

MODELING AND CONTROL OF A PEM FUEL CELL SYSTEM

A THESIS SUBMITTED TO  
THE GRADUATE SCHOOL OF NATURAL AND APPLIED SCIENCES  
OF  
MIDDLE EAST TECHNICAL UNIVERSITY

BY

YASEMİN SAYGILI

IN PARTIAL FULFILLMENT OF THE REQUIREMENTS  
FOR  
THE DEGREE OF MASTER OF SCIENCE  
IN  
CHEMICAL ENGINEERING

SEPTEMBER 2013



Approval of the thesis:

**MODELING AND CONTROL OF A PEM FUEL CELL SYSTEM**

submitted by **YASEMİN SAYGILI** in partial fulfillment of the requirements for the degree of **Master of Science in Chemical Engineering Department, Middle East Technical University** by,

Prof. Dr. Canan Özgen  
Dean, Graduate School of **Natural and Applied Sciences**

\_\_\_\_\_

Prof. Dr. Deniz Üner  
Head of Department, **Chemical Engineering**

\_\_\_\_\_

Asst. Prof.Dr. Serkan Kıncal  
Supervisor, **Chemical Engineering Dept., METU**

\_\_\_\_\_

Prof. Dr. İnci Eroğlu  
Co-supervisor, **Chemical Engineering Dept., METU**

\_\_\_\_\_

**Examining Committee Members:**

Assoc. Prof. Halil Kalıpçılar  
Chemical Engineering Dept., METU

\_\_\_\_\_

Asst.Prof. Dr. Serkan Kıncal  
Chemical Engineering Dept., METU

\_\_\_\_\_

Prof. Dr. İnci Eroğlu  
Chemical Engineering Dept., METU

\_\_\_\_\_

Dr. Yılser Devrim  
Project Manager., TEKSİS

\_\_\_\_\_

Eyüp Töngel,.M.Sc.  
Senior Lead Design Engineer., ASELSAN

\_\_\_\_\_

**Date: September 4, 2013**

**I hereby declare that all information in this document has been obtained and presented in accordance with academic rules and ethical conduct. I also declare that, as required by these rules and conduct, I have fully cited and referenced all material and results that are not original to this work.**

Name, Last name: YASEMIN SAYGILI

Signature:

## ABSTRACT

### MODELING AND CONTROL OF A PEM FUEL CELL SYSTEM

Saygılı, Yasemin

M.Sc., Department of Chemical Engineering

Supervisor: Asst. Prof. Dr. Serkan Kınca

Co-supervisor: Prof. Dr. İnci Erođlu

September 2013, 104 pages

Polymer electrolyte membrane (PEM) fuel cells attract an extensive interest due to their advantageous properties. To compete with the conventional power generators fuel cell systems should ensure safe and efficient operations at any time. To achieve satisfactory operations, all the process requirements should be determined and implemented within the operational constraints. Thermal management, reactant supply, water management and power management are some of the main issues for which proper and sufficient control strategies should be developed and implemented by the control system.

In this study a portable 3kW PEM fuel cell system is modeled to understand the system dynamics. The system model includes the fuel cell stack, humidifier, compressor, inlet and outlet manifolds, and cooling system. Model development is carried out by the mass and energy balances, thermodynamics and kinetics. To define unknown system parameters some experiments are performed on stack and the cooling system and a semi-empirical model is constructed.

For the compressor a feedback (PI) controller is combined with a static feed-forward controller. It is observed that the compressor adapts to dynamic changes within small durations. A membrane type, shell and tube structured humidifier is modeled and compared with literature and a reasonable agreement is observed. Two different humidifiers are simulated to see the effect number of tubes involved in humidifier. It is observed that increasing the number of tubes results in better humidification as expected.

Three different control strategies are analyzed for the cooling system involving a pump, radiator and fan. The performances of different controllers for thermal management are evaluated in terms of stack temperature, integral time weighted absolute error (ITAE) and the parasitic energy requirements. Minimizing fan usage with an on/off controller while keeping the pump voltage as a variable gives better results. MATLAB Simulink is used for development and implementation of models and controllers.

**Keywords:** PEM fuel cells, fuel cell system modeling, fuel cell control

## ÖZ

### PEM YAKIT PİLİ SİSTEMİ MODELLEME VE KONTROLÜ

Saygılı, Yasemin  
Yüksek Lisans, Kimya Mühendisliği Bölümü  
Tez Yöneticisi : Yard. Doç. Dr. Serkan Kınçal  
Ortak Tez Yöneticisi: Prof. Dr. İnci Eroğlu

Eylül 2013, 104 sayfa

Polimer elektrolit membranlı (PEM) yakıt pilleri avantajlı özellikleri nedeniyle yoğun bir ilgi görmektedir. Bilinen güç jeneratörleriyle rekabet edilebilmesi için yakıt pilleri her zaman güvenli ve verimli işleyişi sağlamalıdır. Yeterli işleyişi başarmak için bütün proses gereklilikleri operasyon sınırları dâhilinde belirlenmeli ve uygulanmalıdır. Isıl yönetim, tepken tedariki, su yönetimi ve güç yönetimi, yerinde ve yeterli kontrol stratejileri geliştirilmesi ve uygulanması gereken bazı ana konulardandır.

Bu çalışmada sistem dinamiklerini anlamak için 3kWlık portatif bir PEM yakıt pili modellenmiştir. Sistem modeli yakıt pili yığını, nemlendirici, kompresör, giriş ve çıkış hacimleri ve soğutma sistemini içermektedir. Model geliştirilmesi kütle ve enerji denklileri, termodinamik ve kinetik ile yürütülmüştür. Bilinmeyen sistem parametrelerini tanımlamak için yakıt pili yığını ve soğutma sistemi üzerinde deneyler yapılmış ve yarı deneysel bir model kurulmuştur.

Kompresör için statik ileri besleme kontrolörü, geri besleme (PI) kontrolörü ile birleştirilmiştir. Kompresörün dinamik değişikliklere kısa sürede adapte olduğu gözlemlenmiştir. Zarlı boru-kovan yapısındaki nemlendirici modellenmiş, literatür ile kıyaslanmış ve makul bir örtüşme gözlemlenmiştir. Nemlendiricide bulunan tüp sayısının etkisini görmek için iki farklı nemlendirici simule edilmiştir. Tahmin edildiği gibi, tüp sayısının artırılmasının daha iyi nemlenmeyle neticelendiği görülmüştür.

Pompa, radyatör ve fandan oluşan soğutma sistemi için üç farklı kontrol stratejisi incelenmiştir. Isıl yönetim için farklı kontrolörlerin performansları, yakıt pili yığınının sıcaklığı, zaman ağırlıklı mutlak hata entegrali (ITAE), ve parazit enerji gereksinimleri açılarından değerlendirilmiştir. Pompa voltajını değişken olarak tutup, fan kullanımını aç/kapa kontrolörle en aza indirmek daha iyi sonuçlar vermiştir. Model ve kontrolörlerin geliştirilmesi ve uygulanmasında MATLAB Simulink kullanılmıştır.

**Anahtar kelimeler:** PEM yakıt pilleri, yakıt pili modelleme, yakıt pili kontrolü

To the ones we lost in the fight of human rights and democracy,

## ACKNOWLEDGEMENTS

I would like to express my appreciations to my supervisor Asst.Prof. Dr. Serkan Kıncal for his guidance, suggestions and comments through my study. His relaxed and friendly approach created a comfortable environment during the study.

I would like to thank Prof.Dr. İnci Erođlu, my co-supervisor, for her support, guidance and contributions about gaining experience in fuel cell technology.

I am grateful to the people involved in the project ‘Development of a 3 kW PEM fuel cell’, Prof Dr. Nurcan Baç, Asst. Prof. Dr. Ayşe Bayrakçeken, Dr. Yılser Devrim, Dr. Ertuđrul Başıđme, Hüseyin Devrim, Semih Altunay and Ogeday Çapar due to their contributions on my thesis, information and experience sharing.

I would like to thank my colleagues Dominic Deo Androga and Sevler Gökçe Avcıođlu for their helps and encouragements. I also thank to Dr. Serdar Erkan due to his helps and contributions.

I would like to thank Özgen Yalçın and Seval Gündüz for their friendship, support and advices.

I am grateful to my mother for her patience and efforts, and the memories of my beloved father.

I would like to thank my cousins Dilan Saygılı and Ezgi Saygılı for giving me smiles.

I thank to my friends Alkım Göktaş, Damla Ceylan, İrem Kaya and Haydar Dirik for their companionship and sincerity.

TUBITAK is acknowledged for providing scholarship for the project 109M221.

UNIDO-ICHET is kindly acknowledged for the project ‘Development of a 3 kW PEM Fuel Cell- TF/ INT/ 03/ 002’.

## TABLE OF CONTENTS

ABSTRACT.....	v
ÖZ .....	vii
ACKNOWLEDGEMENTS .....	x
TABLE OF CONTENTS.....	xi
LIST OF TABLES .....	xiii
LIST OF FIGURES .....	xiv
LIST OF SYMBOLS .....	xvii
LIST OF ABBREVIATIONS .....	xix
CHAPTERS .....	1
1. INTRODUCTION .....	1
2. PEM FUEL CELL TECHNOLOGY .....	5
2.1. PEM Fuel Cell Operation Principles.....	5
2.2. PEM Fuel Cell components .....	6
2.2.1. Membrane .....	7
2.2.2. Catalyst .....	8
2.2.3. Gas Diffusion Layer.....	9
2.2.4. Bipolar plates (Current collectors).....	9
2.3. Process control subsystems .....	9
2.3.1. Reactant supply subsystem .....	10
2.3.2. Water management .....	12
2.3.3. Thermal management.....	13
2.3.4. Purge valve.....	14
2.3.5. Power management .....	15
2.3.6. Control of individual cell voltages.....	15
3. MODEL DEVELOPMENT .....	17
3.1. Review of Fuel Cell Modeling.....	17
3.2. Modeling Approach .....	19
3.2.1. Stack Model .....	19

3.2.1.1.	Anode Flow Model.....	19
3.2.1.2.	Cathode Flow Model.....	21
3.2.1.3.	Stack Voltage Model.....	22
3.2.1.4.	Membrane Hydration Model.....	24
3.2.2.	Cooling system.....	26
3.2.3.	Humidifier Model.....	28
3.2.4.	Inlet and Outlet Manifolds.....	34
3.2.5.	Compressor Model.....	35
4.	SYSTEM DESIGN AND IMPLEMENTATION.....	37
4.1.	Prototype Design and Selections.....	37
4.2.	Flow chart and control instrumentation.....	39
5.	SYSTEM IDENTIFICATION AND MODEL VALIDATION.....	43
5.1.	Cooling System Experiment Design and Analysis.....	43
5.2.	Stack tests.....	54
5.3.	Humidifier model validation.....	62
5.4.	Compressor model.....	68
5.5.	Final form of the model.....	69
6.	CONTROLLER EVALUATION.....	79
6.1.	Control of Air Supply.....	79
6.2.	Cooling System.....	82
7.	CONCLUSION AND RECOMMENDATIONS.....	89
	REFERENCES.....	91
	APPENDICES.....	95
A.	EQUIPMENT SPECIFICATIONS.....	95
A.1.	Water Circulation Pump.....	95
A.2.	Humidifier.....	96
B.	PROGRAM CODES FOR DATA ANALYSIS.....	97
B.1.	Cooling system regression code.....	97
B.2.	Polarization curve regression code.....	97
B.3.	JMP Script for reducing test data.....	98
B.4.	Humidifier Model Subsystems.....	98
B.5.	Model Parameters.....	102

## LIST OF TABLES

### TABLES

Table 3.1 Time constants for the processes involving in a fuel cell system [18].....	18
Table 3.2 Mass Balances for Humidifier Model.....	31
Table 3.3 Energy Balances for Humidifier Model.....	32
Table 3.4 Nusselt number parameters for shell side [48].....	33
Table 4.5 Fuel Cell System Design Specifications.....	38
Table 5.1 Test Procedure 2 .....	49
Table 5.2 Set parameters and experimental values of stack testing.....	58
Table 5.3 Constants obtained for stack test for polarization curve model.....	61
Table 5.4 Perma Pure FC 200-780 parameters [21].....	63
Table 5.5 Constants for stack compressor model [18].....	69
Table 5.6 Integrated Model Subsystem Details.....	70
Table A.1 Humidifier Specifications .....	96

## LIST OF FIGURES

### FIGURES

Figure 1.1 Number of patents for different alternative energy movements by years .....	1
Figure 2.1 Representation of a single PEM fuel cell.....	5
Figure 2.2 Pathways involved in a fuel cell cathode compartment [4] .....	6
Figure 2.3 Nafion® membrane structure [3].....	7
Figure 2.4 Fuel Delivery System studied by He et. al [19] .....	11
Figure 2.5 Rectangular membrane humidifier studied by Chen et. al [23] .....	12
Figure 2.6 Cooling system provided by Hu et. al [27] .....	14
Figure 3.1 Cooling system integration with stack.....	26
Figure 3.2 Schematic of the humidifier.....	29
Figure 3.3 The structure of the humidifier .....	29
Figure 3.4 Cross section of the Nafion tubes in the humidifier.....	30
Figure 3.5 Defined systems for modeling. ....	31
Figure 4.1 Fuel Cell Stack With 44 Cells.....	37
Figure 4.2 Representation of the Fuel Cell System.....	38
Figure 5.1 Water flow rate by voltage change. ....	44
Figure 5.2 Pump current demand according to voltage.....	44
Figure 5.3 Fan current demand according to voltage .....	45
Figure 5.4 Cooling system tests setup .....	45
Figure 5.5 Cooling system.....	46
Figure 5.6 Cooling system test procedure-1 .....	46
Figure 5.7 Change in fan voltage during test-1. ....	47
Figure 5.8 Change in pump voltage during test-1. ....	47
Figure 5.9 System response when Test-1 Procedure is applied (1Data/second) .....	48
Figure 5.10 System response when test procedure-2 is applied (1000Data/second).....	49
Figure 5.11 Fan voltage profile during test-2.....	50
Figure 5.12 Pump voltage profile during test-2.....	50
Figure 5.13 The U.A curve obtained according to the data fitted .....	51
Figure 5.14 Comparison of the experimental and modeled u.A profiles. ....	51
Figure 5.15 The deviation from '0' .....	52
Figure 5.16 Comparison of radiator outlet temperature for experiment-1 and model.....	52
Figure 5.17 Comparison of radiator outlet temperature for experiment-2 and model.....	53
Figure 5.18 Cooling system model in Simulink.....	53
Figure 5.19 HENATECH Test Station connected to short stack (5 cells).....	54
Figure 5.20 3 kW PEMFC stack and pin integration for individual cell voltage monitoring	55
Figure 5.21 Cell voltage monitoring apparatus for 3kW PEMFC Stack.....	55

Figure 5.22 Data Acquisition Device.....	56
Figure 5.23 Test Station Flow Diagram.....	57
Figure 5.24 A typical screen shot during performance test of 3kW PEMFC stack. ....	58
Figure 5.25 Screen shot of open circuit cell voltage (OCV) distribution for the 3kW PEMFC stack (Test conditions are given in Table 5.2). ....	59
Figure 5.26 Open circuit cell voltage (OCV) distribution for the 3kW PEMFC stack.....	59
Figure 5.27 Stack voltage vs. stack current at 55°C. ....	60
Figure 5.28 Stack power vs. current at 55°C. ....	60
Figure 5.29 Variation of cooling water outlet temperature, stack voltage and current with time .....	61
Figure 5.30 Cell potential vs. cell number at 5.7 A .....	62
Figure 5.31 Recommended humidifier performance evaluation test setup.....	63
Figure 5.32 Humidifier Model in Simulink .....	65
Figure 5.33 Comparison of heat transfer rate of humidifier with literature model. ....	66
Figure 5.34 Comparison of vapor transfer rate of humidifier with literature model. ....	66
Figure 5.35 Comparison of the humidified air temperature.....	67
Figure 5.36 Dynamic simulation results for step change in dry air flow rate. ....	68
Figure 5.37 Compressor model in Simulink. ....	69
Figure 5.38 Block Diagram of the Integrated System Model. ....	70
Figure 5.39 Integrated prototype model in Simulink. ....	71
Figure 5.40 Stack current applied as the disturbance.....	72
Figure 5.41 Simulated stack voltage for the current profile given in Figure 5.31. ....	73
Figure 5.42 Power and heat generation simulation results for the current disturbance. ....	73
Figure 5.43 Simulation of humidifier performances in terms of a step change in stack current. ....	74
Figure 5.44 Air flow rate through the compressor.....	74
Figure 5.45 Water contents of anode, cathode and the membrane obtained by Simulink. ....	75
Figure 5.46 Water flux through the membrane of a single cell due to back diffusion obtained by simulations. ....	76
Figure 5.47 Water flux through the membrane of a single cell due to electro-osmotic drag obtained by simulations. ....	76
Figure 5.48 Water transfer rate from anode compartment to cathode compartment obtained by simulation for full stack .....	77
Figure 6.1 Compressor voltage command determination by a feedback coupled static controller. ....	79
Figure 6.2 Stack current step change applied as the disturbance .....	80
Figure 6.3 Response of compressor output flow to current changes .....	80
Figure 6.4 Response of compressor voltage command to current changes. ....	81
Figure 6.5 Response of oxygen excess ratio with current changes. ....	81
Figure 6.6 Control strategy-1 (Fan voltage:PI, Pump voltage:constant).....	82
Figure 6.7 Control strategy-2 (Fan voltage:on/off, Pump voltage:follows compressor voltage) .....	83
Figure 6.8 Control strategy-3 (Fan voltage:on/off, Pump voltage:PI) .....	83
Figure 6.9 On/off controller in Simulink .....	84
Figure 6.11 Stack temperature change by a stack current changes .....	85

Figure 6.12 Response of fan voltage .....	86
Figure 6.13 Response of pump voltage .....	86
Figure 6.14 ITAE values for the three control strategies. ....	87
Figure 6.15 Parasitic power required for three control strategies.....	87
Figure 6.16 Total parasitic energy requirements during the simulation.....	88
Figure A.1 Water circulating pump ( <a href="http://www.kormas.com/urunler.asp?id=311">http://www.kormas.com/urunler.asp?id=311</a> accessed at 20.06.2013.).....	95
Figure A.2 Structure of themembrane humidifier ( <a href="http://www.permapure.com/prod-sub-pages/fc300/?ind=Product%20Support%20Pages&amp;prod=">http://www.permapure.com/prod-sub-pages/fc300/?ind=Product%20Support%20Pages&amp;prod =</a> accesses at 20.06.2013.) ....	96
Figure B.1 Inlet gas properties subsystem involved in humidifier model .....	100
Figure B.2 Mass balance subsystem involved in humidifier model.....	101
Figure B.3 Energy balance subsystem involved in humidifier model.....	102

## LIST OF SYMBOLS

Symbol	Definition	Unit
A	Areas	m <sup>2</sup>
A <sub>fc</sub>	Fuel cell active area	cm <sup>2</sup>
a <sub>i</sub>	Water activities	-
C <sub>p</sub>	Constant pressure heat capacity	J/ (kg. K)
C <sub>v</sub>	Constant volume heat capacity	J/ (kg.K)
C <sub>v,i</sub>	Membrane water concentration	mol/cm <sup>3</sup>
D <sub>in</sub> , D <sub>out</sub>	Diameter of the tube	m
D <sub>w</sub>	Diffusion coefficient of water	cm <sup>2</sup> /s
E	Open circuit voltage	V
f	Friction factor	-
F	Faraday's constant	96485 C
$\widehat{H}_1$	Enthalpy	J/ kg
h	Heat transfer coefficients	W/ (m <sup>2</sup> .K)
I <sub>st</sub>	Stack current	A
i	Stack current density	A/cm <sup>2</sup>
J <sub>cp</sub>	Combined inertia for the motor and compressor	kg.m <sup>2</sup>
k	Thermal conductivity	Wm <sup>-1</sup> K <sup>-1</sup>
k <sub>ca,out</sub>	Orifice constant	m <sup>2</sup> /s
L	Tube length	m
M <sub>m,dry</sub>	Membrane equivalent weight	kg/mol
m <sub>i,an</sub>	Mass	kg
$\dot{m}$	Mass flow rate	kg/s
M <sub>i</sub>	Molecular weight	kg/mol
n <sub>d</sub>	Electroosmotic drag coefficient	-
n <sub>tube</sub>	Number of tubes involved in the humidifier	-
Nu	Nusselt number	-
n <sub>cell</sub> , n	Number of cells	-
N <sub>v,membrane</sub>	Water flux	mol/(cm <sup>2</sup> .s)
P <sub>i</sub>	Pressure of component i	bar
Pr	Prandl number	-
P <sub>sat</sub>	Saturation pressure	bar
Q	Heat transfer	W
Re	Reynolds number	-
R	Ideal gas constant	8.314 J.mol <sup>-1</sup> .K <sup>-1</sup>
R <sub>ohm</sub>	Internal electrical resistance	Ω.cm <sup>2</sup>
T	Temperature	K, °C
T <sub>∞</sub>	Ambient air temperature	K, °C

$t_m$	Membrane thickness	cm
$U$	Internal energy	J
$u$	Overall heat transfer coefficient	W/(m <sup>2</sup> .K)
$V_{act}$	Activation losses	V
$V_{cm}$	Compressor voltage command	V
$V_{conc}$	Concentration losses	V
$V_{ohm}$	Ohmic losses	V
$V$	Mean velocity of the flow	m/s
$V_{fan}$	Fan voltage	V
$V_{pump}$	Pump voltage	V
$V_i$	Volume	m <sup>3</sup>
$W$	Mass Flow rate	kg/s
$w_i$	Humidity ratio	kg/kg
$W_{v,membrane}$	Total flow rate across the membrane	kg/s
$w_{cp}$	Compressor speed	rad/sec
$W_{cp}$	Compressor air mass flow rate	kg/sec
$\Delta T_{lm}$	Log-mean temperature	-
$\eta$	Efficiency	-
$\lambda_m$	Membrane water content	-
$\rho$	Density	kg/m <sup>3</sup>
$\rho_{m,dry}$	Membrane dry density	kg/cm <sup>3</sup>
$\sigma_m$	Membrane conductivity	( $\Omega.cm$ ) <sup>-1</sup>
$\tau_{cp}$	Torque need by the compressor	N.m
$\tau_{cm}$	Torque input to the compressor motor	N.m
$\phi$	Relative humidity	-

## LIST OF ABBREVIATIONS

AFC	Alkaline fuel cells
DC	Direct current
GDL	Gas diffusion layers
ITAE	Integral time weighted absolute error
MCFC	Molten carbonate fuel cells
MEA	Membrane electrode assembly
OCV	Open circuit voltage
PAFC	Phosphoric acid fuel cells
PEM	Polymer electrolyte membrane
PI	Proportional integral
PTFE	Polytetrafluoroethylene
SOFC	Solid oxide fuel cells



# CHAPTER 1

## INTRODUCTION

Usage and development of technology brings out a drastic increase in energy consumption in all areas of life. It is known that today's energy supplies mainly depend on the combustion of fossil fuels cannot be continued forever due to depletion of fossil fuels and environmental concerns [1-2]. The need for more energy, decrease in available sources and the rise in the awareness of environmental issues attracts many groups in the area of research on both process intensification and alternative energy developments. Fuel cell technology is one of the areas that receive attention since it can be considered as a solution to energy and environmental concerns. Figure 1.1 shows the number of patents awarded for different clean energy trends and popularity of fuel cells. (Cleantech Group., Heslin Rothenberg Farley., Mesiti PC., Clean Energy Patent Growth Index. [http://cepgi.typepad.com/heslin\\_rothenberg\\_farley\\_/](http://cepgi.typepad.com/heslin_rothenberg_farley_/) [accessed 24.04.2013])

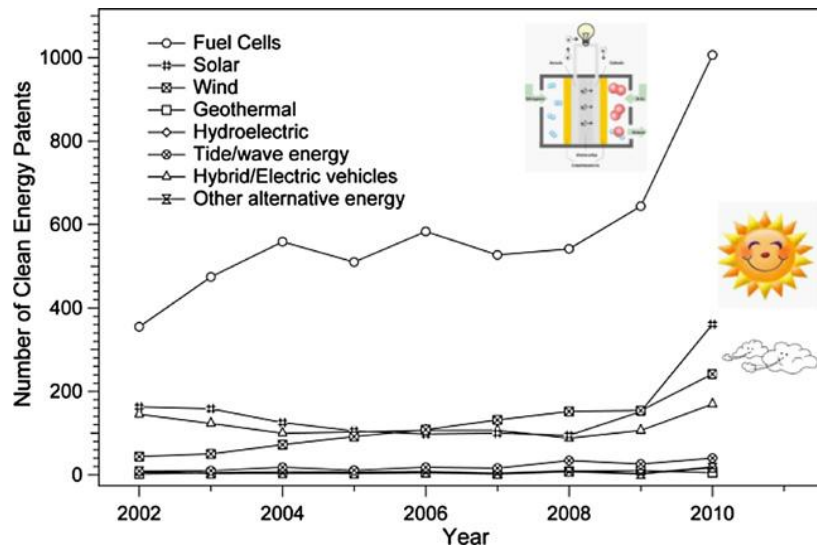


Figure 1.1 Number of patents for different alternative energy movements by years

Fuel cells are the electrochemical reactors that directly convert the chemical energy of a fuel, mainly hydrogen, into electricity by eliminating the energy conversion steps occurring in conventional energy generators and this principle makes fuel cells thermodynamically more efficient than other power generating systems. A fuel cell involves two electrodes; anode and cathode which are negative and positive parts respectively. The electricity is produced by the

electrochemical reactions that occur on these electrodes, typically oxidation of fuel on the anode and reduction of oxidant (mainly oxygen) on the cathode, also water and heat is obtained as the by-products.

Fuel cell and its operating principles are discovered in 1839 and stayed in theory until the 1950's. The technology development is still going on today [3]. What fuel this continuous research on fuel cells are advantages such as higher efficiency, operation with low or zero emissions, modularity, ease to scale-up, promise of long life time, simplicity, and promise of low cost. An intensive research is still being carried out about fuel cell manufacturing methods and component improvements to achieve these accepted advantages in practice.

Fuel cells can be classified according to the electrolyte involved in the system. This electrolyte determines the electrochemical reactions proceed in the system, fuel cell working principles and conditions, especially the operating temperature. Some fuel cell types are Polymer electrolyte membrane fuel cells (PEM), Phosphoric acid fuel cells (PAFC), Molten carbonate fuel cells (MCFC), Solid oxide fuel cells (SOFC), and Alkaline fuel cells (AFC). Fuel cells are applicable in many areas with a wide range of power scale from micro power to MWs such as automobiles, small scale distributed power generators, back-up power systems, space programs, stationary electricity generators, and portable power generators [3]. Each fuel cell type can be preferred for a specific application area due to the operating temperature, cell material, and reactants involved in the electrochemical reactions.

PEM fuel cells attract high attention since they can be applied in automobiles, small scale stationary power generators and portable generators. As the name indicates, PEM fuel cells include a polymer membrane, usually perfluorosulfonated polymers, as the electrolyte which has the ability of conducting protons while behaving as an electron insulator. Other components of PEM fuel cells are electrocatalysts, gas diffusion layers (GDL) and bipolar plates, which are all sandwiched on two sides of membrane respectively and form a single cell. In order to have the desired electric power, single cells should be connected in series to build a stack.

Each of fuel cell components has a specific and important role in the system and direct effect on fuel cell performance. But it can be stated that the membrane is the dominant component that limits and defines the operating conditions, such as fuel cell temperature and humidification level in the system. Fuel cell temperature, membrane hydration, reactant pressures in the cell, individual cell voltages, reactant supply to the system are important topics for a proper fuel cell operation. To satisfy these fuel cell operating conditions, fuel cell stack should be combined with the necessary auxiliary equipment such as fuel supply, humidification and cooling sub-systems, which results in parasitic energy losses. These auxiliary equipment should meet the system requirements such as desired power, humidification, cooling and provide the necessary conditions to the fuel cell stack. This harmony between auxiliaries and stack must be implemented by a control system. The control system must ensure safe and efficient operation at steady-state and transient operations. The fuel cell should practice smooth start-up and shut-downs, make necessary attempts in case of any disturbances and emergency situations.

For a process control application, the fuel cell system model should be developed. Model should include all auxiliary units and the stack. Mass balances, energy balances, kinetic and thermodynamic relationships are the tools for model development. After using these tools, the model should be tested to determine the unknown system specific parameters, and a semi-empirical model should be validated. Different control strategies can then be developed over the generated model. Model based analysis provides the analysis of system behaviors in various conditions, eliminating extensive experiment requirements.

Fuel cell system designs differ widely. There are lots of alternatives of fuel supply modes, cooling systems, humidification systems, handling power options. Therefore modeling approaches and control issues are specific to each individual fuel cell system. However it can be stated that control systems are mainly divided into thermal management, water management, power management, and reactants supply management.

Fuel cells must be thermally managed in order to have a good performance and high efficiency without any degradation in the construction materials. Both reaction kinetics, proton conduction and hydration via the membrane are affected by temperature, hence the temperature of the fuel cell stack should be kept close to a set value to have higher efficiency. The operating temperature of PEM fuel cell is limited between 60 and 80°C due to membrane character and this can be achieved by a cooling system that can be designed with various equipment and control strategies.

In order to have proton conductivity in the system, the polymer membrane (usually Nafion®) humidity should be carefully adjusted. Proton conduction occurs via the water molecules appearing in the membrane which necessitates humidification to some extent. On the other hand excess water can cause flooding by closing the pathways for reactant flow. To achieve a proper water management different types of humidifiers are used in PEM fuel cell systems which can be operated static or with dynamic control algorithms.

Power management subsystem is required to control the power drawn from the fuel cell system. A battery can compensate the power requirements in case of insufficient electricity generations also it can be recharged at extra electricity generations. Usage of the battery can be controlled by analyzing the stack voltage. At low stack voltages the battery can be put into use, such as at start-ups.

Reactant flow subsystem includes the hydrogen flow to anode side and air flow to cathode at desired amounts and pressures. Sufficient amounts of reactants should be supplied to the system to avoid any degradation at catalyst sites. While hydrogen is obtained from pressurized tanks air flow requires additional equipment such as compressor and blowers. The equipment used for reactant flow should have small response times to adapt dynamic load changes as well as low power consumption.

The aim of this thesis is to develop a model and control strategies for a 3kW PEM fuel cell system designed for portable applications. The presented work is carried out as a part of the project 'Development of a 3 kW PEM Fuel Cell System' which is funded by UNIDO-ICHET. In Chapter 2 a literature review for PEM fuel cell operation principles and process

control requirements is given. Chapter 3 consists of the models developed for cooling system, humidifier, stack, compressor and manifolds. The prototype design, operational selections, and process flow charts are given in Chapter 4. System tests and semi-empirical model derivation is expressed in Chapter 5. In Chapter 6, final form of the prototype model is evaluated for different control strategies for thermal management.

## CHAPTER 2

### PEM FUEL CELL TECHNOLOGY

PEM fuel cells have been considered as a promising power source for many applications therefore related technology gain an extensive interest worldwide. Despite the basic principles in theory, there are many drawbacks on practice preventing the commercialization so the component development stage is still continuing. Component integration, stack development, system integration and control should be achieved effectively for smoothly operating fuel cell systems. To construct a fuel cell control system, the system operating principles, material properties and characteristics should be analyzed and understood clearly. The following subsections summarize the component properties, fuel cell operating principles and related drawbacks and important points to be focused on a control system.

#### 2.1. PEM Fuel Cell Operation Principles

The main components of a PEM fuel cell are polymer membrane, catalyst, gas diffusion layers and bipolar plates. The polymer membrane is the center of a cell, followed by catalyst layers for hydrogen oxidation and oxygen reduction reactions at anode and cathode sides respectively. After the catalyst layers gas diffusion layers (GDL) present at anode and cathode. These three structures in a cell called membrane electrode assembly (MEA) together. The MEA is packed with bipolar plates and forms a basic single cell as shown in Figure 2.1.

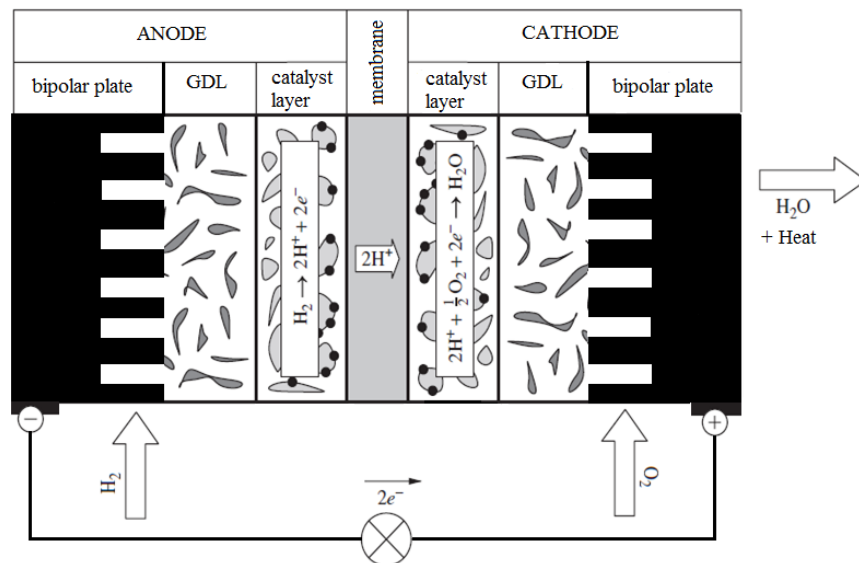
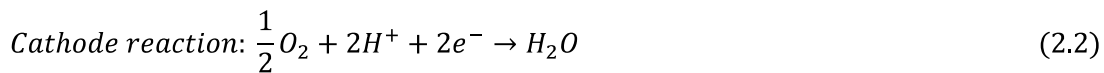


Figure 2.1 Representation of a single PEM fuel cell

During the operation, hydrogen gas passes through the gas channels involved in bipolar plates and reaches to gas diffusion layer. Porous structure of GDL allows hydrogen gas to reach the anode catalyst layer and hydrogen oxidation reaction given in Equation (2.1) occurs at catalyst active sites. The product protons pass through the membrane while the electrons follow an external path to reach cathode catalyst surface. At cathode catalyst sites oxygen reduction proceeds as given in Equation (2.2) with protons and electrons transferred from anode and oxygen coming through the cathode bipolar plate and GDL.



Water transfer occurs through the membrane by the electro-osmotic drag and back diffusion mechanisms. The resultant heat of reactions is transferred by conduction and convection within the system.

A single cell is usually operated at 0.5-0.7 V to have maximum power at load conditions. For sufficient electricity production the single cells must be connected in series and a stack needs to be put together. Fuel cell stack should be equipped with fuel supply equipment, manifold, humidifiers, cooling auxiliaries to construct an independent power generating system.

## 2.2. PEM Fuel Cell components

The materials constructing a fuel cell system has specific roles and properties. The polymer membrane is an electric insulator while transferring protons and water. Electrochemical reactions occur on catalyst surface. The catalyst should also contain proton conducting and electron conducting media, and pores for water transport. Gas diffusion layer distributes reactant gases homogeneously on the fuel cell active area, provide electrically conductive paths for electric conduction and pores for water transport. Figure 2.2 presents the proton and electron pathways at cathode on a single cell. Lastly, bipolar plates collect current and complete electrical circuit on the fuel cell [3].

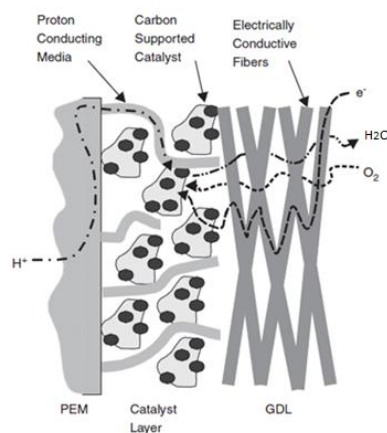


Figure 2.2 Pathways involved in a fuel cell cathode compartment [4]

### 2. 2.1. Membrane

Polymer membrane is the electrolyte that provides ions for proton transfer in PEM fuel cells. To be used in PEM fuel cells, the membrane should provide high proton conductivity while supporting the high currents with minimum resistive losses. It should isolate anode and cathode compartments electrically, so electrons are constrained to follow an external circuit to produce electricity. With adequate mechanical strength and stability, it should behave as a barrier to the mixing of fuel and oxidant gases under operating conditions. It should be chemically and electrochemically stable with a high water mobility that satisfies uniform humidity by preventing localized dryings [5, 6].

Some of the materials used as proton conducting membrane are perfluorinated ionomers, partially fluorinated polymers, non-fluorinated hydrocarbons with or without aromatic backbone and acid-base blends [6]. Among these different membrane types Nafion® produced by Dupont™ became as an industry standard. Nafion® replaced other types of membranes due to its high proton conductivity and life-time, and it is the reference material to be compared with any newly developed membrane [5]. Like a typical ionomer membrane Nafion® is a sulfonated polymer, perfluoro-sulfonylfluoride ethyl-propyl-vinyl, which both includes hydrophobic and hydrophilic parts. The structure of Nafion® can be seen at Figure 2-3. Hydrophilic domain (sulfonic acid functional groups) provides proton conductivity whereas hydrophobic parts (Teflon-like structures) provide mechanical strength and dimensional stability [3, 7].

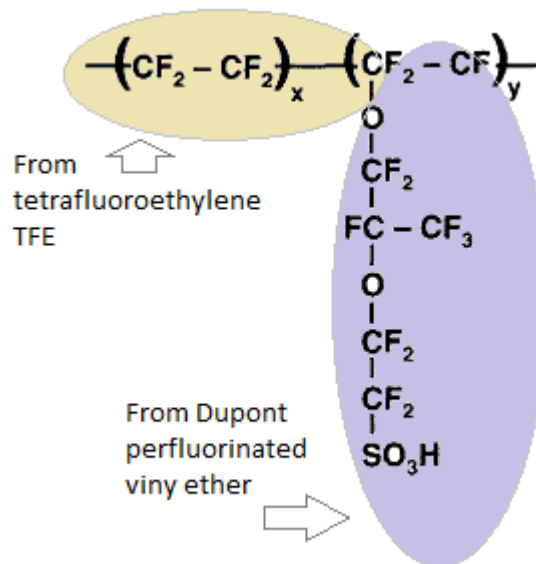


Figure 2.3 Nafion® membrane structure [3]

Nafion® proton conductivity highly depends on the water uptake ratio which is the number of water molecules present per sulfonic acid group. High water uptake ratios results in high conductivity therefore the membrane should be humidified enough to achieve high proton conductivity. But the excess water amount in the system should be prevented because excess water in the cell may fill the pores of catalyst and gas diffusion layer and prevent gases to reach reaction sites. It is also observed that above 80°C, membrane's proton conductivity decreases due to dehydration and to prevent this phenomenon in the system the membrane temperature should be kept at 60-80°C [8]. Therefore it can be stated that to keep the membrane operable with high proton conductivity both temperature and water content should be managed in the control system.

### 2.2.2. Catalyst

Catalysts are the electrodes appearing at two sides of the membrane, at anode and cathode for hydrogen oxidation and oxygen reduction reactions respectively. Besides providing active sites for reaction, PEM fuel cell catalyst should satisfy both proton and electron conductive paths and contain pores allowing water and reactant gas transfer (Figure 2.2). They should include the active ternary phase boundaries where all the reactants can meet. The catalyst should be chemically stable under the operating pH and voltage conditions, and tolerable to fuel and oxidant composition [3, 9].

Pt or Pt supported alloys are commonly used in PEM fuel cells due to their high electrocatalytic activities, resistance to corrosion and oxidation. But as being a precious metal, Pt constitutes a high percentage of stack cost. Over time Pt loading is decreased by studies with using smaller particles, maximizing the surface area and making Pt usage more efficient. There are also many studies in which other precious metals, non-precious metals and incorporated ones are investigated to reduce the catalyst cost [9, 10]. In general Pt is dispersed on carbon support; the support material should have a high surface area, be electrically conductive and create pathways for electrons, and be durable in corrosive environments.

Catalysts are usually prepared by adding Nafion as a binder to the membrane for proton conduction. Also hydrophobic materials (polytetrafluoroethylene (PTFE)) can be added to the catalyst particles to supply dry regions for reactant gas transport. To reduce the transport losses Pt, carbon, Nafion and PTFE (if used) amounts should be efficiently distributed and the ternary phase boundaries should be maximized [10].

There are two ways of MEA preparation. First, the catalyst could be applied on gas diffusion layer then the membrane is sandwiched between these layers and pressed. Secondly, the catalyst can be directly applied on membrane and pressed with GDLs [11]. The contact resistance between membrane and catalyst should be minimized to have lower potential losses.

### **2.2.3. Gas Diffusion Layer**

Gas diffusion layer is the porous diffusion media to distribute reactant gases homogeneously on the fuel cell active area. It is placed between catalyst layer and bipolar plates on anode and cathode. GDL should be electrically conductive for electron transfer and thermally conductive to distribute generated heat from catalysts to other fuel cell components. Carbon paper and carbon cloth are the GDLs used generally. By using hydrophobic (PTFE Teflon) and hydrophilic additives in GDLs, water is managed within the MEA. Water produced at catalyst surface is transferred to outlet gas channels via the hydrophilic channels of GDL. So reactant gases follow the hydrophobic channels and species transport is balanced without any interference [3, 12]. Water management should be effectively carried out to prevent flooding and sustain gas transport.

### **2.2.4. Bipolar plates (Current collectors)**

There are several functions of bipolar plates in fuel cell systems. They are electrically conductive and they enable electron transfer to complete the circuit. They connect the anode of a cell to the cathode of the adjacent cell, and build a stack formed of single cells connected in series. These plates structurally support the MEA, so they should have mechanical strength and durability. They provide fuel and oxidant flows with a flow field. They need to be impermeable to gases, so the reactants are forced to follow the gas channels to reach GDL. Bipolar plates also ensure stack cooling by the cooling channels, so their thermal conductivities should be high. Bipolar plate weight is the biggest portion of stack weight, so light weight materials are preferred. The material should be easily machined and manufactured with a low cost. It should withstand corrosive environment of a fuel cell [3].

The materials used as bipolar plates are graphite, polymer-graphite composites and metals. Graphite shows chemical stability and high electronic conduction but due to their brittle structure they lack mechanical durability. The cost of machining flow fields on graphite plates is also expensive. In order to increase mechanical strength of graphite some polymer additives are also used. These polymers give flexibility to the plates without any effect on chemical stability, but they cause a decrease in electrical conductivity of graphite. Metals shows better electric conduction and mechanical strength but they cannot stand the acidic environment of fuel cell and expose to corrosion. Different coating materials are used to eliminate this problem without any decrease in electrical conductivity [13].

## **2.3. Process control subsystems**

In order to show similar levels of performance of conventional energy generators, fuel cell systems should be operated more efficiently by giving high power density, durability, and reliability. By considering the fuel cell operation principles and component performance requirements it is clear that a control system must be developed and integrated with stack and all the auxiliary equipment. Fuel cell control system can be divided into subsystems of fuel supply, water management, thermal management, power management, purge strategy

and cell voltage check. These subsystems are all related with each other and state the effectiveness of other subsystems and overall system.

### **2.3.1. Reactant supply subsystem**

To assure continuous power supply the system must be charged with reactants with sufficient amounts. The fuel and oxidant supply should be optimized in terms of excess reactant amounts and parasitic losses introduced by power supplying equipment. Fuel supply should be properly controlled to avoid reactant undersupply; lower partial pressures of reactants. Reactant starvation shows negative effects on fuel cell durability and reliability which can be resulted by improper gas supply, sudden load increases and start-ups. . Voltage reversals caused by fuel starvation degrades catalysts. Pt or Ru dissolutions, carbon corrosion and water electrolysis are some of the phenomena observed in fuel starving fuel cells. Measurements on fuel cell active area also show non-uniform distributions of voltage and current in case of fuel starvations [14]. Oxidant starvation causes a decrease in reaction rate and current densities, also rapid cell reversals [15].

For hydrogen deliver, pressurized tanks or hydrogen reformers can be used. Reformate gas usage have limitations on catalyst performance and durability therefore in control studies pressurized hydrogen tanks are preferred as the hydrogen source. Air is supplied to the fuel cells as oxygen source generally. Air requirement could be satisfied by compressors, blowers etc. The air supplying equipment should include filters and leak-proof lubrication systems for eliminating contamination risks. Also they should response quickly in load changes [16].

Vega-Leal et. al used proportional regulation valves for hydrogen flow in anode dead-end mode operation. The flow is provided proportionally to the pressure difference between cathode and anode inlet by the valves [17]. This approach is followed due to the risk of damaging MEA with high pressure differences between anode and cathode.

Pukrushpan et. al used a valve to control hydrogen flow from a high pressurized source, which allows rapid adjustment. The valve is activated according to the pressure difference between anode and cathode manifolds. To minimize the pressure difference between these compartments a simple proportional controller is used. The controller makes the anode pressure to follow cathode pressure by the feedback of pressure difference [18].

He et. al [19] studied a fuel delivery system consisting of an ejector, blower, pressure regulators, flow control valve, purge valve and related manifolds as shown in Figure 2-4. In the system pressurized hydrogen tank is connected to a high pressure regulator so the pressure kept constant in the line, the gas passing through flow control valve ejected to the supply manifold and then to the stack. The excess hydrogen is recirculated by a blower back to the stack inlet and with periodic purging. To avoid high pressure difference between anode and cathode, supply manifold pressure is also controlled for this system. Control strategy is designed for three levels of current requested: low, medium and high. In low current mode ( $0-6000\text{A/m}^2$ ), a constant amount of hydrogen is fed to the system by low

pressure regulator and the excess hydrogen channeled to supply manifold with blower. For medium ( $6000\text{-}8000\text{A/m}^2$ ) and high (above  $8000\text{A/m}^2$ ) flow control valve, ejector and blower are used. Three different controllers, state-feedback, state-feedforward and PI controllers are simulated to see the response of hydrogen stoichiometric ratio and supply manifold pressure with multiple step changes in load. It is stated that the state-feedback control show the best performance in terms of following cathode pressure and disturbance handling.

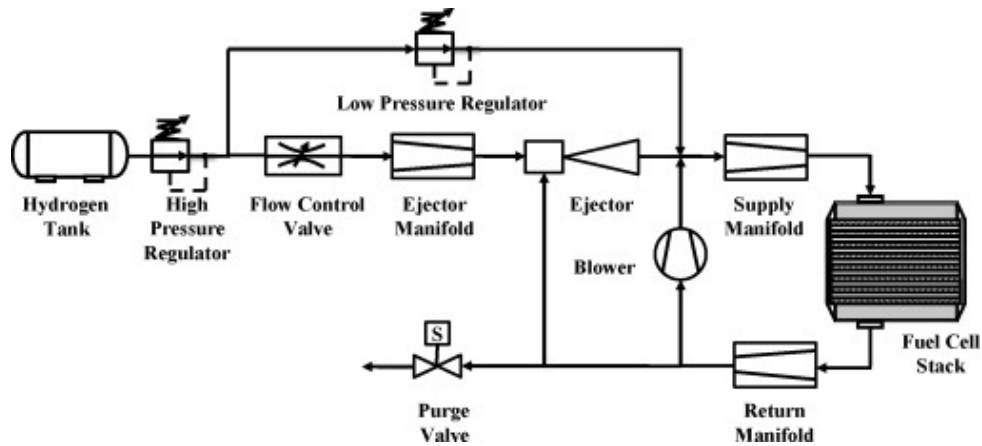


Figure 2.4 Fuel Delivery System studied by He et. al [19]

Vega-Leal et. al applied a feed-forward control strategy for air supply. They calculate the compressor motor input voltage according to stack current and oxygen stoichiometry. The current demanded is measured and with a feed-forward compensator the perturbation is removed. Then the centrifugal compressor is activated by the control signal provided from compensator [17].

Pukruspan et. al proposed three different control configurations for control of air flow. First strategy is static feedforward control that determines the compressor voltage command according to stack current. Secondly dynamic feedforward control is analyzed; this method includes addition of a lead filter to achieve good disturbance rejection. Thirdly, to improve system robustness a feedback (PI) coupled static feedforward strategy is studied. It is stated that feedback controller shows better performance due to its inherent robustness limitations [18].

Panos et. al designed model predictive controller to achieve a proper air supply and thermal management. After deriving the detailed system model, dynamic simulations of the system are used to obtain a reduced order approximated model. Then a explicit multi-predictive controller is designed. It is presented that the designed controller is performing effectively for disturbance rejection [20].

### 2.3.2. Water management

In order to ensure high proton conductivity, Nafion's water content should be optimized. Low water content would not give sufficient proton transfer while excess water will cause mass transfer limitations by filling the porous diffusion media [15]. Due to the contradiction in terms of water limit in the system external humidifiers are used in general.

Some popular humidifier types are nozzle spray, gas bubbling, enthalpy wheel and membrane humidifiers. Nozzle spray humidifiers use the cooling water exiting the stack. They spray the water uniformly on a cloth or wire mesh and allow the reactant gases to go on. This method is disadvantageous since the reactant gases could absorb water proportional to their temperature. Therefore cold inlet air could not reach to a satisfactory relative humidity while entering to the stack. Gas bubbling humidifiers are the bottles of heated water where reactant gases pass through. In these types of humidifiers large pressure drops occur. This makes the usage suitable just for low pressure fuel cells. Enthalpy wheel humidifiers uses stack exhaust air to humidify and heat the fresh air. In these humidifiers the rotational speed of the wheel is changed to control the humidity of fresh air. Their motor causes additional parasitic losses in the system due to the electric power consumption. Membrane type humidifiers exchange heat and water in case of temperature and vapor concentration gradients. Membrane humidifiers are typically installed behind the stack and cooling water or the stack exhaust gases are usually preferred as the humid source. Rectangular and cylindrical geometries are available for membrane type humidifiers [21-23].

Chen et. al studied a rectangular membrane humidifier as shown in Figure 2.5 in which stack exhaust gas is used for humidification. The humidifier includes three channels shown as A, B and C. Dry gas flow is directed to the channels B and A with controlling the sliding plate, while stack exhaust flows through channel C. They applied a proportional controller that based on the error between desired and obtained vapor transfer rates and decides opening ratio of channel A with sliding plate. It is observed that at steady-state proportional control and no control vapor transfer rates are identical but the transient effects can be reduced by the proportional controller [24].

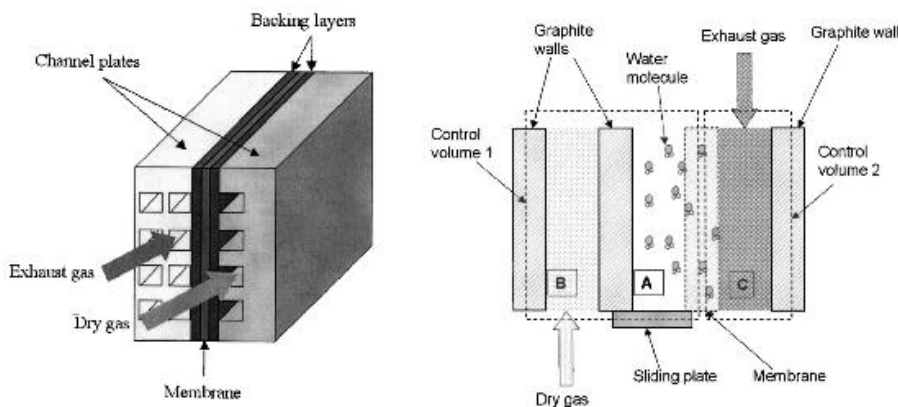


Figure 2.5 Rectangular membrane humidifier studied by Chen et. al [23]

Jong Woo-Ahn studied a cylindrical membrane type humidifier that uses stack exhaust air as the vapor source. In this study the amount of stack exhaust air directed to the humidifier is determined by changing the bypass valve opening factor. Static feed-forward control is applied and results are compared with the uncontrolled humidifier findings. It is observed that the uncontrolled humidifier results in flooding with high water contents whereas the controlled humidifier keeps the membrane water content at desired levels [25].

Pukrushpan et. al studied a static injector humidifier that calculates the amount of water to be added to dry air according to the desired humidity value. While the inlet dry gas conditions such as temperature, humidity and flow rate are known, the water flow rate for injection can be calculated [18].

### **2.3.3. Thermal management**

Keeping the stack temperature at a desired level has a significant effect on safe and efficient operation of fuel cells. Unless sufficient heat is removed, the stack overheating can cause severe hydration in the polymer membrane which would lead to large resistance and loss of proton conductivity. Especially the cells positioned at stack center can show sharp voltage drops due to drying out at high temperatures. Another point is that high temperatures can cause membrane leaks formed by hot spots. This situation can result in unsafe positions since the leaks allow mixing of hydrogen and oxygen [26]. To avoid performance losses and membrane leaks a cooling system should be installed to the fuel cell stack which can reduce the excess heat from the system at any stack current and keep the stack temperature at the set point with a minimum parasitic loss.

Vega-Leal et. al [17] developed a proportional feedback controller for temperature control. This study represents an air cooled fuel cell system that uses a fan to give cooling air to the stack. The cooling strategy in this study is changing fan speed according to the difference of the stack temperature and desired temperature with a proportional controller.

Hu et. al [27] proposed a fuzzy controller with integrator for a cooling system consisting of coolant reservoir, cooling water pump, bypass valve and a heat exchanger as represented on Figure 2.6. Pump voltage and bypass valve opening are determined according to the temperature error sent to the fuzzy controller. The fuzzy control results are compared with conventional PI controllers and it is stated that the fuzzy controller have smaller overshoot and better response times.

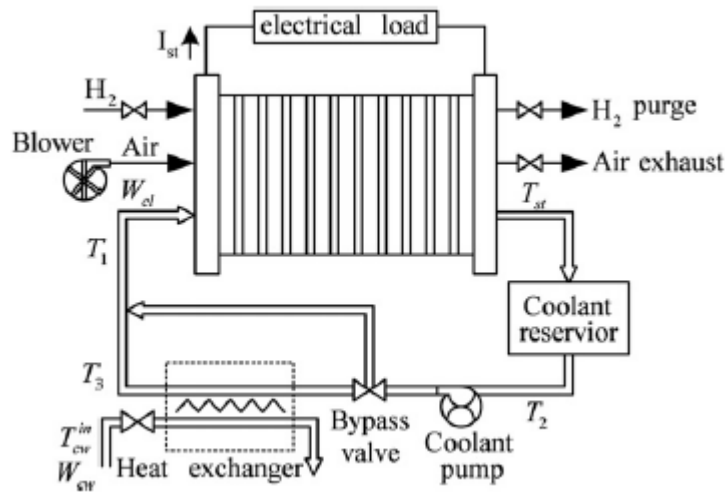


Figure 2.6 Cooling system provided by Hu et. al [27]

Rabbani et. al applied PI controllers on an automobile system consisting of a pump for coolant water flow and radiator with fan. The coolant temperature exiting the stack is measured and compared with the temperature set point. Then this error signal is sent to PI controllers for the pump and fan. It is stated that the temperature control system is slower than the electrochemical reactions. To compensate the heat produced by fast electrochemical reactions high coolant mass flows are used [28].

#### 2.3.4. Purge valve

Dead-end operation is a reactant supply mode in which anode gas exit is normally kept closed, and hydrogen is kept at a constant pressure. During dead-end operation, some impurities and water can be accumulated at anode side due to the permeation through the membrane. Accumulation of these impurities can lead to uneven distribution of hydrogen and fuel starvation [15]. To remove these unwanted species a purging process should be carried out. The frequency and duration of purges should be determined for an efficient purge with minimum fuel consumption [3].

There are two more reasons for purging, performed in shutdown periods. Firstly residual hydrogen should be purged to prevent the degradation of carbon support of cathode catalyst. Secondly, the water removal should be achieved at shutdowns to eliminate the risk of freezing of water if the stack is exposed to sub-freezing temperatures [29]. In order to avoid these phenomena shutdown purge strategy should also be developed.

He et. al [19] proposed a periodic purging for the fuel delivery system given in Figure 2.4. Belvedere et. al [30] suggest to determine purge intervals as a function of stack current or stack voltage. The stack current can be observed and purge valve can be opened in

unfavorable current variations. Similarly the stack voltage can be compared with a threshold voltage value and purge valve can be opened until the voltage is recovered.

Chen et. al performed optimization studies for purging interval and cycle durations. They build a 1 dimensional, two phase model and investigate the effects of purging. They concluded that while shorter cycle durations and long purge intervals increase the efficiency, longer cycle durations and short purging time decreases the hydrogen usage [31].

### **2.3.5. Power management**

The power management system in a fuel cell system has an objective that is to supply a balanced power distribution among the fuel cell and battery to perform at any load demand. Zhang et. al [32] aimed to achieve a power management by comparing the load power demand with fuel cell-battery power. By using a DC/DC converter the system voltage is tried to be kept at 12 V at any condition. If the load demand is lower than the fuel-cell battery rated power (100W) the power would be obtained by the fuel cell while the battery power will be used for parasitic losses. If the battery state of charge, drops lower than lower battery limit the fuel cell will charge the battery until the upper battery limit is obtained. Parasitic losses also need to be powered by the fuel cell during the charging period. If the load demand is between 100-150% of the system rated power, the battery will also be controlled to supply power to the load and auxiliary equipment. If the power demand exceeds 150% of the rated power the system will perform shut-down operation to avoid permanent losses. To understand the battery charging behavior a lithium ion battery is simulated with lower and upper state of charge 58% and 60% respectively. These control objectives are achieved by an embedded micro-controller.

Kim et. al [33] also studied to implement a duty cycle control for the bidirectional battery in terms of deciding the charging or discharging the battery with fast responses by keeping the stack voltage constant at 400V for a 85kW fuel cell system. A ‘dynamic evolution control’ is used to balance the battery charging and discharging. The duty cycle is modeled by using the charging mode dynamic equation and state error function. It is observed that the ‘dynamic evolution control’ improves fuel cell transient dynamics while providing an effective control at steady-states.

### **2.3.6. Control of individual cell voltages**

Some of the diagnosis techniques for a fuel cell system can be listed as obtaining polarization curve, current interruption test, electrochemical impedance spectroscopy and pressure drop measurement [34]. But these techniques are only suitable for non-adapted stacks and not applicable for the fuel cell systems operating as a real electricity generator. The fuel cell stacks are generally tested by individual cell monitoring since cell voltages reflect the fuel cell conditions such as temperature, hydration, oxygen excess ratio and the

related changes. Some cells can respond faster than other cells due to their position on the stack, to illustrate the cells in the center have higher temperatures and exposed dehydration which results in sharp voltage drops. If such cells are analyzed and the requirements are fulfilled a decrease in the overall stack voltage can be prevented at early stages.

The aim of individual cell voltage monitoring mainly has three reasons which are safety, control and long-term analysis. From safety point of view, declined cell voltages can be result by internal problems appearing in the MEA such water droplets preventing gas flow or pinholes and hotspots in the membrane. Individual cell voltages can also be used for control purposes because they directly response to the conditions such as impurity accumulations, water droplets in the gas pathways, unequal gas distribution, membrane drying or flooding and electrical connectivity problems. With the available sensors and operating conditions the cause of the voltage drop can be understood and the necessary procedure can be applied [35]. The degradation of fuel cell stack can be observed by cell voltage monitoring. The degradation is generally expressed as drop in microvolt in terms of the operating hour which can be received directly with cell voltages [36, 37].

It is also reported that cell voltages below 0.4 V gives higher current densities which results in higher water production. Unless the sufficient water removal is applied operation below 0.4 V should be avoided to prevent flooding and its unavoidable results [36].

## CHAPTER 3

### MODEL DEVELOPMENT

#### 3.1. Review of Fuel Cell Modeling

Models are the tools that represent defined system behaviors within the probable conditions. System models can be built by applying mass and energy conservation laws, reaction kinetics, thermodynamics and transport phenomena. These models are defined as the fundamental models and they are preferred in general due to their capturing capacity over a larger range of conditions. Empirical findings can also be used for modeling since they provide an easier option to understand and analyze the system characteristics but they are limited to regions and conditions where the experiments had conducted. Empirical models can be replaced by the fundamental models including complexities. Semi-empirical models can also be created to remove complexity and get system specific parameters and unknowns [38].

For fuel cell systems various models are developed to obtain a deeper understanding on fuel cell operations or process control applications. There are examples of fuel cell modeling to gain an insight about fuel cell water transport, degradation etc.[39- 41] These models can be in macroscopic or microscopic levels while some of the tools used for these scales are computational fluid dynamics and estimation particle interactions respectively. Although these models are satisfactory in terms of capturing fuel cell behaviors their complexity prevents them being applicable in process control applications.

Khandelwal et. al [42] studied one-dimensional thermal model of cold-start in a PEM fuel cell. With this model, temperature distribution in the stack, start-up time, and cold-starting ability and energy requirements are predicted. Although this work addresses the fundamentals related to start-up behavior, it lacks the simplicity requirement for process control studies. Seinderberger et. al [39] developed a model to estimate the water transport and degradations in GDLs. A three-dimensional GDL substrate is simulated by the model but the complexity prevents usage of this model for process control.

The models developed for process control applications should include sufficient details to capture process characteristics but they should also be simple enough to be solvable with the available computers and programs with small durations. The simplifications over the fuel cell dynamics can be carried out by considering the time constants of processes involved in fuel cell operations. The orders of magnitudes and simplification explanations for a fuel cell system are proposed as in Table 3.1 [18].

Table 3.1 Time constants for the processes involving in a fuel cell system [18]

	Order of magnitude (sec)	Explanations
Electrochemical reactions	$10^{-19}$	Reaction dynamics are too fast to be included in the model; they have minimal effects on the overall fuel cell system.
Manifolds	$10^{-1}$	Manifold filling dynamics affect the fuel cell performance since they provide the reactants to the system with desired pressures. Manifold models are important especially at the transients.
Membrane water content	Unclear	The time constant for membrane water content cannot be separated from the temperature and fluid flow; therefore it is given as unclear. But it has a dominant effect on fuel cell performance, so should be included in the model.
Flow dynamics	$10^0$	For an efficient operation, the reactants should be supplied with the selected stoichiometries to the fuel cell. Fluid flow should be included in the model.
Inertia dynamics of the auxiliaries	$10^1$	The auxiliaries such as compressor and cooling system equipment are generally the manipulated systems. They have a direct effect on control system design and must be included in the model.
Cell and stack temperature	$10^2$	Temperature time constant has a larger value when compared with other dynamics. Stack would observe slower temperature dynamics therefore the temperature effect can be ignored instantly. While fast dynamics are enduring, the temperature can be considered as a constant value.

Grötsch et. al [43] derived a nonlinear, two-phase model which includes spatial variations by assuming isothermal and isobaric operation, gases behave ideally, Fick's diffusion is applicable for the hydrogen, oxygen and vapor transport from GDLs to catalyst layers, electro-osmotic drag from the membrane is valid, Butler-Volmer kinetics are applicable, constant gas compositions are available at anode and cathode bulks and dynamics of double layers are fast enough to be neglected. With these assumptions and applying finite volume elements method a 130 dynamic and 413 algebraic equations are obtained. Long simulation times made the model inapplicable for process control and therefore a model reduction process is carried out compulsorily.

Jinglin He et. al [19] derived a two-phase anode model and focused on the fuel delivery system as described in Figure 2.4. The assumptions hold for the study are; constant outlet pressure of the high pressure regulator, no pressure drop, no spatial variations, hydrogen source is pure, membrane is impermeable to gases, ideal gas law is applicable, system is isothermal, no liquid water circulation by the blower or ejector, gaseous and liquid water are in equilibrium in the system. With these assumptions the model stated to be became control oriented, allowing simulations for different conditions and disturbances.

## 3.2. Modeling Approach

Within the scope of this study a semi-empirical model is developed for a PEM fuel cell prototype. The spatial variations are ignored thus complexity is reduced. By considering the slow response time of stack temperature an isothermal model is derived with perfect cooling assumption. For stack voltage model and cooling system experimental data are used to develop a semi-empirical model that reflects the prototype system better and simplifies the model for cooling system.

### 3.2.1. Stack Model

Stack model includes anode and cathode flow models, membrane hydration model and stack voltage model. Anode and cathode flow models enables the estimation of the gas amounts, pressures and humidity of anode and cathode compartments, hydrogen and oxygen excess ratios by developing mass balances with thermodynamics. The main assumptions involved in stack model development can be listed as

- Isothermal operation: temperature dynamics have larger time constants among the other processes involved in fuel cell stack. Therefore stack temperature can be considered as a constant instantly. By assuming a perfect cooling system that directly remove generated heat from the stack, isothermal operation at any time is acceptable.
- Gases behave ideally.
- System is uniform: the subsystem outlet properties such as temperature, pressure, relative humidity are same with the subsystem properties where subsystems are anode and cathode. It is assumed that the anode and cathode channels are uniform by ignoring the spatial variations.
- The Nafion® membrane can be accepted as impermeable to the species rather than water due to its structure. Permeation of hydrogen to cathode, oxygen and nitrogen to anode can be ignored since the permeation rate is not at considerable amounts.

#### 3.2.1.1. Anode Flow Model

The stack in scope of this work is selected to operate at dead-end mode at anode side. A pressurized hydrogen tank is considered as hydrogen source, and the anode pressure would be adjusted with a diaphragm valve and check valve used in the hydrogen line. Anode side mass balance can be written for hydrogen and water as in Equation (3.1) and Equation (3.2),  $m_{i,an}$ (kg) denotes the amount of gas accumulated in the anode for hydrogen or water and  $W$  (kg/s) is be the amount of hydrogen or water inlet, outlet, reacted or transferred. For dead-end mode the outlet terms for hydrogen and water would appear just in purge conditions.

$$\frac{dm_{H_2,an}}{dt} = W_{H_2,anin} - W_{H_2,anout} - W_{H_2,reacted} \quad (3.1)$$

$$\frac{dm_{H_2O,an}}{dt} = W_{vapor,anin} - W_{vapor,anout} - W_{vapor,membrane} - W_{H_2Oliq,anout} \quad (3.2)$$

In anode volume, water could be in either liquid or vapor form. By assuming equal vapor phase and anode volumes, maximum vapor in the anode can be calculated with ideal gas law as in Equation (3.3) where  $P_{sat}$  (Pa) is the saturation pressure given in Equation (3.4),  $V_{anode}$  ( $m^3$ ) is the anode volume,  $M_{H_2O}$  (kg/mol) is the molecular weight of water,  $T_{stack}$  (K) is the stack temperature and  $R$  is the ideal gas constant as  $8.314 \text{ J}\cdot\text{mol}^{-1}\cdot\text{K}^{-1}$

$$m_{vapor,max.anode} = \frac{P_{sat} V_{anode} M_{H_2O}}{RT_{stack}} \quad (3.3)$$

$$\log(P_{sat}) = -1.69 \times 10^{-4} T^4 + 3.85 \times 10^{-7} T^3 - 3.39 \times 10^{-4} T^2 + 0.143 T - 20.92 \quad (3.4)$$

If the water amount in anode compartment exceeds the maximum allowable vapor amount, liquid water will form as given in Equation (3.5).

$$m_{H_2O,liq,anode} = m_{H_2O,an} - m_{vapor,max.anode} \quad (3.5)$$

The total pressure in anode volume stated in Equation (3.6) is the addition of hydrogen and vapor partial pressures as given in Equation (3.7) and (3.8) respectively.

$$P_{anode} = P_{H_2,anode} + P_{vapor,anode} \quad (3.6)$$

$$P_{H_2,anode} = \frac{m_{H_2,anode} RT_{stack}}{V_{anode} M_{H_2}} \quad (3.7)$$

$$P_{vapor,anode} = \frac{m_{vapor,anode} RT_{stack}}{V_{anode} M_{H_2O}} \quad (3.8)$$

Anode relative humidity,  $\phi$ , is expressed by Equation (3.9) where saturation pressure is a temperature dependent function estimated in Equation (3.4) [18].

$$\phi_{anode} = \frac{P_{vapor,anode}}{P_{sat}(T_{stack})} \quad (3.9)$$

With known anode inlet humidity, temperature and pressure, the hydrogen and vapor inlet flow rates can be calculated by the Equations (3.10)-(3.14).

$$P_{vapor,anodein} = \phi_{anodein} P_{sat}(T_{anodein}) \quad (3.10)$$

$$P_{H_2,anodein} = P_{anodein} - P_{vapor,anodein} \quad (3.11)$$

$$w_{anodein} = \frac{M_{H_2O}}{M_{H_2}} \times \frac{P_{vapor,anodein}}{P_{anodein}} \quad (3.12)$$

where  $w_{anodein}$  is the humidity ratio (kg/kg).

$$W_{H_2,anodein} = \frac{1}{1 + w_{anodein}} \times W_{anodein} \quad (3.13)$$

$$W_{vapor,anodein} = W_{anodein} - W_{H_2,anodein} \quad (3.14)$$

The amount of hydrogen consumed in the reaction,  $W_{H2reacted}$  (kg/s), is given by Faraday's law as in Equation (3.15).  $I$  (A) is the current,  $F$  is the Faraday's constant 96485 C,  $n$  is the number of cells in the stack.

$$W_{H2reacted} = \frac{n \cdot I}{2F} \times M_{H2} \quad (3.15)$$

Hydrogen and vapor amount in the anode outlet stream can be calculated by the Equations (3.16)-(3.18). There would be no exit flows in dead-end operation normally, so hydrogen and vapor outlet terms would only appear in purge conditions.

$$w_{anodeout} = \frac{M_{H2O}}{M_{H2}} \times \frac{P_{vapor,anode}}{P_{H2,anode}} \quad (3.16)$$

$$W_{H2,anodeout} = \frac{1}{1 + w_{anodeout}} \times W_{anodeout} \quad (3.17)$$

$$W_{vapor,anodeout} = W_{anodeout} - W_{H2,anodeout} \quad (3.18)$$

### 3.2.1.2. Cathode Flow Model

Cathode flow model is related with the air flow in the cathode volume and the governing electrochemical reactions. For this study cathode compartment is selected to be operating at through flow mode; the air depleted in terms of oxygen would pass through outlet manifold. Cathode flow model strategy is similar to anode flow model, the mass balances for cathode species are completed with ideal gas law and Faraday's law. Oxygen, nitrogen and water mass balances are given in Equations (3.19)-(3.21). The water transfer rate through the membrane involved in Equation (3.21) is assumed to be at pseudo-steady state since it is considered to be a small value.

$$\frac{dm_{O2,ca}}{dt} = W_{O2,cathodein} - W_{O2,cathodeout} - W_{O2,reacted} \quad (3.19)$$

$$\frac{dm_{N2,ca}}{dt} = W_{N2,cathodein} - W_{N2,cathodeout} \quad (3.20)$$

$$\begin{aligned} \frac{dm_{H2O,cathode}}{dt} = & W_{vapor,cathodein} - W_{vapor,cathodeout} + W_{vapor,cathodegen} \\ & + W_{vapor,membrane} - W_{H2Oliq,cathodeout} \end{aligned} \quad (3.21)$$

Faraday's law gives the amounts of oxygen reacted and water produced by the electrochemical reactions involving in the system in Equation (3.22) and Equation (3.23) respectively.

$$W_{O2reacted} = \frac{n \cdot I}{4F} \times M_{O2} \quad (3.22)$$

$$W_{H_2O, cathode generated} = \frac{n \cdot I}{2 F} \times M_{H_2O} \quad (3.23)$$

The partial pressures of oxygen, nitrogen and vapor in the cathode volume can be stated by Equation (3.24) where i=oxygen, nitrogen and vapor.

$$P_{i,ca} = \frac{m_{i,ca} R T_{stack}}{V_{cathode} M_i} \quad (3.24)$$

Cathode outlet pressure is assumed to be equal to the cathode pressure due to the uniformity assumption, which is equal to the sum of the partial pressures of the species involving in cathode volume as stated in Equation (3.25).

$$P_{ca} = P_{ca,out} = \sum P_{i,ca} \quad (3.25)$$

Cathode exit flow rates for oxygen, nitrogen and vapor are expressed with a simple orifice equation as in Equation (3.26) where  $k_{ca,out}$  is the orifice constant,  $P_{ca}$  and  $P_{rm}$  are the cathode and return manifold pressures respectively.

$$W_{ca,out} = k_{ca,out} (P_{ca} - P_{rm}) \quad (3.26)$$

Cathode inlet and outlet mass flows can be calculated by a similar way with the equations provided in anode flow model.

### 3.2.1.3. Stack Voltage Model

Stack voltage model estimates the losses encountered in polarization curve and calculates the stack voltage according to the stack current. Different models are available in literature to calculate voltage of a cell according to the current, temperature, humidity and reactant partial pressures [3, 18, 44]. The theoretical open circuit voltage (OCV) of a fuel cell is 1.23 V but in practice lower OCV values are observed. When a load is put into use the voltage further drops from OCV values due to the activation losses ( $v_{act}$ ), ohmic losses ( $v_{ohm}$ ) and concentration losses ( $v_{conc}$ ) as given in Equation (3.27) and (3.28), where E is OCV value and  $i$  ( $A/cm^2$ ) is the stack current density given as the ratio of stack current ( $I_{st}$ ) to fuel cell active area ( $A_{fc}$ ) as in Equation (3.29) [18].

$$v_{singlecell} = E - v_{act} - v_{ohm} - v_{conc} \quad (3.27)$$

$$v_{singlecell} = E - [v_0 + v_a(1 - e^{-c_1 i}) - [i R_{ohm}] - [i \left( c_2 \frac{i}{i_{max}} \right)^{c_3}] ] \quad (3.28)$$

$$i = \frac{I_{st}}{A_{fc}} \quad (3.29)$$

The open circuit potential is expressed as a function of stack temperature, hydrogen and oxygen partial pressures in the system as in Equation (3.30) [18].

$$E = 1.229 - 8.5 \times 10^{-4}(T_{fc} - 298.15) + 4.308 \times 10^{-5}T_{fc} \left[ \ln \frac{P_{H_2}}{1.01325} - \frac{1}{2} \ln \frac{P_{O_2}}{1.01325} \right] \quad (3.30)$$

Activation losses are related with the sluggish reaction kinetics. A voltage difference is required for the electrochemical reaction to proceed and it is stated that the activation losses are dominant in cathode side of PEM fuel cells [44]. The activation loss is estimated with the Equation (3.31), where  $c_1$  is a constant, and  $v_o$  and  $v_a$  are given in Equations (3.32) and (3.33) [18].

$$v_{act} = v_o + v_a(1 - e^{-c_1 i}) \quad (3.31)$$

$$v_o = 1.229 - 8.5 \times 10^{-4}(T_{fc} - 298.15) + 4.308 \times 10^{-5}T_{fc} \left[ \ln \frac{P_{ca} - P_{sat}}{1.01325} - \frac{1}{2} \ln \frac{0.1173(P_{ca} - P_{sat})}{1.01325} \right] \quad (3.32)$$

$$v_a = (-1.618 \times 10^{-5}T_{fc} + 1.618 \times 10^{-2}) \left( \frac{P_{O_2}}{0.1173} + P_{sat} \right)^2 + (1.8 \times 10^{-4}T_{fc} - 0.166) \left( \frac{P_{O_2}}{0.1173} + P_{sat} \right) + (-5.8 \times 10^{-4}T_{fc} + 0.5736) \quad (3.33)$$

Ohmic losses are observed due to the flow of protons through the membrane, electrons through the electrically conductive components of the cell and external circuit, and contact resistances of materials that effects conduction within the system. These losses can be shown by Ohm's law as in Equation (3.34) [3].

$$v_{ohm} = iR_{ohm} \quad (3.34)$$

Where  $R_{ohm}$  ( $\Omega\text{cm}^2$ ) is cell's total internal resistance that captures ionic, electronic and contact resistances given in Equation (3.35) as a function of membrane thickness  $t_m$  and membrane conductivity  $\sigma_m$ [45].

$$R_{ohm} = \frac{t_m}{\sigma_m} \quad (3.35)$$

Membrane ionic conductivity is determined as fuel cell temperature ( $T_{fc}$ ) and membrane water content ( $\lambda_m$ ) as in Equation (3.36)[46].

$$\sigma_m = (0.005139\lambda_m - 0.00326) \exp \left( 350 \left( \frac{1}{303} - \frac{1}{T_{fc}} \right) \right) \quad (3.36)$$

Concentration losses occur in case of the drop of the reactant concentrations at the reaction sites especially at higher current densities. Equation (3.37) gives the concentration polarization where  $i_{max}$  and  $c_3$  are constants to be determined experimentally, and  $c_2$  is calculated by Equation (3.38) [18].

$$v_{conc} = i \left( c_2 \frac{i}{i_{max}} \right)^{c_3} \quad (3.37)$$

$$c_2 = \begin{cases} (7.16 \times 10^{-4}T_{fc} - 0.622) \left( \frac{P_{O_2}}{0.1173} + P_{sat} \right) + (-1.45 \times 10^{-3}T_{fc} + 1.68) \\ \quad \text{for } \left( \frac{P_{O_2}}{0.1173} + P_{sat} \right) < 2atm \\ (8.66 \times 10^{-5}T_{fc} - 0.068) \left( \frac{P_{O_2}}{0.1173} + P_{sat} \right) + (-1.6 \times 10^{-4}T_{fc} + 0.54) \\ \quad \text{for } \left( \frac{P_{O_2}}{0.1173} + P_{sat} \right) \geq 2atm \end{cases} \quad (3.38)$$

By assuming all the cells are identical, stack voltage would be simply the multiplication of single cell voltage with number of cells as in Equation (3.39).

$$v_{stack} = n_{cell}v_{singlecell} \quad (3.39)$$

### 3.2.1.4. Membrane Hydration Model

Membrane hydration model estimates the water transfer through the membrane by the mechanisms of electro osmotic drag and diffusion. For membrane hydration model it is assumed that the water transfer is uniform over the fuel cell active area and the water concentration changes linearly within the membrane thickness. Water flux  $N_{v,membrane}$  (mol/ (s.cm<sup>2</sup>)) through a membrane is given in Equations (3.40)-(3.41) and the overall water transfer  $W_{v,membrane}$ (kg/s) for the stack is given as in Equation (3.42) [18].

$$N_{v,membrane} = N_{v,osmotic} - N_{v,diffusion} \quad (3.40)$$

$$N_{v,membrane} = n_d \frac{i}{F} - D_w \frac{C_{v,ca} - C_{v,an}}{t_m} \quad (3.41)$$

$$W_{v,membrane} = N_{v,membrane} \times M_v \times A_{fc} \times n_{cell} \quad (3.42)$$

During proton conduction through the membrane electrons are also dragged from anode to cathode. Proton transfer so the water transfer strongly depends on membrane water content  $\lambda_m$  and the current drawn from the stack. Water transfer by the electro-osmotic drag is given in Equation (3.43) , where  $n_d$  is the electroosmotic drag coefficient expressed as a function membrane water content in Equation (3.44),  $i$  is the current density (A/cm<sup>2</sup>) and  $F$  is Faradays constant [18],[47].

$$N_{v,osmotic} = n_d \frac{i}{F} \quad (3.43)$$

$$n_d = 0.0029\lambda_m^2 + 0.05\lambda_m - 3.4 \times 10^{-19} \quad (3.44)$$

Water content  $\lambda_i$ , can be related to the water activities ( $a_i$ ) as in Equation (3.45) where  $i$  could either represent anode, cathode or membrane [47]

$$\lambda_i = \begin{cases} 0.043 + 17.81a_i - 39.85a_i^2 + 36.0a_i^3, & 0 < a_i \leq 1 \\ 14 + 1.4(a_i - 1), & 1 < a_i \leq 3 \end{cases} \quad (3.45)$$

Membrane water activity can be calculated as the arithmetic mean of anode side and cathode side water activities as in Equation (3.46) where activities ( $a_i$ ) are defined as the ratio of vapor pressure  $P_{v,i}$  and saturation pressure  $P_{sat,i}$  by Equation (3.47) [18].

$$a_m = \frac{a_{an} + a_{ca}}{2} \quad (3.46)$$

$$a_i = \frac{P_{v,i}}{P_{sat,i}} \quad (3.47)$$

Water generation due to chemical reactions and electro-osmotic drag makes a concentration gradient between anode and cathode. The diffused water amount  $N_{v,diffusion}$  (mol/ (cm<sup>2</sup>.s)) can be expressed as in Equation (3.48) where  $D_w$  is the diffusion coefficient (cm<sup>2</sup>/s),  $C_{v,i}$  is the concentration of anodic and cathodic sides (mol/cm<sup>3</sup>) and  $t_m$  is the membrane thickness.

$$N_{v,diffusion} = D_w \frac{C_{v,ca} - C_{v,an}}{t_m} \quad (3.48)$$

Water concentrations can be stated as Equations (3.49) and (3.50) for anode and cathode compartments respectively, where  $\rho_{m,dry}$  (kg/cm<sup>3</sup>) is the membrane dry density,  $m_{m,dry}$  (kg/mol) is membrane equivalent weight and  $\lambda_i$  is the water content given in Equation (3.45) [18].

$$C_{v,an} = \frac{\rho_{m,dry}}{m_{m,dry}} \lambda_{an} \quad (3.49)$$

$$C_{v,ca} = \frac{\rho_{m,dry}}{m_{m,dry}} \lambda_{ca} \quad (3.50)$$

The diffusion coefficient is dependent on stack temperature  $T_{fc}$  (K) and membrane water content as given in Equations (3.51) and (3.52) [47].

$$D_w = D_\lambda \exp\left(2416 \left(\frac{1}{303} - \frac{1}{T_{fc}}\right)\right) \quad (3.51)$$

$$D_\lambda = \begin{cases} 10^{-6} & , \lambda_m < 2 \\ 10^{-6}(1 + 2(\lambda_m - 2)) & , 2 \leq \lambda_m \leq 3 \\ 10^{-6}(3 - 1.67(\lambda_m - 3)) & , 3 < \lambda_m < 4.5 \\ 1.25 \times 10^{-6} & , \lambda_m \geq 4.5 \end{cases} \quad (3.52)$$

### 3.2.2. Cooling system

While the electricity is produced by the fuel cell stack there will be heat generation caused by irreversibilities. To keep the system temperature at a desired set point a cooling system should be operated. Cooling can be achieved by using different cooling equipment integrated to the system. The cooling system considered in this thesis consists of a cooling water pump and a fan connected to a radiator and the related model is derived accordingly. The cooling water passes through the water channels machined on bipolar plates of stack and pumped back to the radiator as seen on Figure 3.1.

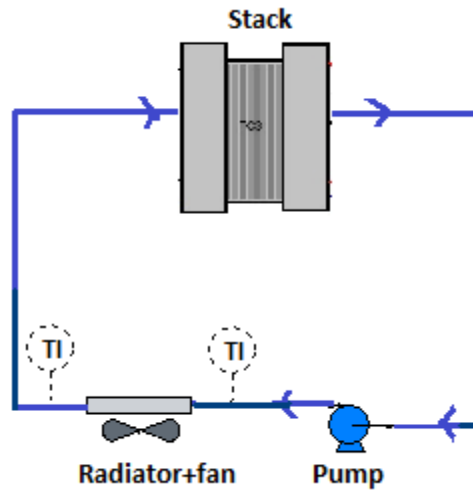


Figure 3.1 Cooling system integration with stack.

To derive cooling system modeling equations the system is defined as the contents of the radiator. The mass balance for cooling water can be written as in Equation (3.53) where  $\dot{m}_{in} \left( \frac{kg}{s} \right)$  is the hot water of stack that is entering to radiator,  $\dot{m}_{out} \left( \frac{kg}{s} \right)$  is the cooled water in radiator and  $m_r$  (kg) is the water staying in radiator volume.

$$\dot{m}_{in} - \dot{m}_{out} = \frac{dm_r}{dt} \quad (3.53)$$

The radiator will be filled with water during installation therefore  $\dot{m}_{in}$  will be equal to  $\dot{m}_{out}$  at any time as in Equation (3.54). Therefore the mass accumulation terms would diminish as in Equation (3.55).

$$\dot{m}_{in} = \dot{m}_{out} = \dot{m} \quad (3.54)$$

$$\frac{dm_r}{dt} = 0 \quad (3.55)$$

Water flow rate could be determined by the pump characteristics and voltage as in Equation (3.56).

$$\dot{m} = \dot{m}(V_{pump}) \quad (3.56)$$

The general energy balance for the radiator could be given as in Equation (3.57) by assuming constant physical properties and neglecting the kinetic and potential energy terms.

$$Energy_{in} - Energy_{out} = Energy_{accumulation} \quad (3.57)$$

Inlet energy term is formed by the hot water leaving the stack and entering to the radiator while the energy removal term is formed by the cold water leaving the stack and heat removed by from the radiator surface to surroundings as given in Equations (3.58) and (3.59) respectively. Energy accumulation term is given in Equation (3.60) for the contents of the radiator.

$$Energy_{in} = \dot{m}_{in} \times \hat{H}_{in} = \dot{m}_{in} \times C_{p_{water}} \times T_{in} \quad (3.58)$$

$$Energy_{out} = \dot{m}_{out} \times \hat{H}_{out} + Q_{removed\ by\ air} = (\dot{m}_{out} \times C_{p_{water}} \times T_{out}) + (u \times A \times \Delta T_{lm}) \quad (3.59)$$

$$\begin{aligned} Energy_{accumulation} &= \frac{dU}{dt} = V_{rad} \times \rho \times C_{p_{water}} \times \frac{d(T - T_{ref})}{dt} \\ &= V_{rad} \times \rho \times C_{p_{water}} \times \frac{dT}{dt} \end{aligned} \quad (3.60)$$

where  $C_{p_{water}}$  (J/ (kg. K)) is the heat capacity of water,  $T$  (K) is the temperature,  $u$  (W/(m<sup>2</sup>.K)) is the overall heat transfer coefficient,  $A$  (m<sup>2</sup>) is the heat transfer area of the radiator,  $\rho$  (kg/m<sup>3</sup>) is the density of water.

Equation (3.58) could be rewritten as Equation (3.61) by substituting Equations (3.54)-(3.60).

$$\dot{m}(V_{pump}) \cdot C_{p_{water}} \cdot (T_{in} - T_{out}) - (u \times A \times \Delta T_{lm}) = V_{rad} \cdot \rho \cdot C_{p_{water}} \cdot \frac{dT}{dt} \quad (3.61)$$

It is assumed that the temperature of the system is the average of radiator inlet and outlet temperatures as stated by Equation (3.62).

$$\frac{dT}{dt} = \frac{1}{2} \left( \frac{dT_{in}}{dt} + \frac{dT_{out}}{dt} \right) \quad (3.62)$$

The log-mean temperature is given in Equation (3.63) where  $T_{\infty}$  (K) is the ambient air temperature assumed to be constant [48].

$$\Delta T_{lm} = \frac{(T_{\infty} - T_{out}) - (T_{\infty} - T_{in})}{\ln\left(\frac{(T_{\infty} - T_{out})}{(T_{\infty} - T_{in})}\right)} \quad (3.63)$$

Overall heat transfer coefficient would depend on the water flow rate and air flow rate that correspond to pump and fan voltages therefore  $u$  can be estimated as a function depending on fan and pump voltages as given in Equation (3.64).

$$u = u(V_{fan}, V_{pump}) \quad (3.64)$$

By combining the equations (3.61)-(3.64), the general energy balance takes the form represented in Equation (3.65).

$$\begin{aligned} \dot{m} \times C_{p_{water}} \times (T_{in} - T_{out}) - \left( u(V_{fan}, V_{pump}) \times A \times \frac{(T_{\infty} - T_{out}) - (T_{\infty} - T_{in})}{\ln\left(\frac{(T_{\infty} - T_{out})}{(T_{\infty} - T_{in})}\right)} \right) \\ = V_{rad} \times \rho \times C_{p_{water}} \times \frac{1}{2} \left( \frac{dT_{in}}{dt} + \frac{dT_{out}}{dt} \right) \end{aligned} \quad (3.65)$$

The integration with the stack and cooling system is given by the Equation (3.66) as;

$$\frac{dT_{st}}{dt} = \dot{Q}_{generation} - \dot{Q}_{removed} \quad (3.66)$$

While the stack efficiency is proportional to the stack power, heat generation is proportional to the lack of efficiency. So heat generation can be expressed as in Equation (3.67) while  $\eta$  is the efficiency and  $P_{st}$  (W) is the stack power.

$$\dot{Q}_{generation} = P_{st} \frac{(1 - \eta)}{\eta} \quad (3.67)$$

$$\eta = \frac{v_{single\ cell}}{1.23} \quad (3.68)$$

### 3.2.3. Humidifier Model

In order to supply humidified air to the system different types of humidifiers can be used. [21-24]. For this study a membrane type humidifier with a shell and tube geometry is supposed to humidify the air entering to the stack. To increase system efficiency the cathode exhaust stream is used as the humidification source for the dry gas of compressor output. A representative figure for the humidifier used in the fuel cell system is given in Figure 3.2.

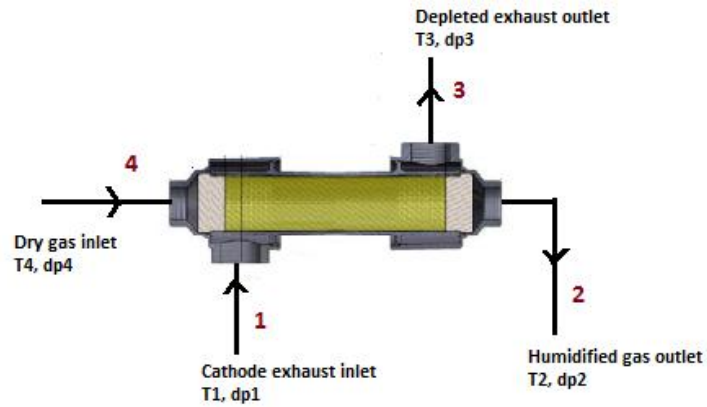


Figure 3.2 Schematic of the humidifier.

The arrangement of the humidifier is similar to shell and tube heat exchangers. The dry gas passes through the bundle of Nafion tubes (stream-4), while the cathode exhaust gas (stream-1) surrounds these Nafion tubes by providing both moisture and heat. The shell and tube structure and the cross section of the Nafion tubes are given in Figure 3.3 and Figure 3.4 respectively (<http://www.authorstream.com/Presentation/Arley33-37254-Fuel-Cell-Humidification-presentation-Using-Nafion-Moisture-Exchange-Devices-as-Education-ppt-powerpoint/> accessed at 04.03.2013).

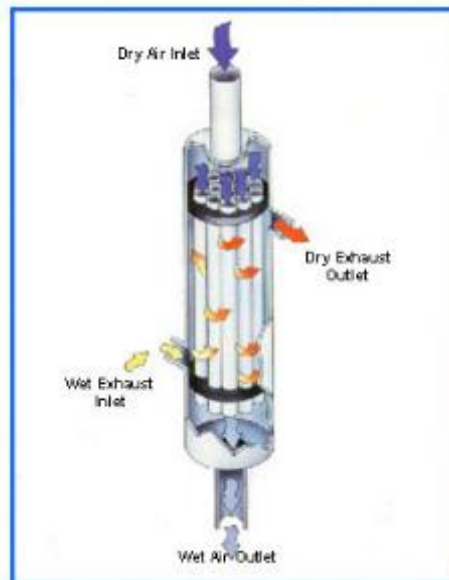


Figure 3.3 The structure of the humidifier



Figure 3.4 Cross section of the Nafion tubes in the humidifier

The assumptions made for the humidifier modeling are listed as;

- Ideal gas law is applicable.
- There is no liquid water in the system and no condensation occurs. It is assumed the stack exhaust does not contain any liquid water and the temperature change in humidifier compensated by the vapor transfer that prevents condensation.
- There is no heat transfer to the surroundings of the humidifier due to insulation. It is assumed that the stack exhaust does not exchange heat with the environment; all available heat is shared within the humidifier.
- Heat capacities are constant. The changing temperature and pressure effects on heat capacities are ignored.
- The kinetic and potential energy terms in the energy balance are neglected.
- Tube side is considered as a one single tube whose area and volume is equal to the number of tubes times one small tube as shown in Figure 3.5. Bundle of small tubes lumped into a larger tube to observe the overall humidifier performance.
- The air permeation through the Nafion® membrane is ignorable and it is assumed that only water can permeate through the membrane, dry air cannot pass from shell side to tube side or vice versa.

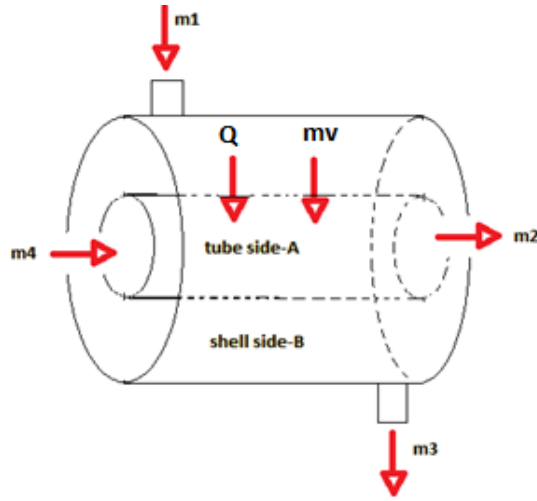


Figure 3.5 Defined systems for modeling.

The model is developed over two control volumes; the bundle of Nafion tubes and shell side as in Figure 3.5. Wet gas coming from the stack ( $\dot{m}_1(kg/s)$ ), passes through the shell volume while the dry gas ( $\dot{m}_4(kg/s)$ ) passes through Nafion tubes counter currently. There will be mass transfer due to concentration difference in shell and tube volumes, also heat transfer due to temperature difference. The mass balances and energy balance equations are developed over control volumes A and B for the dry air and vapor.

General mass balance equation is given in Equation (3.69), where  $i$  represents dry air and vapor. Mass balances for the tube side and shell side are tabulated in Table 3.2 by the Equations (3.69)-(3.73)

$$mass_{in,i} - mass_{out,i} = mass_{accumulation,i} \quad (3.69)$$

Table 3. 2 Mass Balances for Humidifier Model

Control volume	Species	Mass Balance
For tube side(A)	Vapor	$\dot{m}_{4,vapor} + \dot{m}_v - \dot{m}_{2,vapor} = \frac{dm_{A,vapor}}{dt}$ (3.70)
	Dry Air	$\dot{m}_{4,dry\ air} - \dot{m}_{2,dry\ air} = \frac{dm_{A,dry\ air}}{dt}$ (3.71)
For shell side(B)	Vapor	$\dot{m}_{1,vapor} - \dot{m}_v - \dot{m}_{3,vapor} = \frac{dm_{B,vapor}}{dt}$ (3.72)
	Dry Air	$\dot{m}_{1,dry\ air} - \dot{m}_{3,dry\ air} = \frac{dm_{B,dry\ air}}{dt}$ (3.73)

Energy balances for the two control volumes, shell side and tube side are written according to the general energy balance as given in Equation (3.74). Tube and shell side energy balances are tabulated in Table 3.3 by the Equations (3.75)-(3.80), where  $\dot{Q}$  (W) is the heat transfer from shell side to tube side,  $\widehat{H}_i$  (J/ kg) is the enthalpy of the related species,  $U$  (J) is the internal energy accumulated in the control volume,  $C_p$  (J/ (kg.K)) is the constant pressure heat capacity and  $C_v$  (J/ (kg.K)) is the constant volume heat capacity.

$$\text{energyin} - \text{energyout} = \text{energyaccumulation} \quad (3.74)$$

Table 3.3 Energy Balances for Humidifier Model

Control volume	Energy Balance
Tube side(A)	$\dot{m}_4 \widehat{H}_4 + \dot{m}_v \widehat{H}_v + \dot{Q} - \dot{m}_2 \widehat{H}_2 = \frac{dU_A}{dt}$ (3.75)
	$\dot{m}_4 C_{p4} T_4 + \dot{m}_v C_{pv} T_v + \dot{Q} - \dot{m}_2 C_{p2} T_2 = m_A C_{vA} \frac{dT_A}{dt} + C_{vA} T_A \frac{dm_A}{dt}$ (3.76)
	Where $T_A = (T_4 + T_2)/2$ (3.77)
Shell side(B)	$\dot{m}_1 \widehat{H}_1 + \dot{m}_v \widehat{H}_v - \dot{Q} - \dot{m}_3 \widehat{H}_3 = \frac{dU_B}{dt}$ (3.78)
	$\dot{m}_1 C_{p1} T_1 - \dot{m}_v C_{pv} T_v - \dot{Q} - \dot{m}_3 C_{p3} T_3 = m_B C_{vB} \frac{dT_B}{dt} + C_{vB} T_B \frac{dm_B}{dt}$ (3.79)
	Where $T_B = (T_1 + T_3)/2$ (3.80)

Heat transfer between the control volumes can be expressed as Equation (3.81);

$$\dot{Q} = U.A.\Delta T_{lm} \quad (3.81)$$

Where  $U$  is the overall heat transfer coefficient (W/(m<sup>2</sup>.K)),  $A$  is the area between the shell and tube sides that heat exchange occurs and  $\Delta T_{lm}$  is the counter-current log mean temperature as given in Equation (3.82).

$$\Delta T_{lm} = ((T_1 - T_2) - (T_3 - T_4)) / \log((T_1 - T_2)/(T_3 - T_4)) \quad (3.82)$$

For a cylindrical geometry the  $U.A$  term can be expressed as in Equation (3.83) where  $h_A$  and  $h_B$  are the heat transfer coefficients of the corresponding control volumes (W/ (m<sup>2</sup>.K)).  $A_{in}$  and  $A_{out}$  are the inlet and outlet heat transfer areas respectively (m<sup>2</sup>),  $L$  is the humidifier

active length (m),  $k_{mem}$  is the membrane thermal conductivity ( $Wm^{-1}K^{-1}$ ),  $D_{in}$  and  $D_{out}$  are the inlet and outlet diameters of the tube (m).

$$\frac{1}{U.A} = \frac{1}{h_A \times A_{in}} + \frac{\ln\left(\frac{D_{out}}{D_{in}}\right)}{2\pi L k_{mem}} + \frac{1}{h_B \times A_{out}} \quad (3.83)$$

Heat transfer coefficients are expressed as in Equations (3.84) where Nu is the Nusselt number,  $k$  ( $Wm^{-1}K^{-1}$ ) is the thermal conductivity of air, and  $D$  (m) is the diameter, and  $i$  denotes tube and shell sides.

$$h_i = Nu_i \cdot \frac{k_i}{D_i} \quad (3.84)$$

The Nusselt number for internal flow inside tube side volume can be stated as in Equation (3.85) whereas the Nusselt number for the shell side is shown in Equation (3.86) [21]. The Reynolds numbers are given in Equations (3.87) and (3.88) where  $n_{tube}$  is the number of small tubes involved in the humidifier.

$$Nu_A = 0.023 Re^{0.8} Pr^{0.4} \quad (3.85)$$

$$Nu_B = x Re^y Pr^{1/3} \quad (3.86)$$

$$Re_A = \frac{\dot{m}_a}{\frac{\pi \times D_A \times \mu_A}{n_{tube}}} \quad (3.87)$$

$$Re_B = \dot{m}_1 / (\pi \times D_B \times \mu_B) / n_{tube} \quad (3.88)$$

$x$  and  $y$  values for Equation (3.88) are depend on the shell side Reynolds number which are given in Table 3.4.

Table 3.4 Nusselt number parameters for shell side [48].

Range of Reynolds number	x	y
$Re_B \leq 4$	0.989	0.330
$4 < Re_B \leq 40$	0.911	0.388
$40 < Re_B \leq 4000$	0.638	0.466
$4000 < Re_B \leq 40000$	0.193	0.618
$40000 < Re_B$	0.027	0.805

Water transfer  $\dot{m}v\left(\frac{kg}{s}\right)$  between the shell side and tube side occurs due to the concentration gradient at membrane boundaries for these control volumes as given in Equations (3.89) and (3.90) [21]

$$\dot{m}v = W_{diff,mem,B} - W_{diff,mem,A} \quad (3.89)$$

$$W_{diff,mem,i} = \frac{(C_i - C_{middle}) \times A \times D_w \times M_w}{0.5 t_{mem}} \quad (3.90)$$

where  $W_{diff,mem,i}$  ( $\frac{kg}{s}$ ) is the water transfer for the control volume (shell side or tube side) to the middle of the membrane,  $C_i$  ( $\text{mol/m}^3$ ) is the vapor concentration of the control volume,  $C_{middle}$  ( $\text{mol/m}^3$ ) is the vapor concentration at middle of the membrane.  $A$  ( $\text{cm}^2$ ) is the overall mass transfer area,  $D_w$  ( $\text{cm}^2/\text{s}$ ) is the diffusion coefficient,  $M_w$  ( $\text{kg/mol}$ ) molecular weight of water,  $t_{mem}$  ( $\text{cm}$ ) is the membrane thickness.

Vapor concentration at the middle of the membrane  $C_{middle}$  ( $\text{mol/m}^3$ ), is related with the membrane water content as given in Equation (3.91)-(3.93) [21]

$$C_{middle} = \frac{\rho_{dry,mem}}{M_{mem}} \cdot \lambda_{mem} \quad (3.91)$$

$$\lambda_{mem} = \frac{C_{H2O,mass}/M_{H2O}}{\frac{\rho_{dry,mem}}{M_{mem}} - 0.0126 \cdot C_{H2O,mass}/M_{H2O}} \quad (3.92)$$

$$C_{H2O,mass} = \int \frac{\dot{m}v}{A \times t_{mem}} dt \quad (3.93)$$

where  $\rho_{m,dry}$  ( $\text{kg/cm}^3$ ) is the membrane dry density,  $M_{mem}$  ( $\text{kg/mol}$ ) is membrane equivalent weight and  $\lambda_{mem}$  is the membrane water content,  $C_{H2O,mass}$  ( $\text{kg/m}^3$ ) is the mass concentration of the membrane.

Membrane boundary concentrations can be expressed as in Equation (3.94). For the diffusion coefficient calculation Equations (3.51)-(3.52) and (3.45)-(3.46) are applicable.

$$C_i = \frac{\rho_{dry,mem}}{M_{mem}} \cdot \lambda_i \quad (3.94)$$

### 3.2.4. Inlet and Outlet Manifolds

There will be inlet and outlet manifolds connecting the humidifier and stack. To avoid any heat losses in the system these manifolds will be insulated. So the manifolds can be assumed to be kept at constant temperature. Equation (3.95) gives the mass balance for a manifold where  $i$  represents inlet and outlet manifolds.

$$\frac{dP_i}{dt} = \frac{R_a T}{V_i} (m_{air,in} - m_{air,out}) \quad (3.95)$$

The pressure drops in the tube shaped manifolds are calculated by Equation given in Equation (3.96), where  $L$  ( $\text{m}$ ) is the tube length;  $D$  ( $\text{m}$ ) is the tube diameter,  $\rho$  ( $\text{kg/m}^3$ ) is the

fluid density,  $V$  (m/s) is the mean velocity of the flow and  $f$  is the friction factor defined in Equation (3.97) [49].

$$\Delta P_i = f \cdot \frac{2L\rho V^2}{D} \quad (3.96)$$

$$f = 0.0014 + \frac{0.125}{Re^{0.32}} \quad (3.97)$$

### 3.2.5. Compressor Model

Air supply to the fuel cell stack would be achieved by a compressor. The compressor model should provide the compressed air flow rate according to a given voltage. Pukrushpan et. al [18] developed a compressor model consisting of compressor map and, compressor and motor inertia. The compressor map gives static information reflecting the air flow rate according to the desired pressure, motor speed and power. Compressor and motor inertia gives the compressor speed which will be used in compressor map to find flow rate. The dynamics related to compressor speed  $\omega_{cp}$ (rad/sec) is given in Equation (3.98) where  $J_{cp}$  ( $\text{kg.m}^2$ ) is the combined inertia for the motor and compressor,  $\tau_{cm}$  (N.m) is the torque input to the compressor motor,  $\tau_{cp}$  (N.m) is the torque need by the compressor [18].

$$J_{cp} \frac{d\omega_{cp}}{dt} = \tau_{cm} - \tau_{cp} \quad (3.98)$$

Motor input torque is given in Equation (3.99) where  $k_t$ ,  $R_{cm}$ ,  $k_v$  are motor constants and  $\eta_{cm}$  is the mechanical efficiency of the motor [18].

$$\tau_{cm} = \eta_{cm} \frac{k_t}{R_{cm}} (v_{cm} - k_v \omega_{cp}) \quad (3.99)$$

Torque required by the compressor is given in Equation (3.100) as;

$$\tau_{cp} = \frac{C_p}{\omega_{cp}} \frac{T_{atm}}{\eta_{cp}} \left[ \left( \frac{P_{sm}}{P_{atm}} \right)^{\frac{\gamma-1}{\gamma}} - 1 \right] W_{cp} \quad (3.100)$$

Where  $C_p$  is the specific heat capacity of air with a value of  $1004 \text{ J.kg}^{-1}.\text{K}^{-1}$ ,  $\gamma$  is the ratio of specific heats of air as 1.4,  $P_{sm}$  and  $P_{atm}$  are the pressures of supply manifold (compressor outlet) and atmospheric pressures respectively,  $T_{atm}$  is taken as the atmospheric air temperature at  $25^\circ\text{C}$ , and  $W_{cp}$  is the the compressor air mass flow rate (kg/sec) which should be determined by the compressor map [18].



## CHAPTER 4

### SYSTEM DESIGN AND IMPLEMENTATION

Fuel cell system designs can differ by the operational selections and the usage of auxiliaries. In this chapter the fuel cell system which is the subject of modeling and control studies is described in terms of the process design and auxiliary equipment. The fuel cell system subject to this study consists of the stack and auxiliaries supplied by the project 'Development of a 3 kW fuel cell system' given by UNIDO-ICHET. The stack which has 44 cells is shown on Figure 4.1.

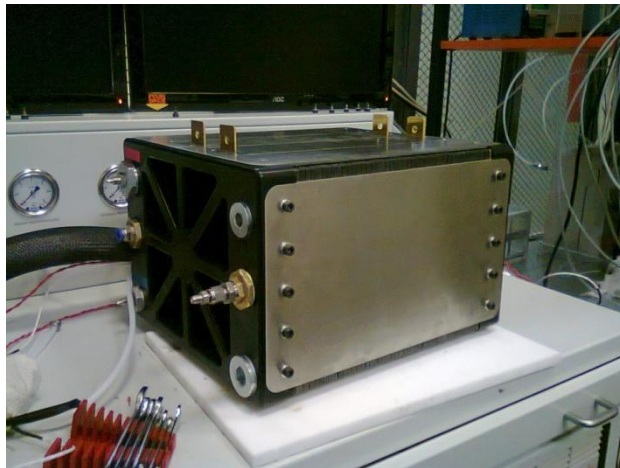


Figure 4.1 Fuel Cell Stack With 44 Cells.

#### 4.1. Prototype Design and Selections

The fuel cell system studied in this thesis has a design basis of net 3 kW that determines the stack properties such as number of cells and active fuel cell area. System selections are done to maximize the delivered power from the fuel cell stack, by minimizing the parasitic losses and fuel usage. Figure 4.2 represents the process flow chart with the main equipment involved in the system. The anode side is selected to be operating at dead-end mode to minimize fuel consumption. Anode outlet would be opened just in purge conditions. For cathode flow, compressed air will be humidified in a membrane type humidifier by using the exhaust air of the stack. Heat removal will be achieved by a closed loop water cooling system consisting of a pump, radiator and a fan. Cooling water will pass through the channels involved in bipolar plates by removing heat from the stack and turn back to radiator by the pump.

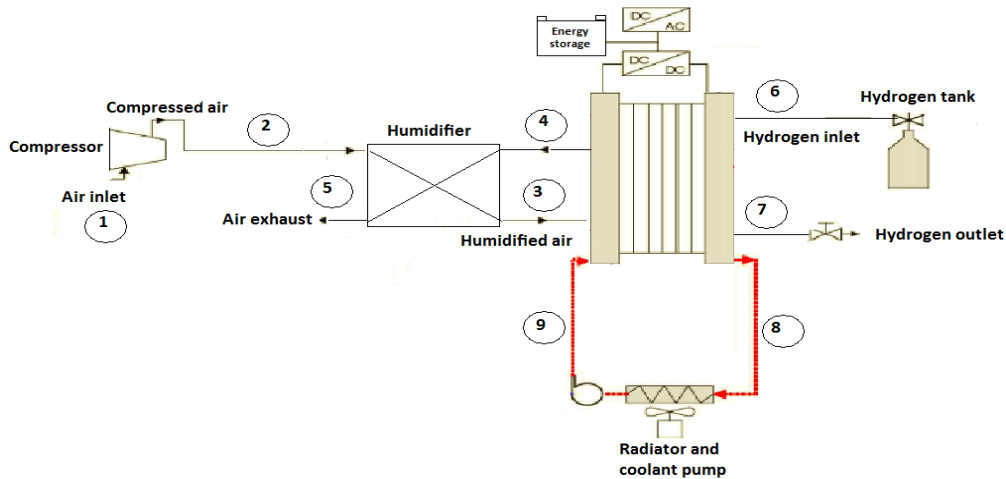


Figure 4.2 Representation of the Fuel Cell System

In order to have a net power of 3 kW, the calculations related with stack sizing and desired gas amounts are developed for a 5.3 kW fuel cell. Table 4.1 gives the fuel cell system design information in terms of operating conditions and selections.

Table 4.1 Fuel Cell System Design Specifications

	Value	Unit
Design power	5.3	kW
Design current density at 0.6 V	0.5	(mA/cm <sup>2</sup> )
Cathode operating pressure	1.2	atm
Anode operating pressure	1.2	atm
Operating temperature	338.0	K
Anode gas inlet temperature	298.0	K
Cathode gas inlet temperature	338.0	K
Number of cell	44.0	-
Cell active area	400.0	cm <sup>2</sup>
Removed heat	7100	W
Operation mode of anode	Dead-end	-
Hydrogen stoichiometry	1	-
H2 consumption rate of fuel cell at maximum power	0.054724	mol/s
	0.110312	g/s
	66.95446	L/min
Operation mode of cathode	Through-flow	-
Oxygen stoichiometry	2	-
Air inlet flow rate at maximum power	0.27	mol/s
	7.85	g/s
	332.91	L/min

The components and auxiliary equipment involved in the system should be consistent to the specifications given in Table 4.1. The catalog data and the specifications of pump and humidifier are given in Appendix A.

#### **4.2. Flow chart and control instrumentation**

The control system should provide an efficient and safe operation for steady and unsteady conditions. The main control objectives are supplying desired amounts of fuel and oxidant, keeping the temperature and pressure at the desired values, managing the power delivered from the stack and battery conditions, checking oxygen and hydrogen amounts in the system environment for safety considerations and keeping individual cell voltages above 0.4 V to prevent the cells from permanent damages. The prototype piping and instrumentation diagram with the control instrumentations is given in Figure 4.3.

Hydrogen will be fed to the system from a pressurized hydrogen tank. The hydrogen line would include a solenoid valve, relief valve, pressure indicator and a pressure regulator. At start-ups the solenoid valve will be opened to feed hydrogen to anode compartment. The pressure indicator will show whether there is a proper hydrogen pressure in the line and tank or not by giving an alarm. The relief valve will control the pressure in the line by avoiding the high pressures. The pressure regulator will let hydrogen flow through anode inlet when the hydrogen inside anode is depleted and it will follow the cathode pressure. The solenoid valve will be closed at shut-down and emergency conditions.

The air flow would be provided by a compressor accompanied by a filter. The compressor command voltage would be controlled according to the stack current. The voltage command to the compressor would define the motor speed and accordingly the compressed air flow rate through the stack.

The cooling system for the prototype consists of a pump, radiator and a fan. Stack cooling water outlet would be measured and the cooling system would be operated accordingly. This temperature feedback can be used for different control strategies.

Power management subsystem is required to control the power drawn from the fuel cell system. The parasitic power requirement increases with increase in stack performance, so the net power obtained from the system would be organized by a battery. The battery usage in the stack would be controlled according to the stack voltage. At low voltages the battery would be used, such as at start-ups. The battery would be recharged when excessive power is available.

During the operation, water and some impurity gases could accumulate in the anode side due to dead-end operation and these impurities should be removed from the system by a purge valve. Purge valve can be used with setting the frequency and duration of the purges or controlling the voltage across the cell nearest to the anode exit. If the voltage is lower than the expected values, purge valve should be opened to remove the impurities.

To prevent cell voltage losses below 0.4 V, individual cell voltages would be monitored. If any cell voltage drops below 0.4 V, purge valve will be opened and if low voltages endure the system would be directed to battery or emergency conditions.

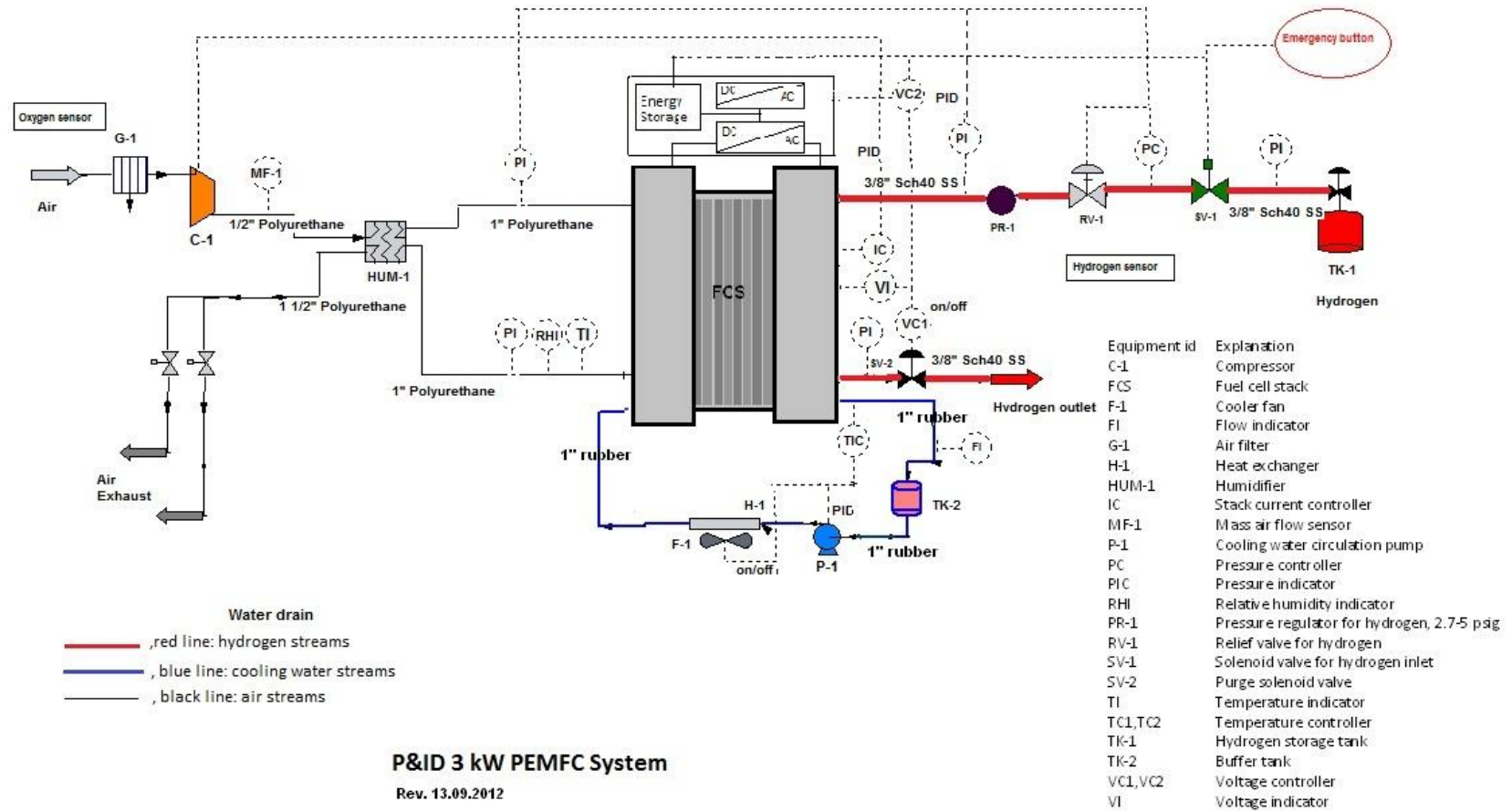


Figure 4.3 Prototype PI Diagram with Control Instrumentation



## CHAPTER 5

### SYSTEM IDENTIFICATION AND MODEL VALIDATION

In Chapter 3, the prototype system including the stack, manifolds, humidifier, compressor, and cooling system is modeled by using the energy and material conservation laws that result in differential equations. These equations are completed with thermodynamics and kinetics describing the critical system parameters. To define the unknown system parameters and create a semi-empirical model experiments are performed on cooling system and stack. The experiments are carried out in the Fuel Cell Technology Laboratory, METU-Department of Chemical Engineering. For humidifier and compressor literature values are used for model verification.

#### 5.1. Cooling System Experiment Design and Analysis

Heat removal from the stack is supplied by a water cooling system including a pump (Kormas centrifugal Pump), radiator and fan system (Tofaş-automobile radiator). Cooling water passes through the cooling channels machined on bipolar plates and remove heat. The heated water pumped through a radiator coupled with fan for cooling.

The cooling system tests are performed to obtain the functions of water flow rate through the pump and multiplication of overall heat transfer coefficient and overall heat transfer area ( $u(V_{fan}, V_{pump}) \times A$ ) given in Equations (3.56) and (3.65) respectively.

$$\dot{m} = \dot{m}(V_{pump}) \quad (3.56)$$

$$\begin{aligned} \dot{m} \times c_{p_{water}} \times (T_{in} - T_{out}) - \left( u(V_{fan}, V_{pump}) \times A \times \frac{(T_{\infty} - T_{out}) - (T_{\infty} - T_{in})}{\ln \left( \frac{(T_{\infty} - T_{out})}{(T_{\infty} - T_{in})} \right)} \right) \\ = V_{rad} \times \rho \times C_{p_{water}} \times \frac{1}{2} \left( \frac{dT_{in}}{dt} + \frac{dT_{out}}{dt} \right) \end{aligned} \quad (3.65)$$

In order to calculate the parasitic losses encountered by the cooling system, current drawn by pump and voltage are also tested for different voltages. The power applied to the pump and the fan are changed with two adjustable AC-DC converters (MW power supply-NES-350-24KO and Yıldıırım Electronics Y-0012 DC power supply).

Volumetric flow rate of water through the pump according to voltage is given in Figure 5.1. The test is performed by measuring the amount of water accumulated in an empty container in a determined time. This data is fit to a linear equation giving the volumetric flow rate

$\dot{q}$  [lt/min] in terms of pump voltage  $V_{pump}$  as in Equation (5.1). Volumetric flow rate can be converted to mass flow rate [kg/s] as in Equation (5.2).

$$\dot{q} = 1.388V_{pump} - 5.662 \tag{5.1}$$

$$\dot{m}(V_{pump}) = 0.023V_{pump} - 0.0944 \tag{5.2}$$

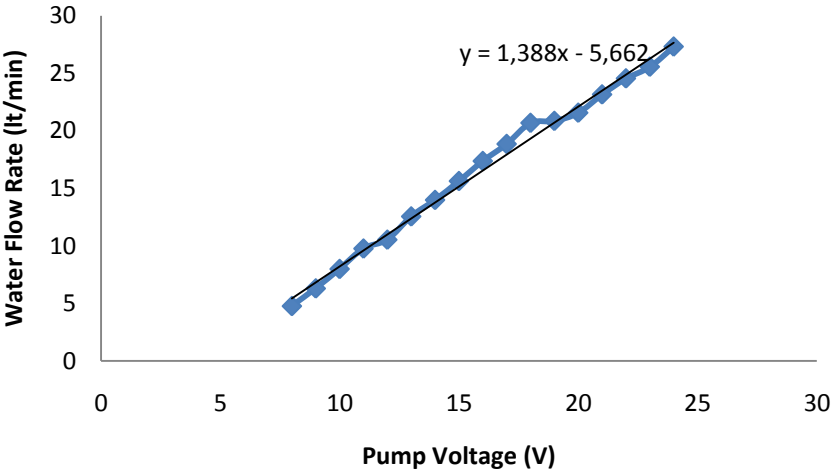


Figure 5.1 Water flow rate by voltage change.

To be able to estimate the parasitic losses encountered by cooling system, current drawn by the pump and fan are determined as functions of voltages. Voltages versus current graphs are formed and the obtained lines are fit into functions. The current drawn from the pump and fan for different voltages are given in Figure 5.2 and Figure 5.3 respectively.

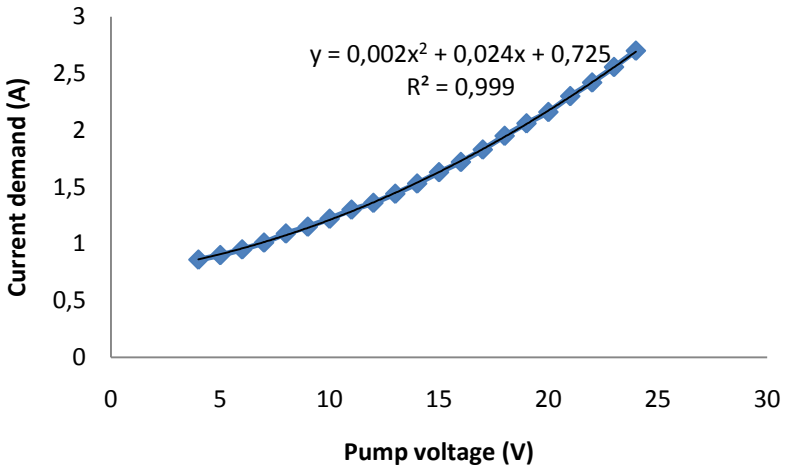


Figure 5.2 Pump current demand according to voltage

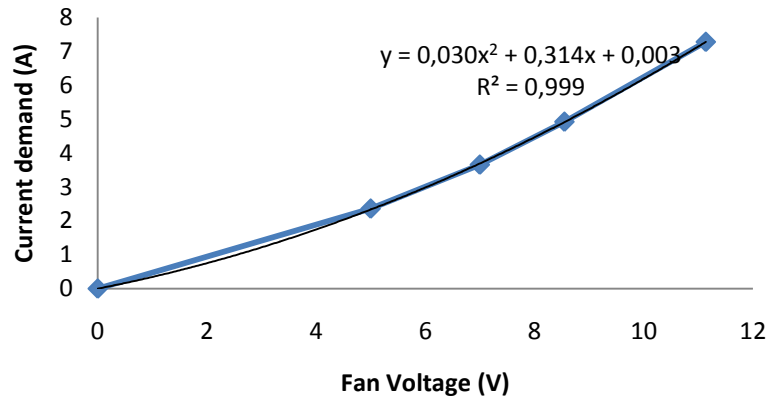


Figure 5.3 Fan current demand according to voltage

The comparison of Figure 5.2 and Figure 5.3 shows the current drawn therefore the parasitic power required by the fan is much higher than the pump when same voltage is applied. Minimum usage of fan would give smaller parasitic losses; this is an important point for the selection of cooling system control strategy.

To characterize  $(u(V_{fan}, V_{pump}) \times A)$ , water circulating pump (Kormas centrifugal Pump), an automobile radiator & fan (Tofaş) and water bath (Nüve BS402) are connected as in Figure 5.4. Hot water obtained from the water bath is pumped through the radiator and then returned to the water bath. Radiator inlet and outlet temperatures are monitored and recorded by a data logger (National Instruments NI USB-6211) that is attached to the thermocouples (Omega Engineering K-type Chromega- Alomega). The test photograph is shown in Figure 5-5. Two test procedures are applied for characterization of the cooling system which aimed changing voltage of the pump or fan while keeping the other's voltage as a constant.

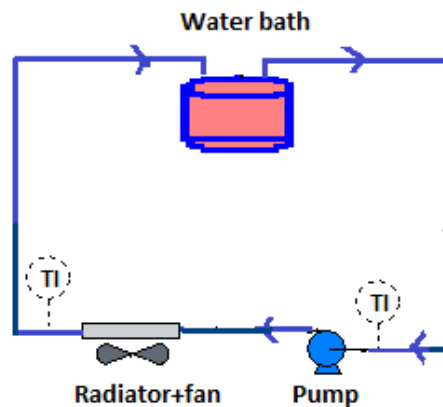


Figure 5.4 Cooling system tests setup



Figure 5.5 Cooling system

**Test Procedure-1:**

In the first test, the pump voltage is set to different values while the fan is operated at on/off mode. Fan voltage is kept constant while operating, at 7V corresponding to 30% of maximum fan power. Pump response to dynamic changes are tried to be understood by this method. The test procedure is given in Figure 5.6 while the radiator inlet and outlet temperatures are recorded per second.

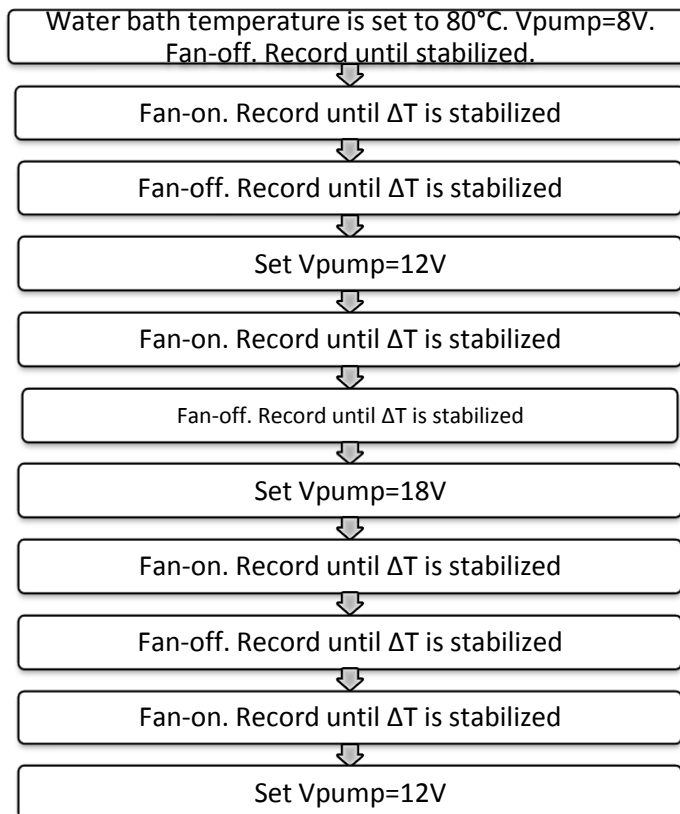


Figure 5.6 Cooling system test procedure-1

Fan voltage and pump voltage adjustment during the experiment-1 is given in Figure 5.7 and 5.8 respectively.

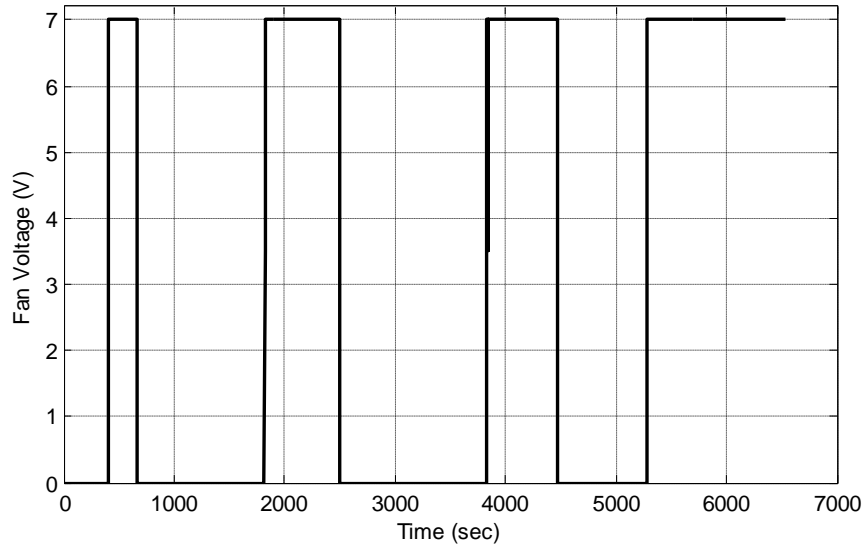


Figure 5.7 Change in fan voltage during test-1.

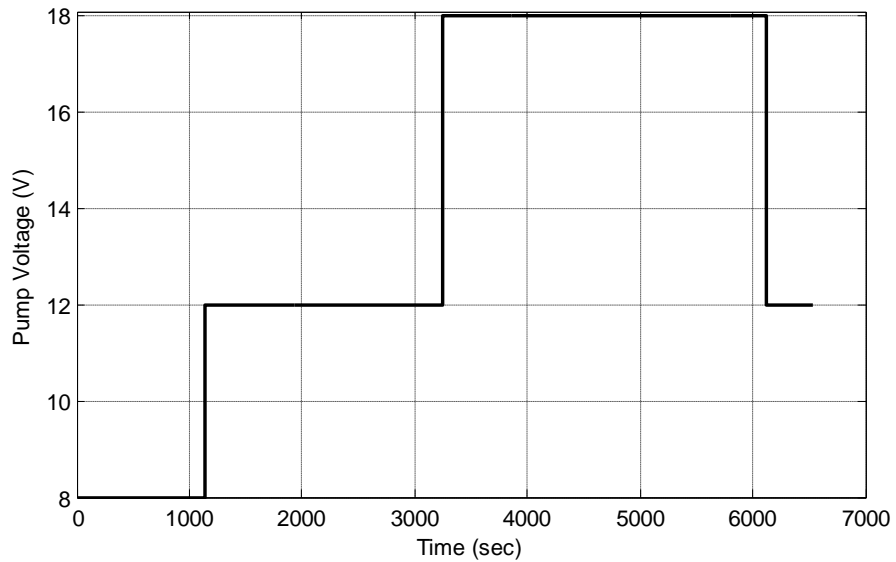


Figure 5.8 Change in pump voltage during test-1.

Water bath capacity (2000W) was insufficient to recover the removed heat and keep the temperature at a constant value while fan and pump are both operated. Figure 5.9 shows the

radiator inlet and outlet temperatures which show a decreasing trend while fan is in operation. Water bath temperature is increased when only pump is working and heat removal is smaller than 2000W.

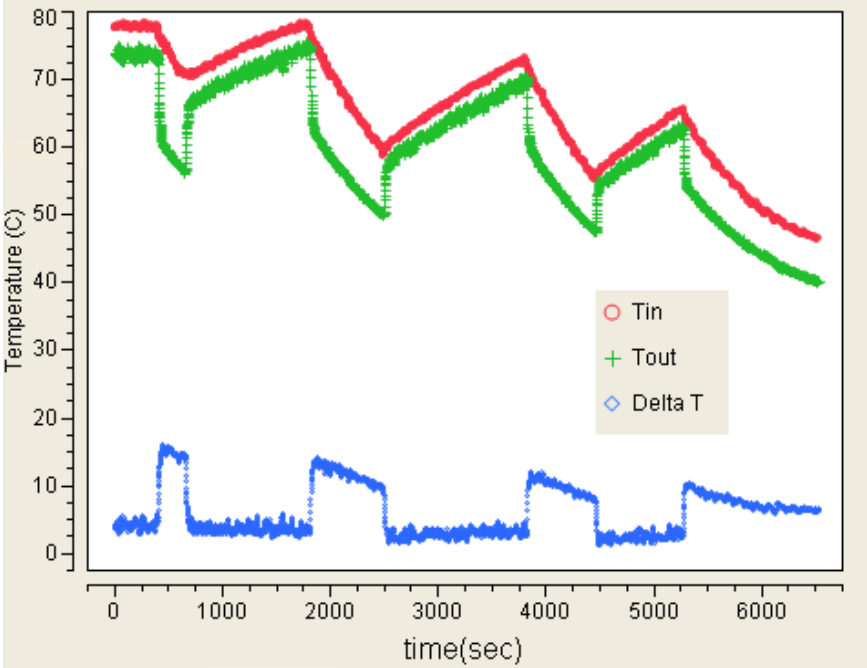


Figure 5.9 System response when Test-1 Procedure is applied (1Data/second)

**Test Procedure-2:**

In the second test, the pump voltage is set to different values while the fan is adjusted to different voltages 0V, 5V, 7V, 8.55V and 11.14 V which corresponds to 0%, 20%, 30%, 40% and 60% of maximum fan power for each pump voltage. In this test the fan performance is tried to be characterized by keeping pump voltage constant. The test procedure is given in Table 5.1.

The data obtained by the test procedure-2 is given at Figure 5.10. During test procedure-2, 1000 data are recorded for each second. Excessive number of data points disallowed the data analysis due to program memory problems. Therefore data number is reduced by a script written in JMP software to 1 data per second which is given in Appendix B.3. Fan voltage and pump voltage adjustment during the experiment-2 is given in Figure 5.11 and 5.12 respectively for the portion of the data used in analysis.

Table 5.1 Test Procedure 2

Step	Fan voltage (V)	Pump voltage(V)	Explanations
1	0.00	12	Water bath temperature is set to 60°C. Record until the water bath temperature is stabilized
2	5.00	12	Wait until $\Delta T$ is stabilized
3	7.00	12	Wait until $\Delta T$ is stabilized
4	8.55	12	Wait until $\Delta T$ is stabilized
5	11.14	12	Wait until $\Delta T$ is stabilized
6	0	12	
7	0	18	
8	5.00	18	Wait until $\Delta T$ is stabilized
9	7.00	18	Wait until $\Delta T$ is stabilized
10	8.55	18	Wait until $\Delta T$ is stabilized
11	11.14	18	Wait until $\Delta T$ is stabilized
12	0	18	
13	0	8	
14	5.00	8	Wait until $\Delta T$ is stabilized
15	7.00	8	Wait until $\Delta T$ is stabilized
16	8.55	8	Wait until $\Delta T$ is stabilized
17	11.14	8	Wait until $\Delta T$ is stabilized

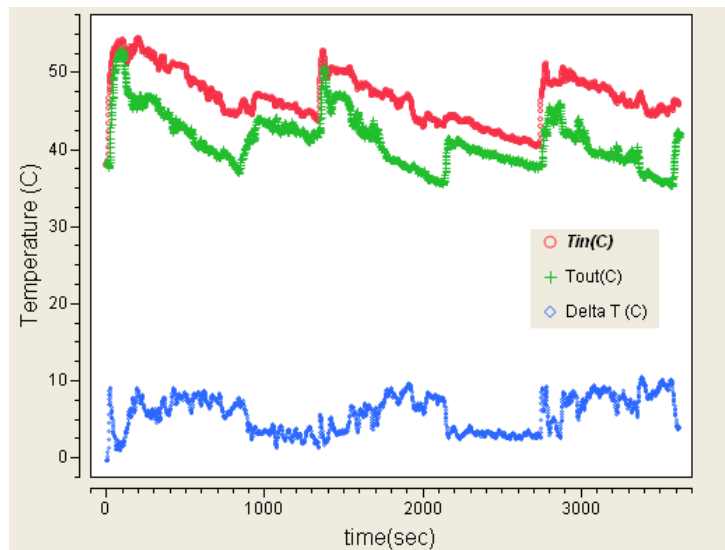


Figure 5.10 System response when test procedure-2 is applied (1000Data/second)

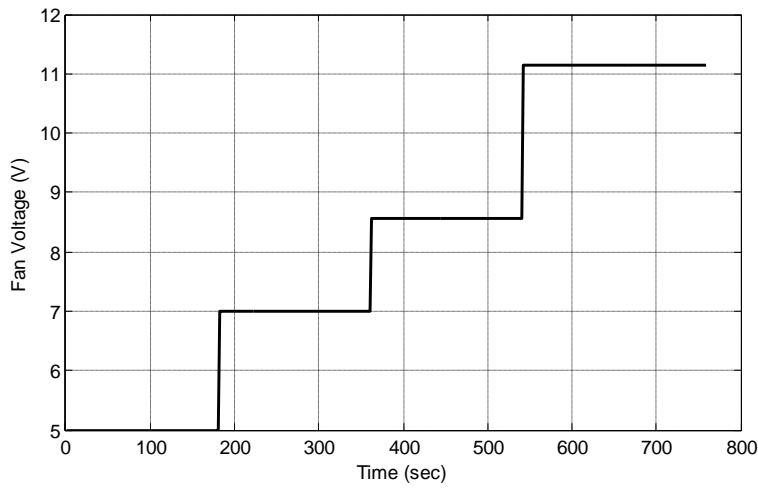


Figure 5.11 Fan voltage profile during test-2

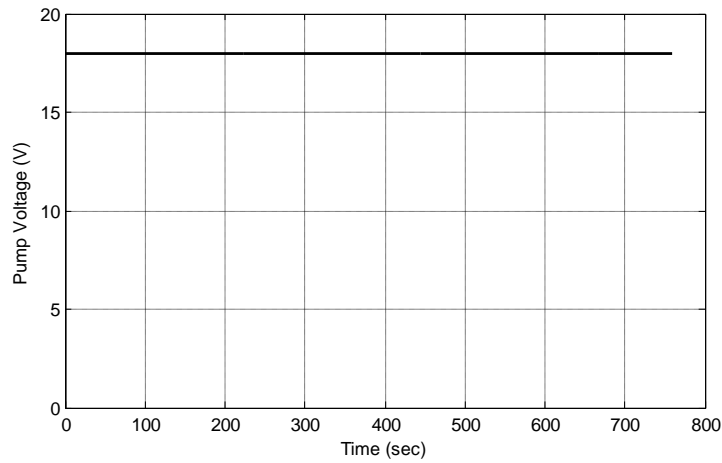


Figure 5.12 Pump voltage profile during test-2

By using the temperature data obtained from tests 1 and 2, it is desired to find an u.A function satisfying the Equation (5.3) given below.

$$\begin{aligned}
 & (0.023V_{pump} - 0.0937) \cdot cp_{water} \cdot (T_{in} - T_{out}) \\
 & - \left( u(V_{fan}, V_{pump}) \cdot A \cdot \frac{(T_{\infty} - T_{out}) - (T_{\infty} - T_{in})}{\ln\left(\frac{T_{\infty} - T_{out}}{T_{\infty} - T_{in}}\right)} \right) \\
 & - V_{rad} \cdot \rho \cdot cp_{water} \cdot \frac{1}{2} \left( \frac{dT_{in}}{dt} + \frac{dT_{out}}{dt} \right) = 0 \tag{5.3}
 \end{aligned}$$

When we simulate the Equation (5.3) in Simulink, with inlet and outlet temperatures obtained from the tests, we have an experimental u.A profile as given in Figure 5.13.

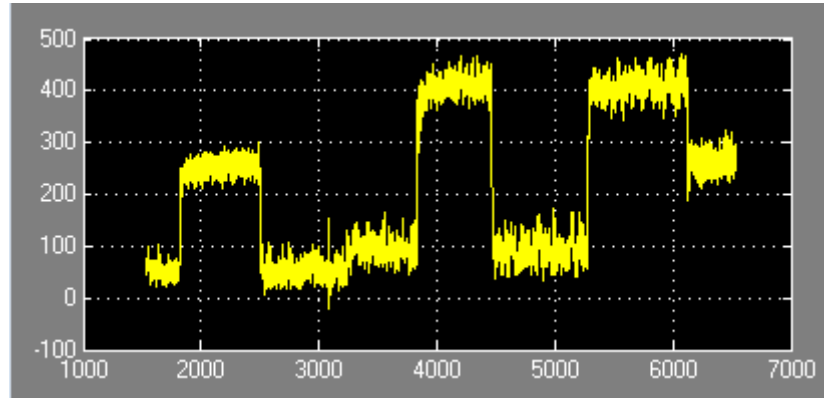


Figure 5.13 The U.A curve obtained according to the data fitted

A function fitting Figure 5.13 is tried to be found in Matlab by nonlinear regression, lsqcurvefit method as given in Appendix B.1. The regression is carried out by inserting the data points of radiator inlet and outlet temperatures, pump and fan voltages into Equation (5.3) for the available data sets, and trying different function types for u.A. The function obtained can be described as in Equation(5.4) and the comparison of the experimental and estimated u.A curve is given in Figure 5.14.

$$uA = 0.782 \times (0.551 \times V_{fan} + 3.639)^{2.08} \times (0.913 \times V_{pump} - 3.97)^{0.815} \quad (5.4)$$

While  $V_{pump} \geq 4.5 V$

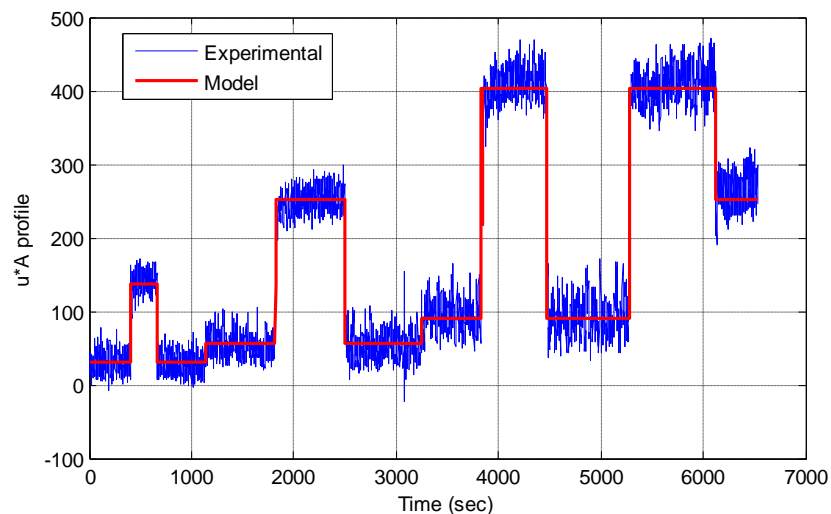


Figure 5.14 Comparison of the experimental and modeled u.A profiles.

When Equation (5.4) is used instead of u.A function in the simulation we obtain Figure 5.15 which must be zero as the result of Equation (5.3). Many deviations at Figure 5.15 are observed but it can be clarified that these are resulted due to the noisy behavior of experimental data, especially originated at the points where voltages of the pump or fan are changed.

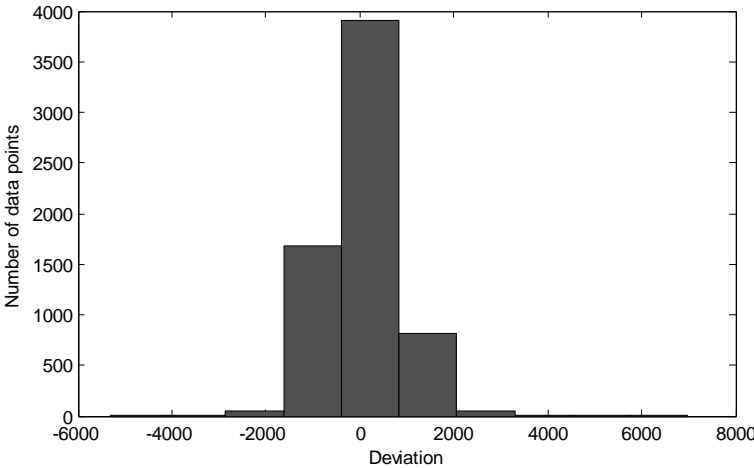


Figure 5.15 The deviation from '0'

When experimental conditions such as radiator inlet temperature, fan voltage and pump voltage are used in the model to predict radiator outlet model by using Equation (5.4) in the cooling system model instead of overall heat transfer coefficient times overall heat transfer area it is observed that the model coincides with the experimental findings. Figure 5.16 and Figure 5.17 compare experimental and model results for radiator outlet temperature for test-1 and test-2 respectively.

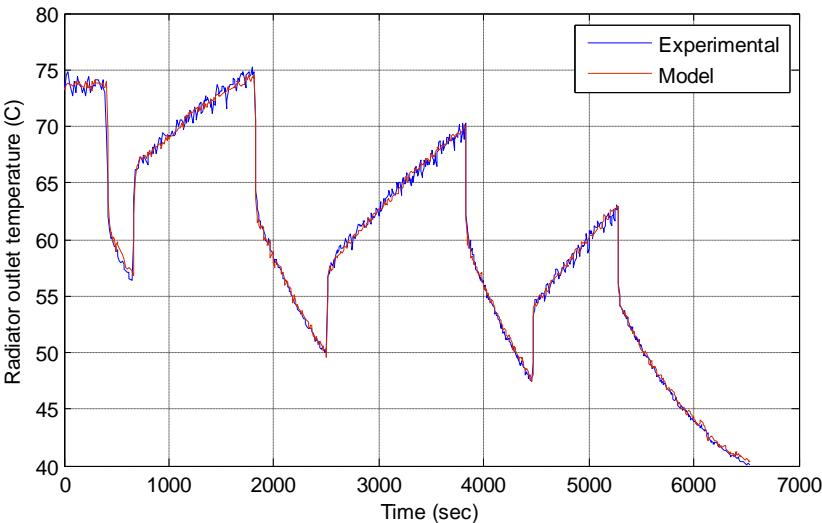


Figure 5.16 Comparison of radiator outlet temperature for experiment-1 and model.

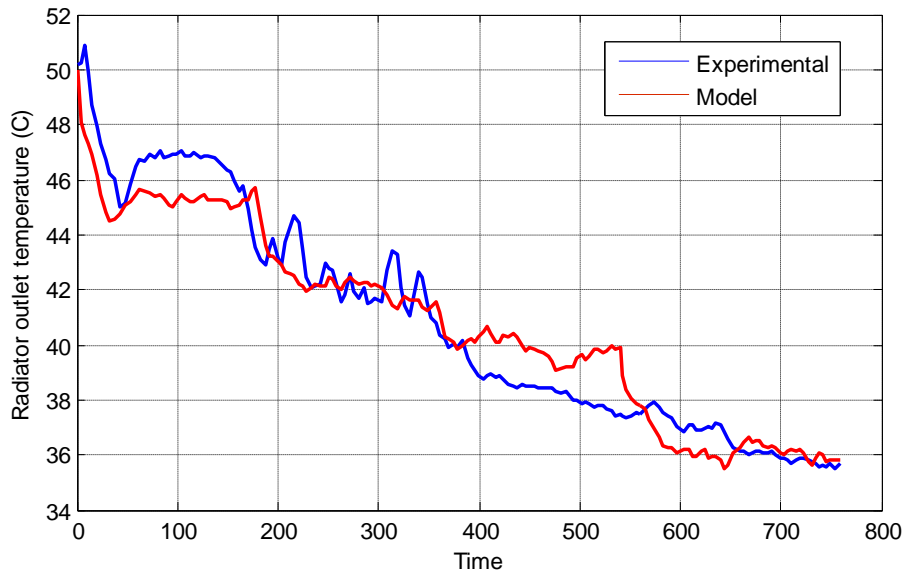


Figure 5.17 Comparison of radiator outlet temperature for experiment-2 and model.

After obtaining  $uA$  function, the cooling system is modified in Simulink, which gives radiator outlet temperature when radiator inlet temperature, pump and fan voltages are the model inputs. Figure 5.18 represents a screen shoot of Matlab- Simulink model of the cooling system.

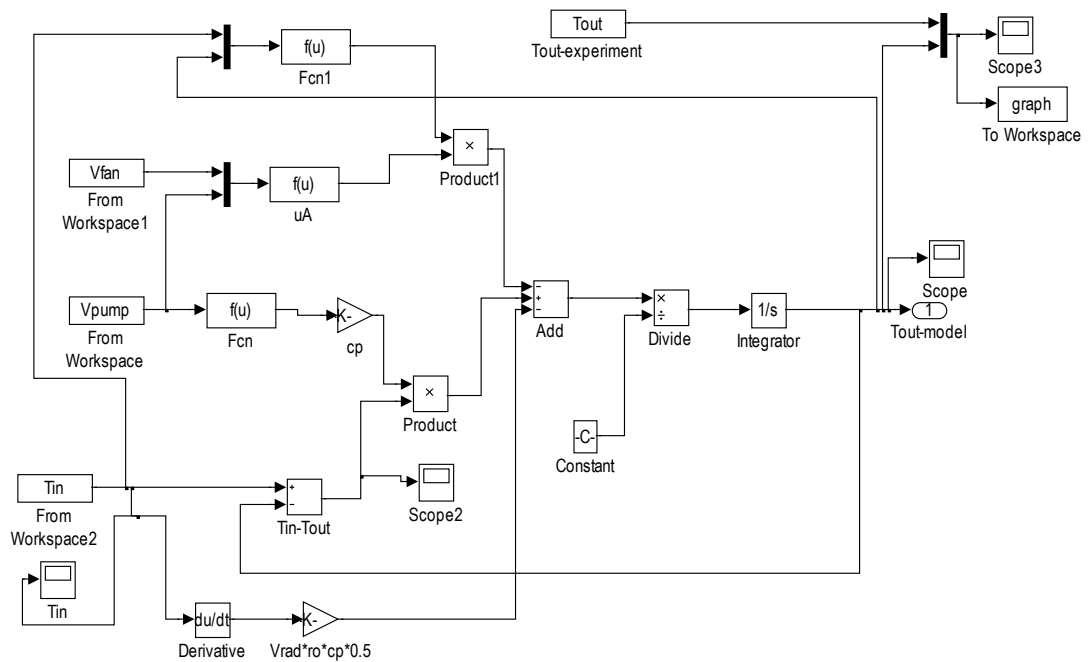


Figure 5.18 Cooling system model in Simulink

## 5.2. Stack tests

Constructing a fuel cell polarization curve model requires the knowledge of the contribution of activation, ohmic and concentration losses. To determine these losses, some system specific parameters and operating conditions should be known, such as temperature, pressure and the constants given in Section 3.2.1.3. In order to generate a semi-empirical polarization curve model, the stack is tested at its specified steady-state working conditions and a polarization curve is obtained. This data is used in a non-linear regression analysis and the constants of Equation (3.28) are determined.

The test set values are selected in accordance with the operation values decided at the design stage. Dry hydrogen is supplied to the system with a stoichiometry of 1.2, while the air relative humidity is hold at 100 % with a 2.5 stoichiometry. Stack temperature is tried to be kept constant near 55 °C.

During the stack test HENATECH test station and software are used for supplying reactant flows, humidification, purging, controlling the temperature of reactant streams, which is shown on Figure 5.19. Individual cell voltages are monitored by Yokogawa MX100 Data Acquisition Device that delivers data from the gold plated spring pins (GATE) which are connected to each 44 bipolar plates. Figure 5.20-5.21 shows the gold plate spring pins that are connected to the stack for individual cell voltage monitoring. Data acquisition device cables which are connected to the individual cells are shown at Figure 5.22. The voltage data are recorded by FC Power software. A water bath (NÜVE BS402) is installed to the stack to keep the stack at a desired temperature. The load on the stack is adjusted by an electronic load (Dynaload RBL488, TDI). The test system set-up scheme is shown at Figure 5.23.



Figure 5.19 HENATECH Test Station connected to short stack (5 cells)

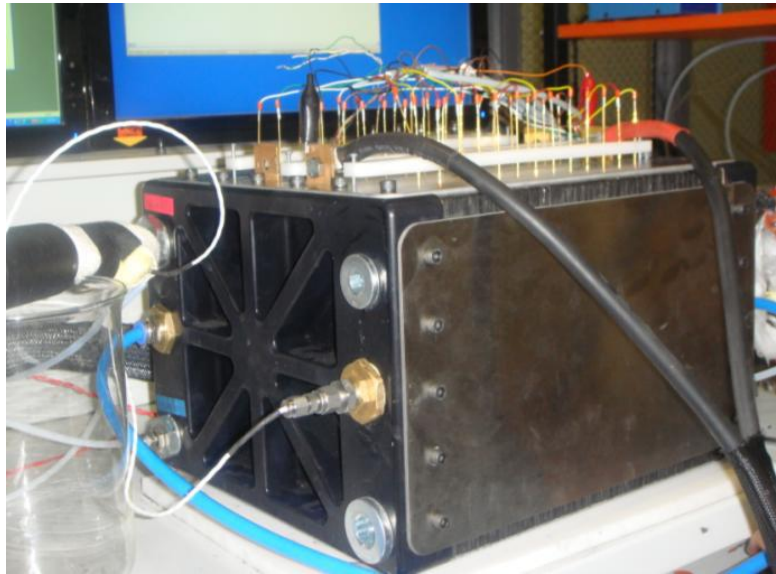


Figure 5.20 3 kW PEMFC stack and pin integration for individual cell voltage monitoring

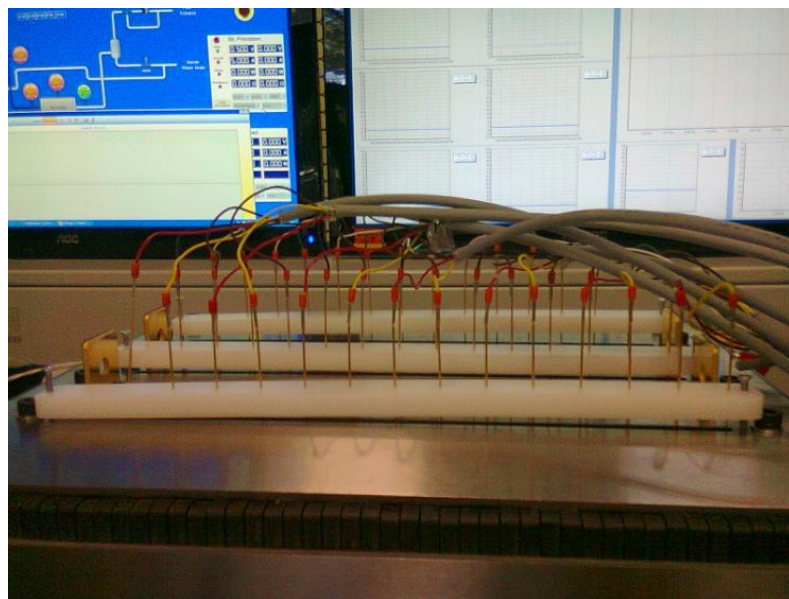


Figure 5.21 Cell voltage monitoring apparatus for 3kW PEMFC Stack.

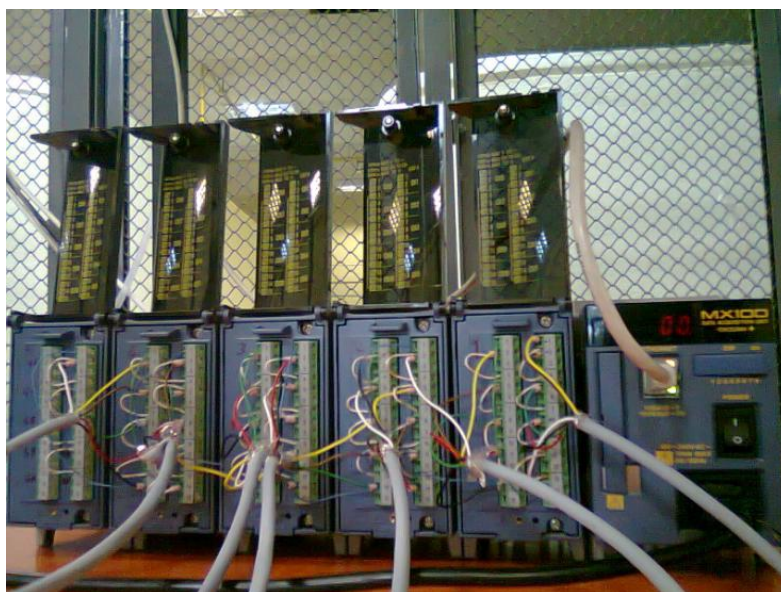


Figure 5.22 Data Acquisition Device

During start-up, firstly the water bath is opened and set to 50°C then nitrogen, air and hydrogen feed lines are opened. Dry nitrogen is passed through the stack and stack testing conditions are set on HENATECH software program. Figure 5.24 and Table 5.2 show a typical screen shoot and process values for the test respectively. Hydrogen and air lines are opened and nitrogen valve is closed. While air is passed through the humidifier, hydrogen is fed dry to the system. To eliminate any condensation in the feed streams and inside the gas channels in the stack, the temperature of the humidifier is increased gradually with the temperature increase in stack. And the stack is operated at 20 A constant current for 30 minutes. In HENATECH test station maximum attainable power is 500 W, due to the capacity of mass flow controllers, so maximum 20 A current is reachable in a 44-cell stack. After reaching steady conditions at 20 A, polarization curve is obtained by decreasing the current 5 A in each step until the OCV is reached. Also to understand the effect of cooling water on stack performance, water bath set temperature is increased and voltage is observed while the current is kept at 20 A.

At shut down nitrogen purge valves are opened, hydrogen and air valves are closed. Nitrogen purge is continued for 15 minutes, and the humidifier and water bath temperatures are decreased to room temperature. Stack is left to cool down by itself gradually. Finally cooling water is removed from the stack.

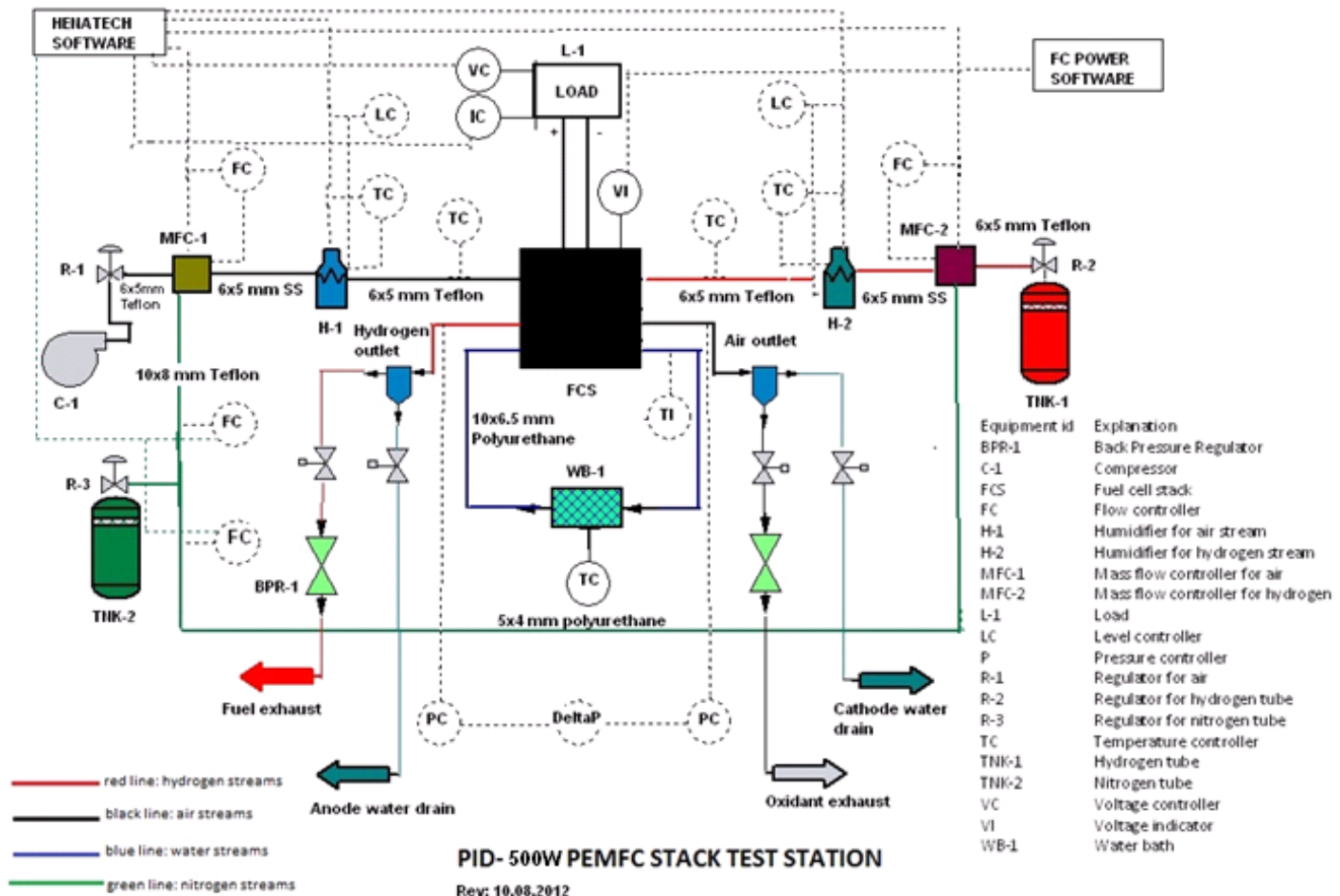


Figure 5.23 Test Station Flow Diagram



Figure 5.24 A typical screen shot during performance test of 3kW PEMFC stack.

Table 5.2 Set parameters and experimental values of stack testing

	<b>Set Value</b>	<b>Process Value</b>
Hydrogen stoichiometry	1.2	1.2
Air stoichiometry	2.5	2.5
Hydrogen pressure	1.2 bar	1.35 bar
Air pressure	1.2 bar	1.52 bar
$\Delta P$	5 psig( 24 mbar)	0.17 bar
Cooler Temperature	50 °C	50-65 °C
Minimum hydrogen flow	1 slpm (calculated for 50 mA/cm <sup>2</sup> )	1 slpm
Minimum air flow	5 slpm (calculated for 50 mA/cm <sup>2</sup> )	5 slpm
Maximum hydrogen flow	8.92 (calculated for 0.8 V, 20A)	7-10 slpm
Maximum air flow	44.3 (calculated for 0.8V, 20A)	44-44.4 slpm
Air Relative humidity	100%	100%
Feed lines	70 °C	70 °C

Due to the limitations of test station, maximum 20 A current delivered from the stack, by giving a maximum power of 500 W. The open circuit voltage for the stack is observed as 41.4 V, while the individual cell voltages were in the range of 0.96 and 0.93 V. Figure 5.25 shows a screen shot of the test station while OCV values are observed and Figure 5.26 shows the OCV values for the individual cells. The polarization curve at 55°C and the stack power change with respect to current are shown on Figure 5.27 and Figure 5.28 respectively.

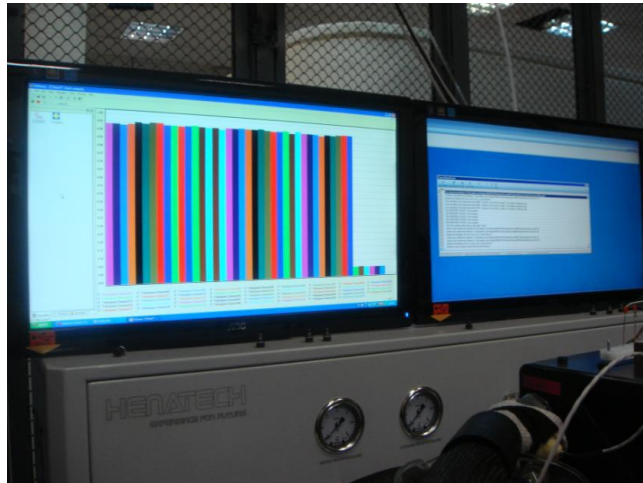


Figure 5.25 Screen shot of open circuit cell voltage (OCV) distribution for the 3kW PEMFC stack (Test conditions are given in Table 5.2).

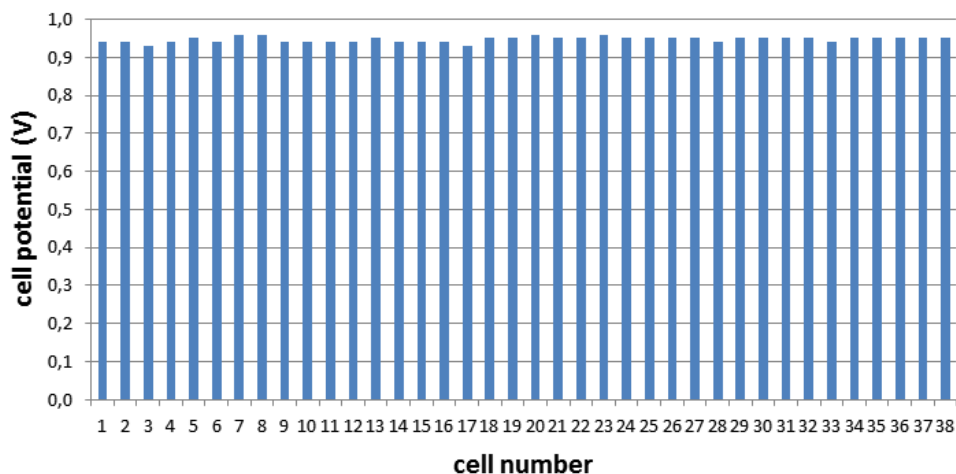


Figure 5.26 Open circuit cell voltage (OCV) distribution for the 3kW PEMFC stack

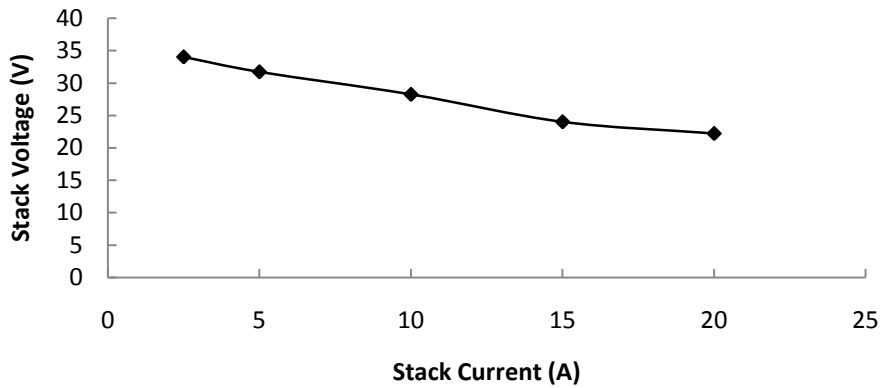


Figure 5.27 Stack voltage vs. stack current at 55°C.

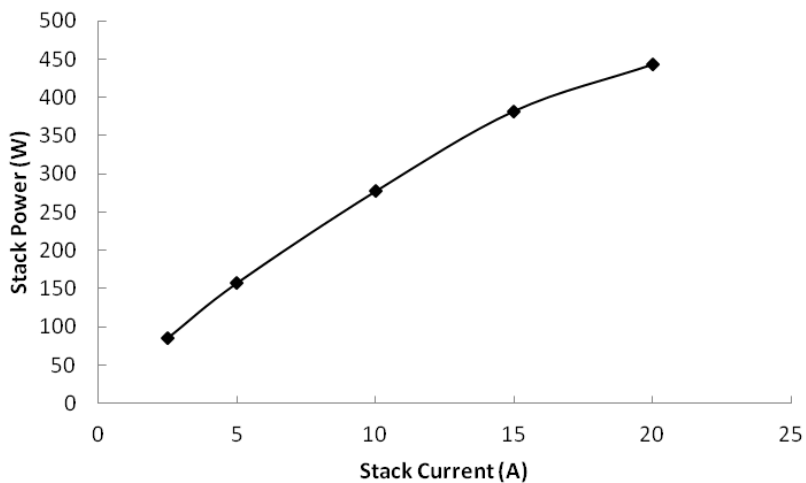


Figure 5.28 Stack power vs. current at 55°C.

Figure 5.29 illustrates the behavior of the stack, while circulating water temperature is increased for the first 20 minutes and current is set to different values. It can be stated that the slight variations in the circulating water temperature, which also contribute to stack temperature, do not have sharp effects on the stack voltage. Since the stack is designed and manufactured to be operated at 55°C and near to this temperature, and the effect of slight temperature variations do not have a considerable effect on stack voltage, the polarization curve obtained for 55°C is used in the determination of constants of Equation (3.28) In MATLAB, lsqcurvefit is used to find the constants which are provided in Table 5.3.(See Appendix B.2)

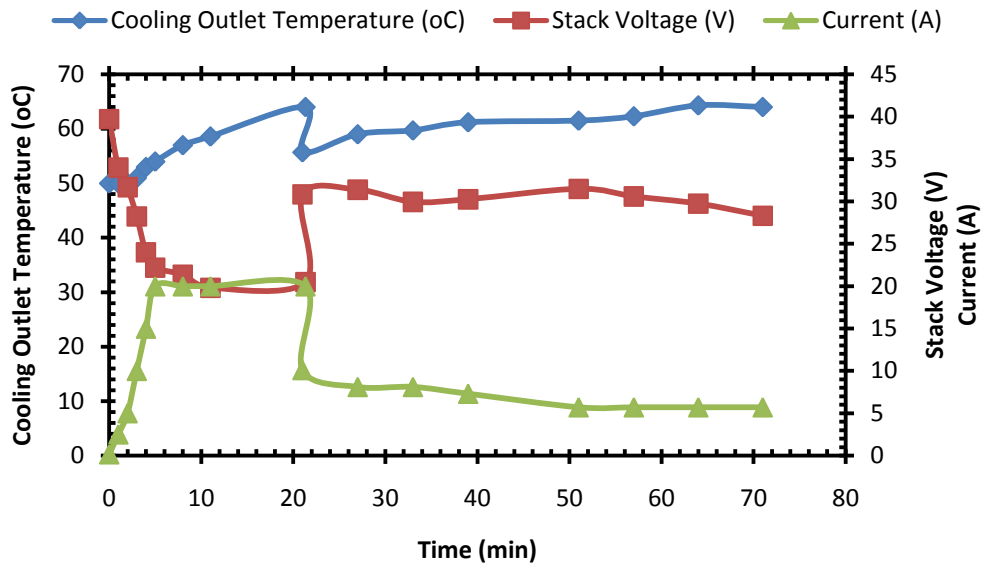


Figure 5.29 Variation of cooling water outlet temperature, stack voltage and current with time

Table 5.3 Constants obtained for stack test for polarization curve model.

Constant	Value
$c_1$	10
$c_3$	2.0004
$i_{\max}$	1.5824

Figure 5.30 shows the voltage of each cell with respect to cell number. The cell voltage varies between 0.43 to 0.85 V while the stack current is kept constant at 5.7 A. It is observed that the increase in cooler outlet temperature from 61.5°C to 62.9°C causes voltage losses of most of the cells. The stack power is 179 W at 61.5 °C. This value decrease to 169 W as the temperature increase to 62.9 °C. This is mainly due to the decrease of stack voltage from 31.47 V to 29.75 V.

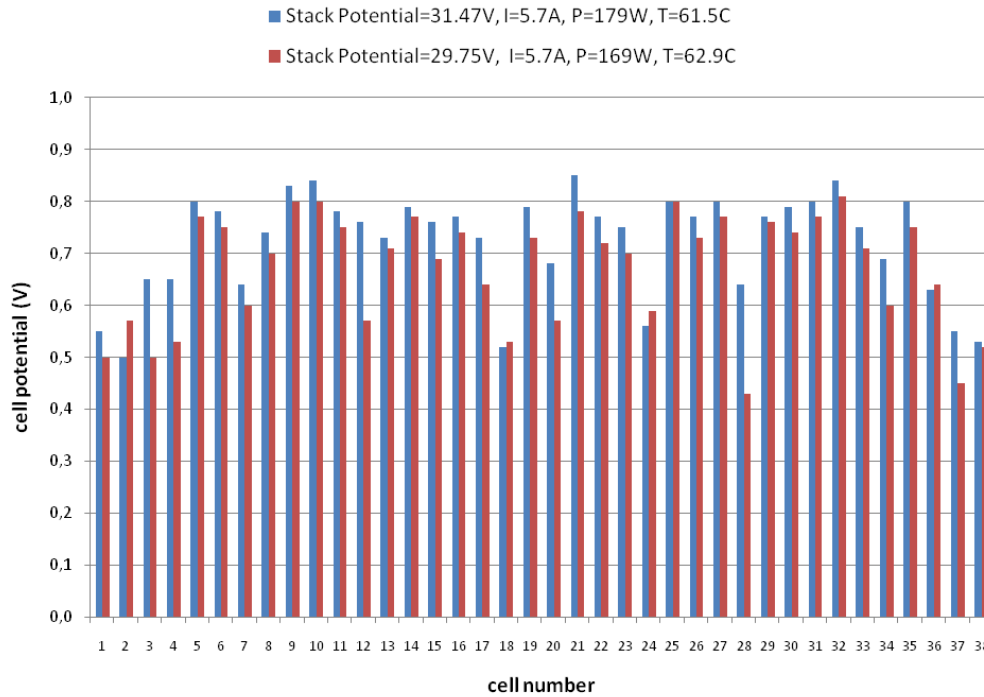


Figure 5.30 Cell potential vs. cell number at 5.7 A

### 5.3. Humidifier model validation

To check the validity of the humidifier model, the recommended performance test is given in Figure 5.31. Dry air coming from the compressor (maximum 330 slpm,  $T=60\text{ }^{\circ}\text{C}$ ) passes through mass flow indicator (MFI) and enters to the humidifier (side 1). Relative humidity of the exit air is measured then the stream enters to a water bubbling column (5 lt), which is placed in a water bath. Saturated air leaving the bubbling column enters to the side 2 of the humidifier. This stream resembles the exhaust air in the actual stack. Temperatures and the relative humidities of the entering and exiting streams can be measured and the model results can be compared with experimental data.

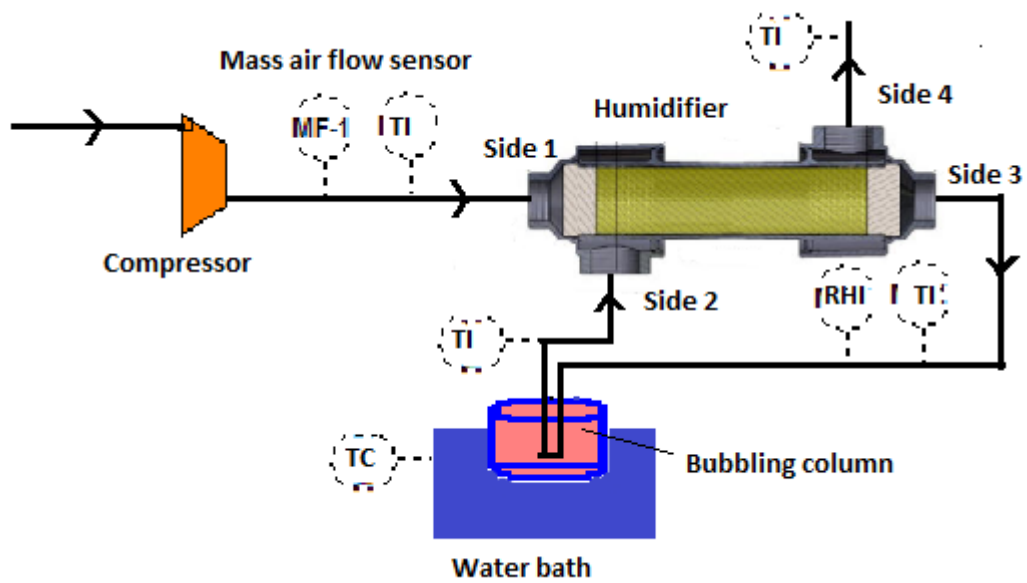


Figure 5.31 Recommended humidifier performance evaluation test setup.

By using the equations involved in section 3.2.3, the humidifier is modeled in Simulink that is shown in Figure 5.32 whose subsystems and details are given in Appendix B.4. Instead of performing the humidifier experiment as described above, the model results are compared with the values available in literature.

Park et. al [21] proposed a mathematical model for a shell and tube type humidifier produced by Perma Pure (FC 200-780-10HP). Although the stated humidifier is adaptable to smaller fuel cell systems it enables us to validate the model by literature model using the parameters given in Table 5.4. After the model is verified by literature effects of various operating conditions are analyzed. The modeling approach and humidifier parameters given by Park et. al correspond to this study, therefore the model results should also have similarities.

Table 5.4 Perma Pure FC 200-780 parameters [21]

Parameter	Value
Membrane tube thickness	0.00005 m
Membrane tube inner diameter	0.00097 m
Membrane tube active length	0.254 m
Overall length of the membrane tube	0.311 m
Number of membrane tubes	1660
Inner diameter of the humidifier housing	0.056 m
Membrane dry density	0.001 kg/cm <sup>3</sup>
Membrane dry equivalent weight	1.0 kg/mol

Figure 5.33-5.36 gives a comparison of the model derived for this study and the model proposed by Park et. al In Figure 5.33 heat transfer rate is compared for the two models, for the simulation fuel cell exhaust air is assigned to be at 343.15 K with 100% relative humidity and 1.3 atm pressure, while the dry air is at 298.15K with 30% relative humidity and 1.3 atm. Exhaust air flow rate selected to be equal to the dry air flow rate. As observed in Figure 5.33, the heat transfers for the two models are overlapping. The increase in heat transfer with the increase in flow rates is an expected behavior since the high flow rates increase the overall heat transfer coefficient by having higher fluid velocities.

In Figure 5.34 vapor transfer rate according to the air flow rate is given, it is observed that the vapor transfer rate increases by the increase in flows of dry and humidified airs. This situation can be related with the increase in heat transfer at higher air flow rates. The driving force that provides vapor transfer is the concentration gradient between tube side and shell side. The concentration is expressed as a function of water activity as given in Equation (3.47) and (3.94). Although the same inlet conditions prevail, increasing air flow rates will result in higher heat transfer from tube side to the shell side. With increasing heat transfer the temperature of tube side will drop lower values by decreasing the saturation pressure which will cause an increase in tube side water activity. On the contrary, heated shell side would have higher saturation pressure that decrease the shell side water activity. While the difference between water activities increases, concentration gradient also increases by resulting higher vapor transfer rates. Figure 5.34 also compares the vapor transfer rate for the two models and a slight deviation is observed. The difference between two models can be related to the different initial conditions used in modeling.

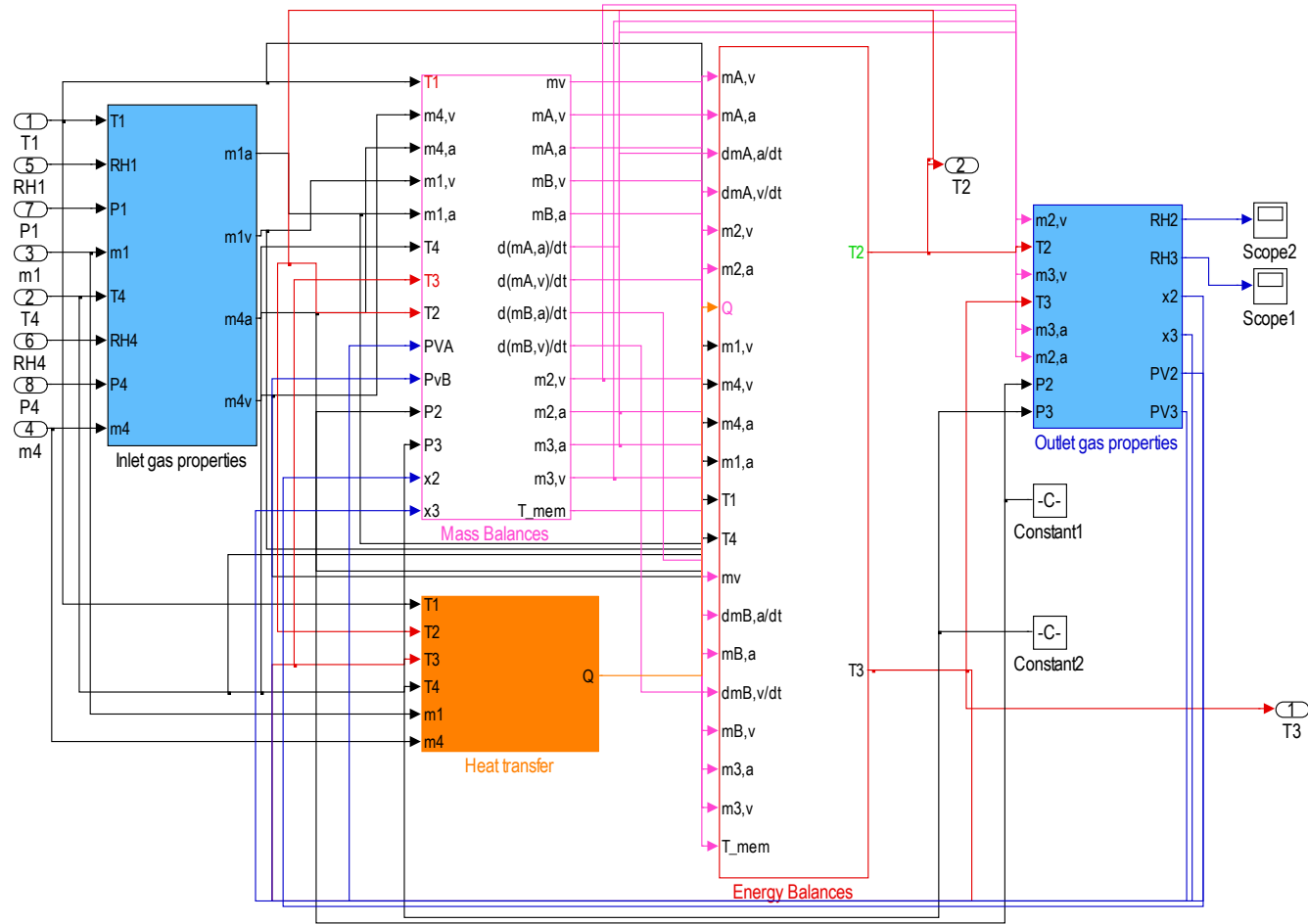


Figure 5.32 Humidifier Model in Simulink

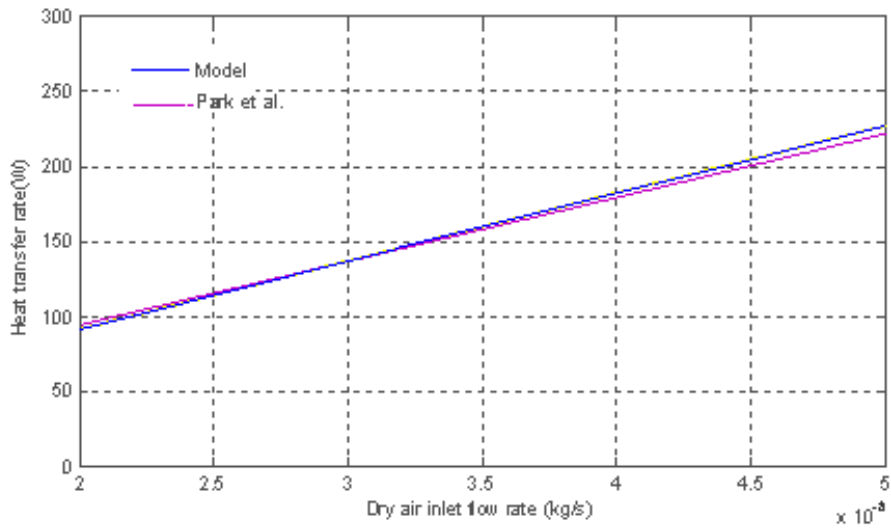


Figure 5.33 Comparison of heat transfer rate of humidifier with literature model.

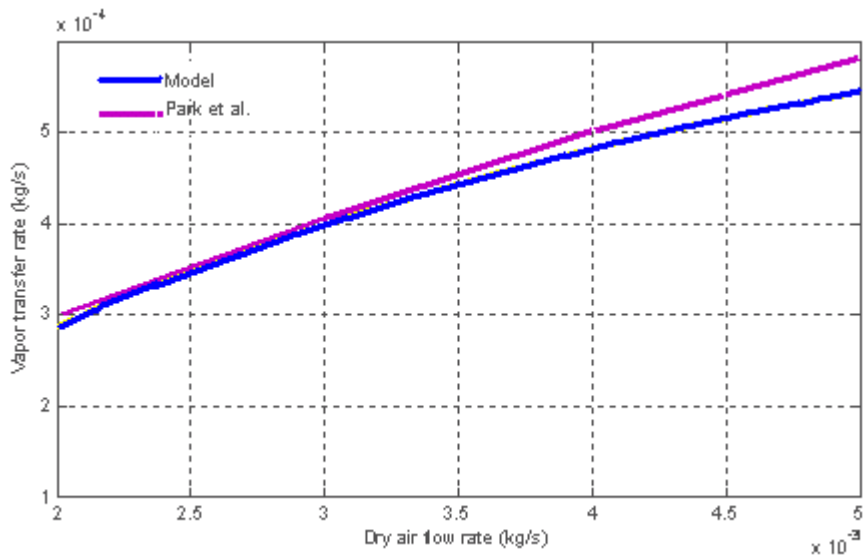


Figure 5.34 Comparison of vapor transfer rate of humidifier with literature model.

In Figure 5.35 the temperature of humidified air that supposed to fed to the stack is given according to the dry air flow rate. Also a comparison is conducted by the modeling and experimental results provided by Park et. al [21]. The simulation temperature, pressure and relative humidity for dry air are 294.25 K, 1 atm and 40% respectively. The stack exhaust air is flow rate is set equal to dry air flow rate while the temperature, pressure and relative

humidity are 343.15 K, 1atm and 100%. Temperature differences are observed especially at the starting region for the simulation. These are considered to be occurring due to the differences in initial conditions that are used in the simulations. Also the rate of change of dry air flow rates thus the simulation times are probably set to different values which may prevent the exact overlapping of the literature data and model data.

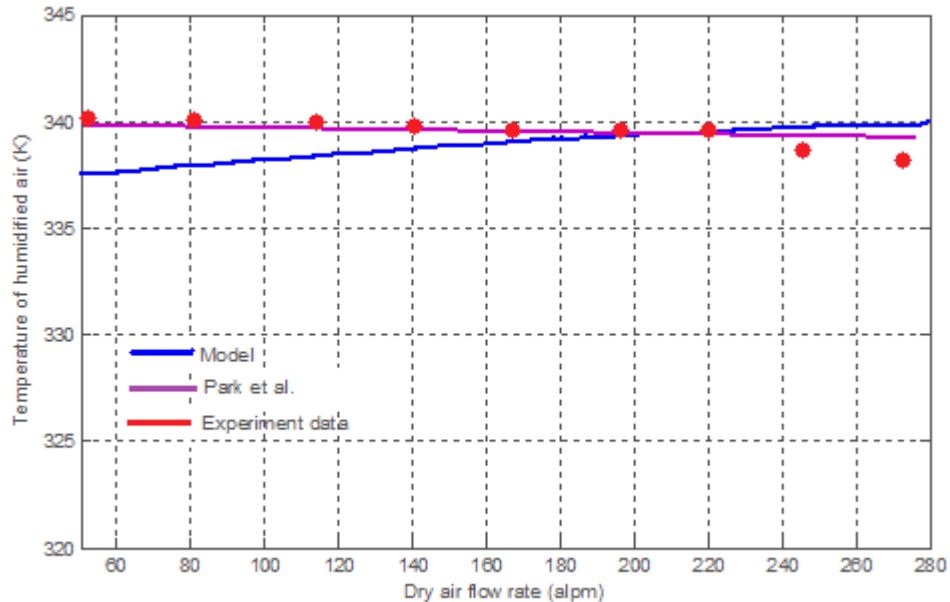


Figure 5.35 Comparison of the humidified air temperature.

By applying a step change on dry air flow rate dynamic simulations of heat transfer rate, vapor transfer rate, wet air outlet temperature, and wet air outlet relative humidity are obtained and given in Figure 5.36 in which literature simulations also appear for comparison. Exhaust gas temperature, pressure, relative humidity and flow rate are selected to be 343.15 K, 1.3 atm, 100%, and 0.003 kg/s respectively. Dry air temperature is 298.15 K with 1.3 atm pressure and 30% relative humidity. From Figure 5.36 it can be stated that dynamic behaviors for the two models are similar. The humidifier model involves 3 differential equations which necessitates initial condition description to obtain solution. In addition, the outlet flow information is lacking since the outlet flow constants are not determined. Thereby initial guesses for the humidity ratios for humidifier outlet gases are required to start simulations. The differences in initial guesses are considered as the differences between the simulation results and literature.

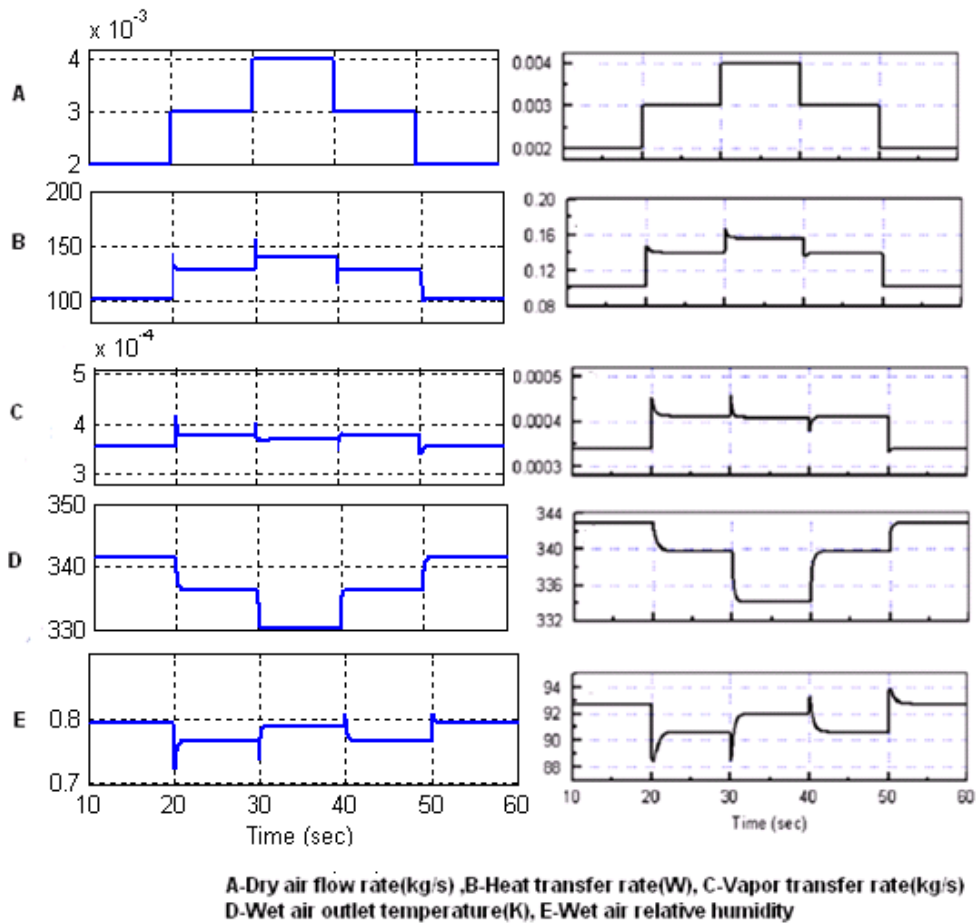


Figure 5.36 Dynamic simulation results for step change in dry air flow rate.

#### 5.4. Compressor model

Air will be supplied to the system with a compressor, the recommended compressor characterization tests aim to build a relation for compressor voltage command in terms of air flow rate and pressure, functionalize the compressor map and define the unknown parameters for the compressor dynamics.

Compressor test can be performed by applying step changes to compressor voltage for a constant pressure while recording compressor speed, air flow rate, output pressure and voltage command by small data intervals (1 data/sec). All these data can be replaced in compressor model as defined in Equations (3.98)-(3.100) and the unknown constants can be found. Also a correlation expressing air flow in terms of pressure and voltage command or compressor speed can be obtained as the compressor map information.

For this study the constants and compressor map data are obtained from the study of Pukrushpan et al.[18]. Table 5.5 gives the constants obtained from literature [18]. The capacity of the compressor adapted [18] exceeds the compressor capacity requirement for a 3 kW fuel cell. Therefore the compressor output air flow rate is multiplied by a factor to reduce flow rate to the desired level. Figure 5.37 shows the Simulink model obtained for compressor.

Table 5.5 Constants for stack compressor model [18].

Constant	Value
$k_v$	0.0153 V/(rad/sec)
$k_t$	0.0153 N.m/Amp
$R_{cm}$	0.82 $\Omega$
$\eta_{cm}$	98%

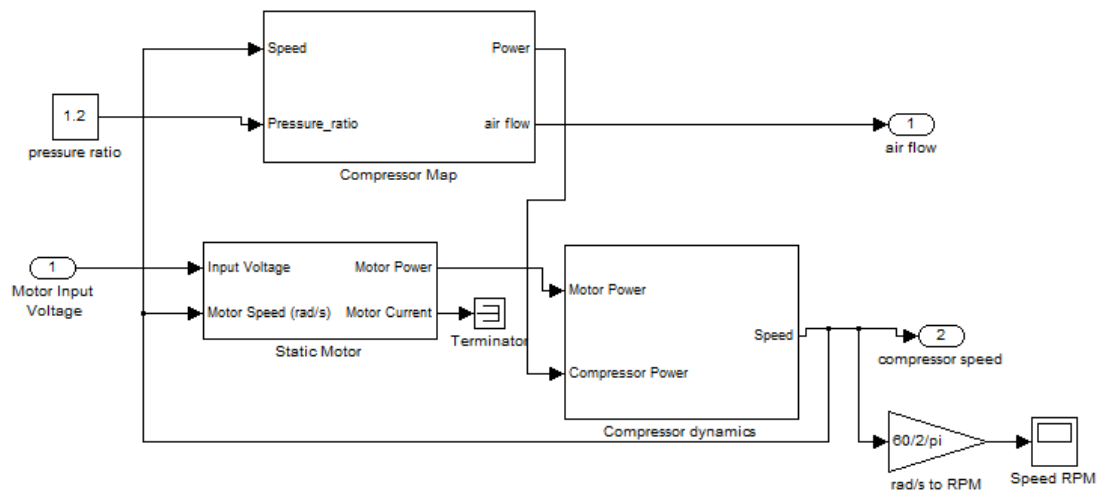


Figure 5.37 Compressor model in Simulink.

### 5.5. Final form of the model

The final form of the model is integrated by using the separate models of compressor, humidifier, stack, manifolds and cooling system. Figure 5.38 represents the integrated system block diagram, by showing the inputs and outputs of each subsystem. Each subsystem consists of set of equations required to find the desired outputs. Table 5.6 gives the inputs, outputs and the related equations used to obtain the outputs for each subsystem.

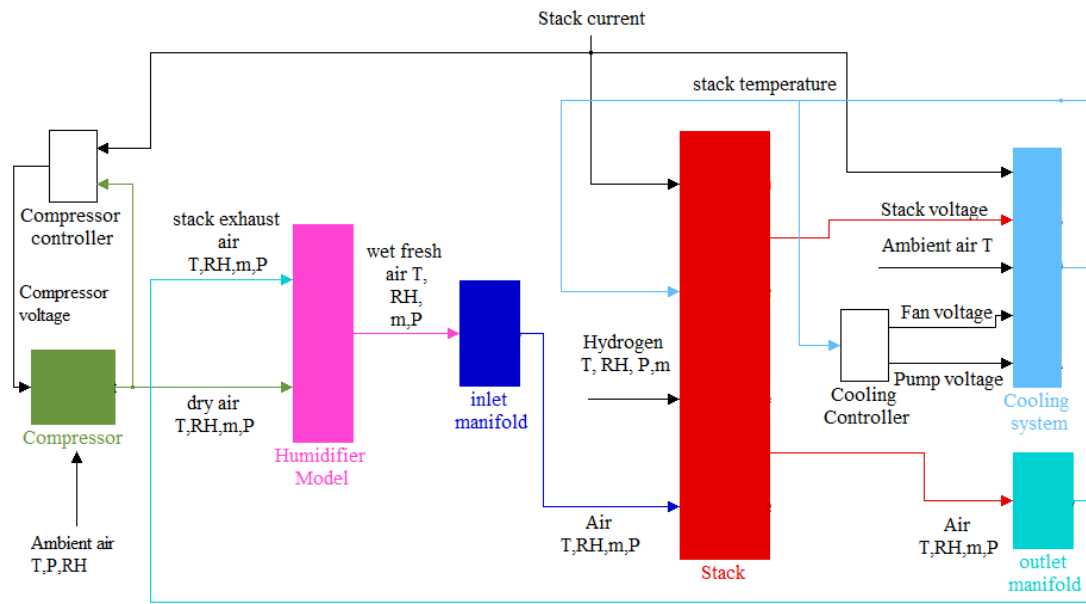


Figure 5.38 Block Diagram of the Integrated System Model.

Table 5.6 Integrated Model Subsystem Details.

Subsystem	Inputs	Outputs	Related Equations
Compressor	$v_{cm}, P_{atm}, T_{\infty}, P_{sm}$ Ambient air $T, RH, m, P$	$W_{cp}$ Compressed air $T, RH, m, P$	(3.98)-(3.100)
Compressor controller	$W_{cp}, I_{st}$	$W_{cp}$	PI controller
Humidifier model	Stack exhaust $T, RH, m, P$ Dry air $T, RH, m, P$	Wet fresh air $T, P, RH, m$	(3.69)-(3.94)
Inlet manifold	Wet fresh air $T, P, RH, m$	Stack inlet air $T, P, RH, m$	(3.95)-(3.97)
Stack	Stack inlet air $T, P, RH, m$ Hydrogen inlet $T, P, RH, m$	Stack exhaust $T, RH, m, P$ Stack voltage	(3.1)-(3.52)
Cooling system	Stack voltage, $T_{\infty}$ , $V_{pump}, V_{fan}$	Stack efficiency Heat generation $T_{stack}$	(3.53)-(3.68)
Outlet manifold	Stack exhaust $T, RH, m, P$	Exhaust air $T, RH, m, P$	(3.95)-(3.97)
Cooling Controller	$T_{stack}$	$V_{pump}, V_{fan}$	Different controllers

The Simulink screen image is given in Figure 5.39. The parameters are given in Appendix B.5.

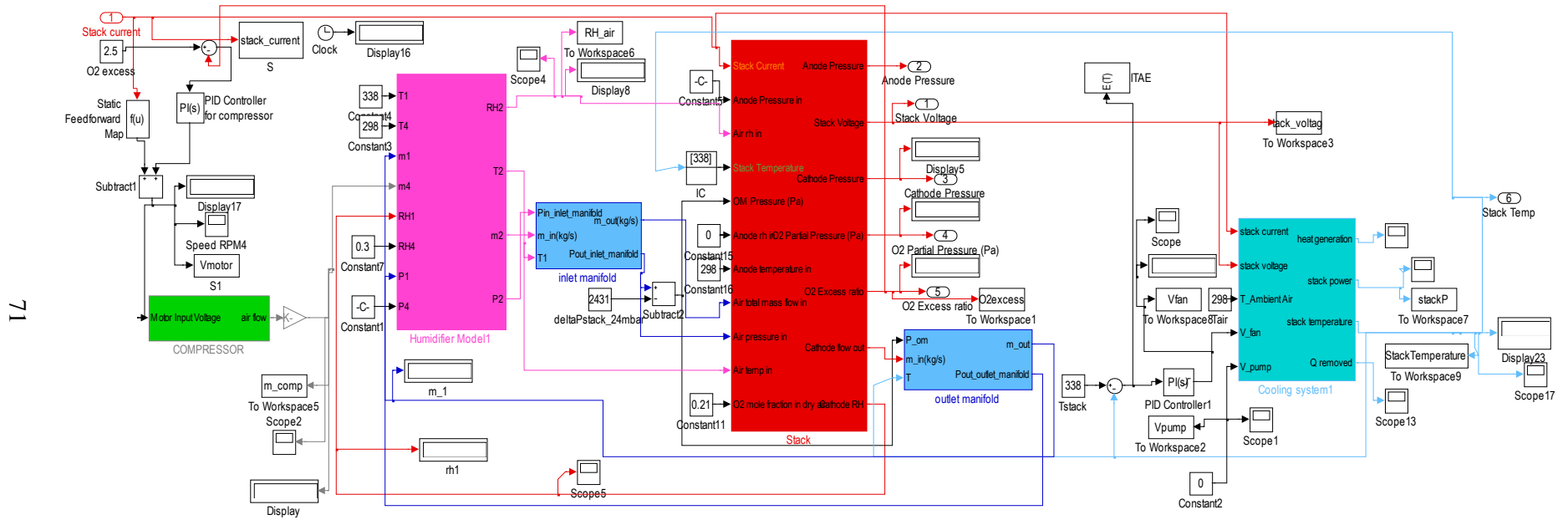


Figure 5.39 Integrated prototype model in Simulink.

In a fuel cell system the main disturbance is the stack current since current changes directly affect required reactant amounts, sufficient heat removal and humidification etc. The current driven from the stack affect the amounts of hydrogen and air required for the reactions. The change in reactant requirements should be compensated by the reactant supply equipment such as compressor which should be manipulated to have sufficient amounts of air. Similarly, higher stack current will result in higher heat generation that necessitates changes in cooling system manipulated variables. At different stack currents, the amount of dry air that needs to be humidified is also changes. To analyze the integrated model a step change in stack current is applied and the resulting stack voltage, power and heat generations, humidifier responses, water fluxes and water contents are observed. Figure 5.40 shows the change in stack current with time which is applied as the disturbance. In the simulation the air requirement is calculated by Faraday's Law coupled with a PI controller following the feedback of the difference of required and supplied air amount and then compressor voltage command corresponding to this air flow rate is determined. The air compressed to 1.2 atm by the compressor. The resulting stack voltage, power and heat generations are is given in Figure 5.41 and 5.42 respectively which are simulated by using the equations (3.28) and (3.67).

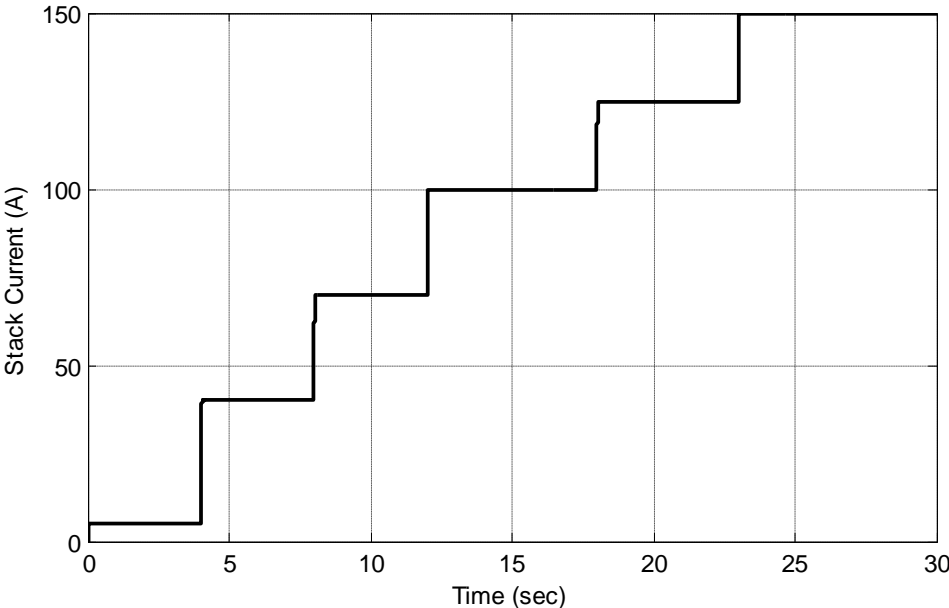


Figure 5.40 Stack current applied as the disturbance

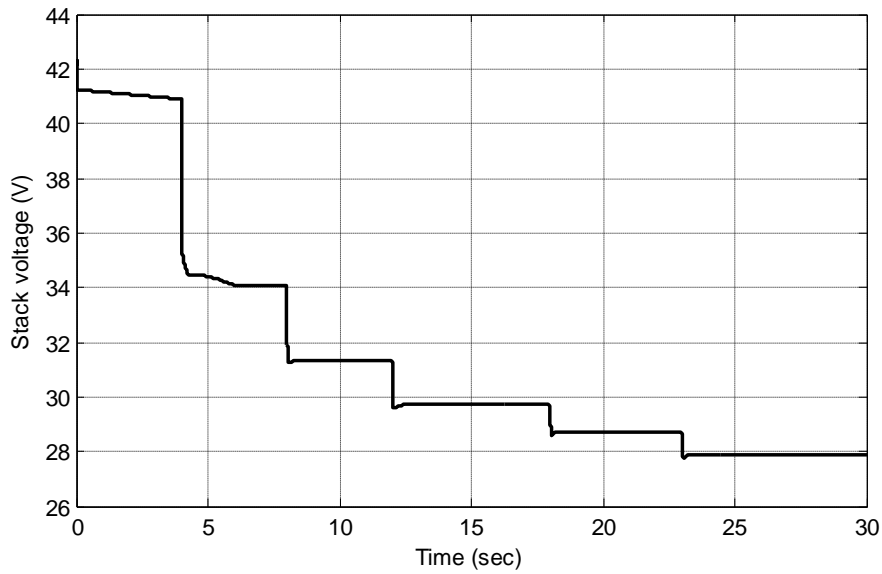


Figure 5.41 Simulated stack voltage for the current profile given in Figure 5.31.

The OCV value for the model is observed as 0.96 V for each cell resulting 42.3 V for the whole stack. The experimental OCV for the stack was obtained as 41.4 V which is compatible with the model. As shown on Figure 5.41, while 150 A current is demanded by the load, the cell voltages remains about 0.61 V which is the desired level to attain for high power densities.

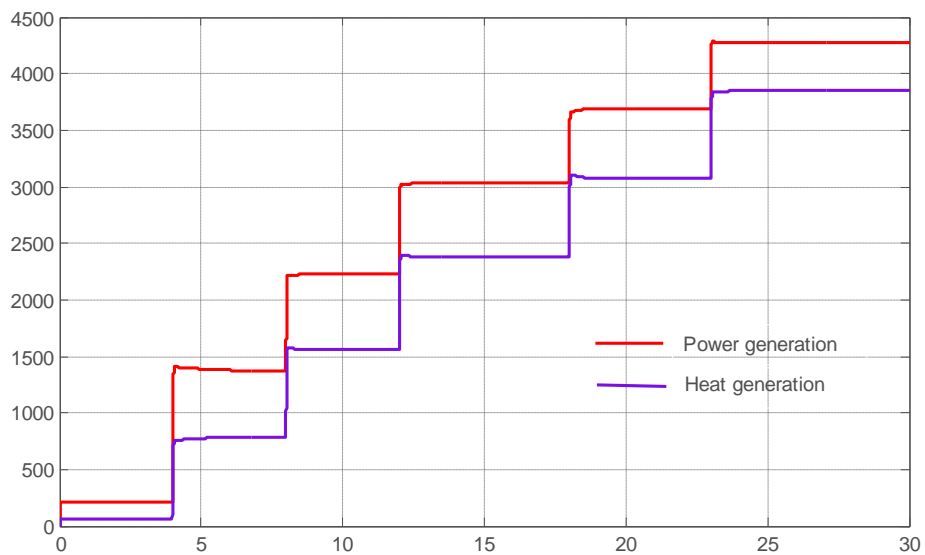


Figure 5.42 Power and heat generation simulation results for the current disturbance.

In order to see the response of humidifier for step changes in stack current Figure 5.43 is plotted. Two humidifiers analyzed, FC200 and FC300 models, which include 780 and 1660 tubes respectively. It is observed that for the first 5 seconds the dry system starts to be humidified by the electrochemical reactions and at the 7<sup>th</sup> second the stack exhaust starts to be fully humidified. Although the water production increase by the increase in stack current, the air flow also gain higher values due to the increasing voltage command by the 8<sup>th</sup> second. At 8<sup>th</sup> second and other step times, the air flow rate through the compressor is increases within a short response time, the stack exhaust humidity becomes insufficient and a sharp decrease is observed for the relative humidity of the fresh air. For FC300 humidifier, the heat and mass transfer area is greater so it shows better performance to humidify the dry air. The air flow rate supplied through the humidifier is also given in Figure5.44 which obtained by the equations (3.98)-(3.100).

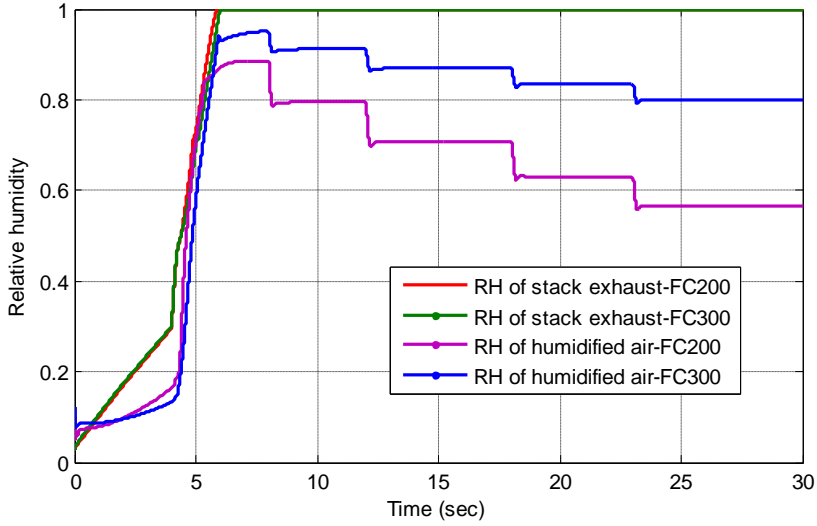


Figure 5.43 Simulation of humidifier performances in terms of a step change in stack current.

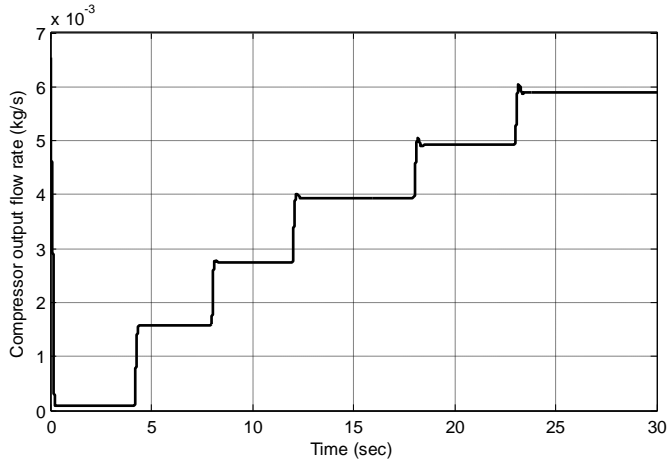


Figure 5.44 Air flow rate through the compressor

Figure 5.45 shows the change in water contents, the ratio of water molecules to the charge sites, of anode, cathode and membrane with respect to time when the stack current disturbance given in Figure 5.40 is applied. While the inlet air humidity increases as given in Figure 5.43, the water contents of anode, cathode and membrane also show an increasing trend. After the 6<sup>th</sup> second cathode water content reaches the maximum, when cathode vapor pressure becomes equal to the saturation pressure. As stack current increases, the anode water content decreases due to the increase in electro-osmotic drag but cathode water content stays constant due to the constant vapor pressure at cathode. Membrane water content which is the arithmetic mean of cathode and anode water contents also shows a decreasing trend due to the decrease in anode water content with increasing electro-osmotic drag.

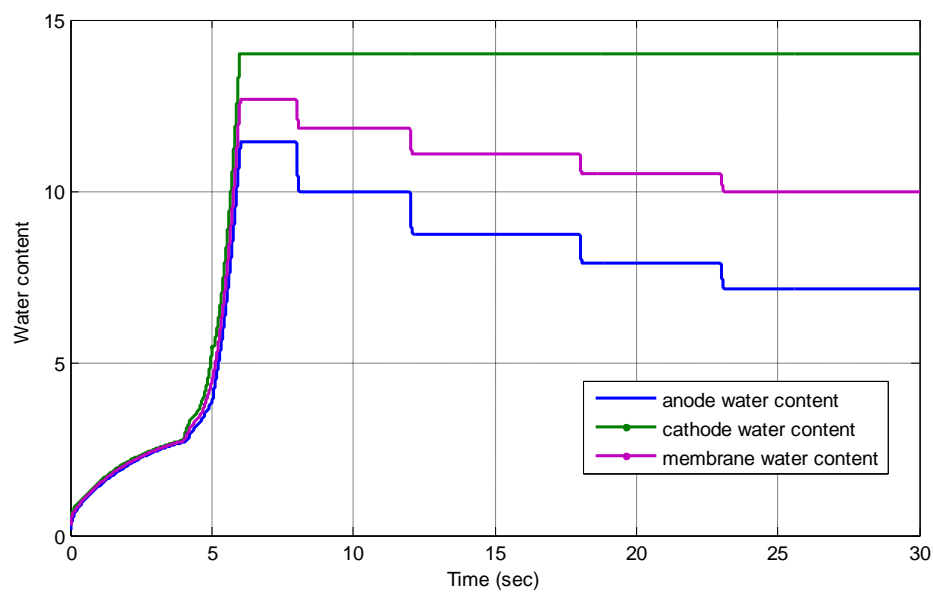


Figure 5.45 Water contents of anode, cathode and the membrane obtained by Simulink.

Water flux through the membrane by osmotic drag and back diffusion are given in Figure 5.46 and Figure 5.47 respectively, which are calculated for a single cell through the equations (3.43)-(3.50). It is observed that the water flux by electro-osmotic drag and back diffusion amounts are similar but the flux directions are reverse. Since the hydrogen gas that is fed to the stack is dry, the water transfer through anode to cathode by electro-osmotic drag is restricted by the water transferred from cathode. Water transfer due to electro-osmotic drag can only be as much as the water transferred from cathode compartment.

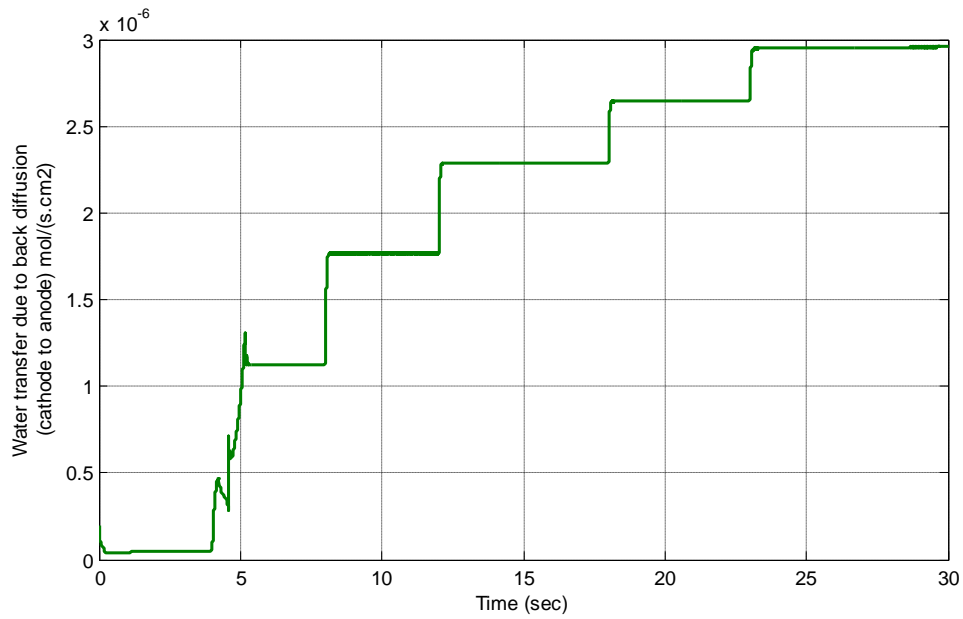


Figure 5.46 Water flux through the membrane of a single cell due to back diffusion obtained by simulations.

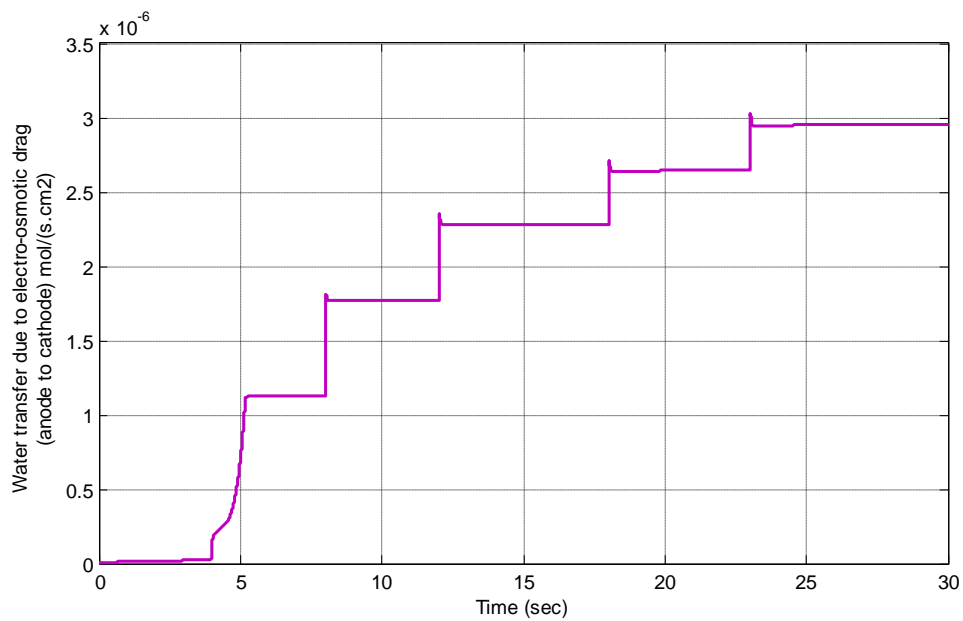


Figure 5.47 Water flux through the membrane of a single cell due to electro-osmotic drag obtained by simulations.

Water transfer rate from anode compartment to cathode compartment for the full stack is given by Figure 5.48, which is simulated by the Equation (3.40) according to the stack

current disturbance as in Figure 5.40. At low stack currents the water transfer from cathode to anode is observed due to the back diffusion. But as the stack current increases water transfer due to the electro-osmotic drag is limited by the water transferred from cathode therefore the net water transfer becomes zero except the overshoots observed at the times of step current changes. At these steps the electro-osmotic drag which is a function of stack current and membrane water content, shows an overshoot due to the step increase in current and a decrease in membrane water content.

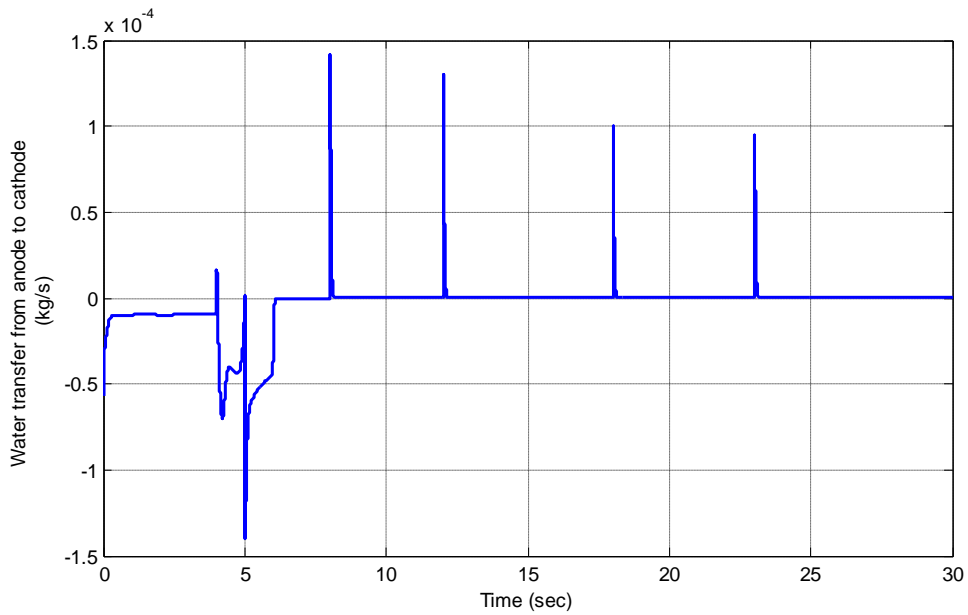


Figure 5.48 Water transfer rate from anode compartment to cathode compartment obtained by simulation for full stack



## CHAPTER 6

### CONTROLLER EVALUATION

#### 6.1. Control of Air Supply

For this study a feedback coupled static feedforward controller is used for air supply. The compressor voltage command is determined according to the air requirement calculated by Faraday's Law which behaves as the set point for air flow. The error between compressor output flow rate and the calculated value is sent to a PI controller for voltage adjustment. A parallel PI controller integrated in the model as given in Equation (6.1). The controller method is represented in Figure 6.1.

$$\frac{P'(s)}{E(s)} = K_c \left[ 1 + \frac{1}{\tau_i s} \right] \quad (6.1)$$

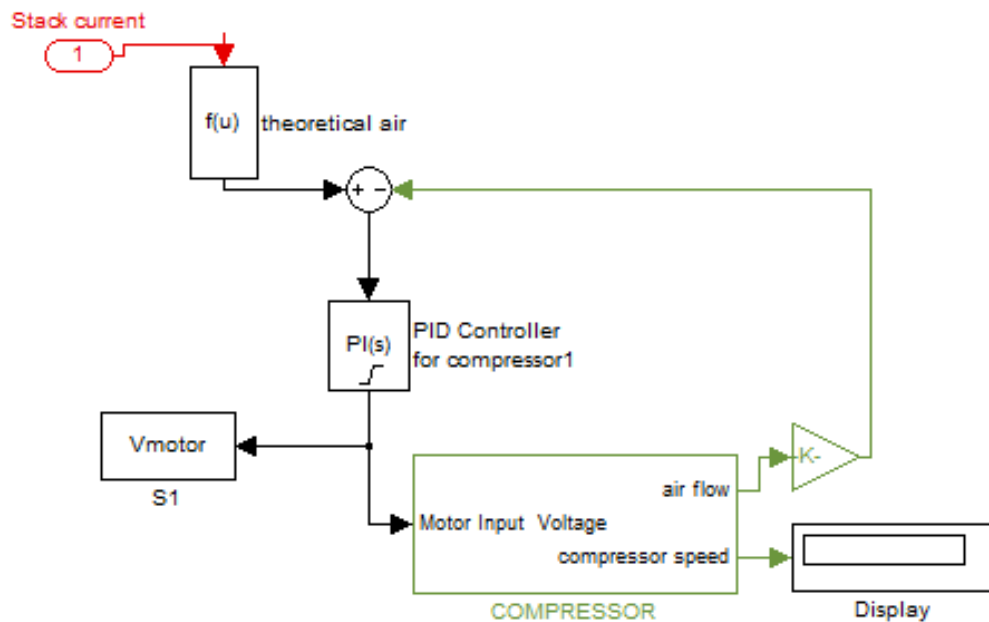


Figure 6.1 Compressor voltage command determination by a feedback coupled static controller.

Step changes in stack current are applied as a disturbance to the system as given in Figure 6.2. The compressor output flow rates, voltage command and oxygen excess ratios are given by the Figures 6.3-6.5 which are simulated by using Equations(3.98)-(3.100) and Equations (3.19)-(3.26).

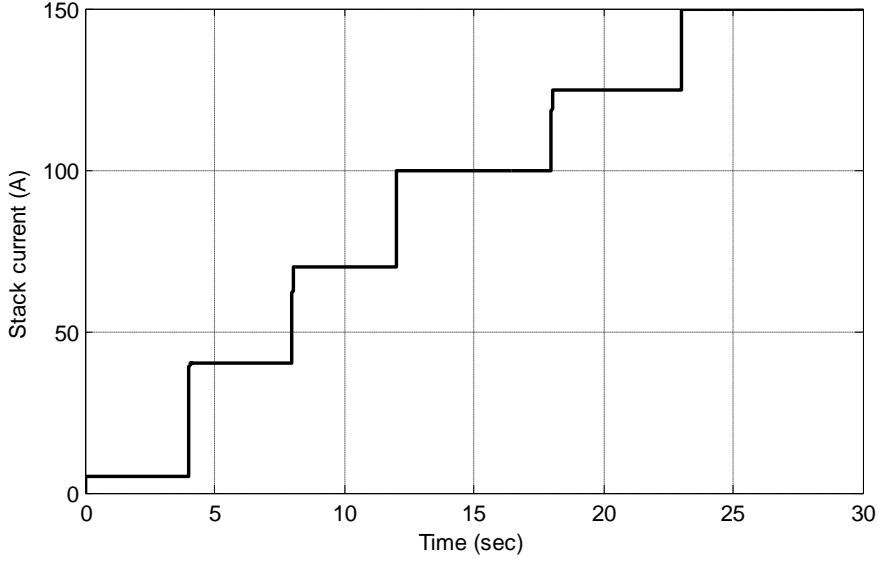


Figure 6.2 Stack current step change applied as the disturbance

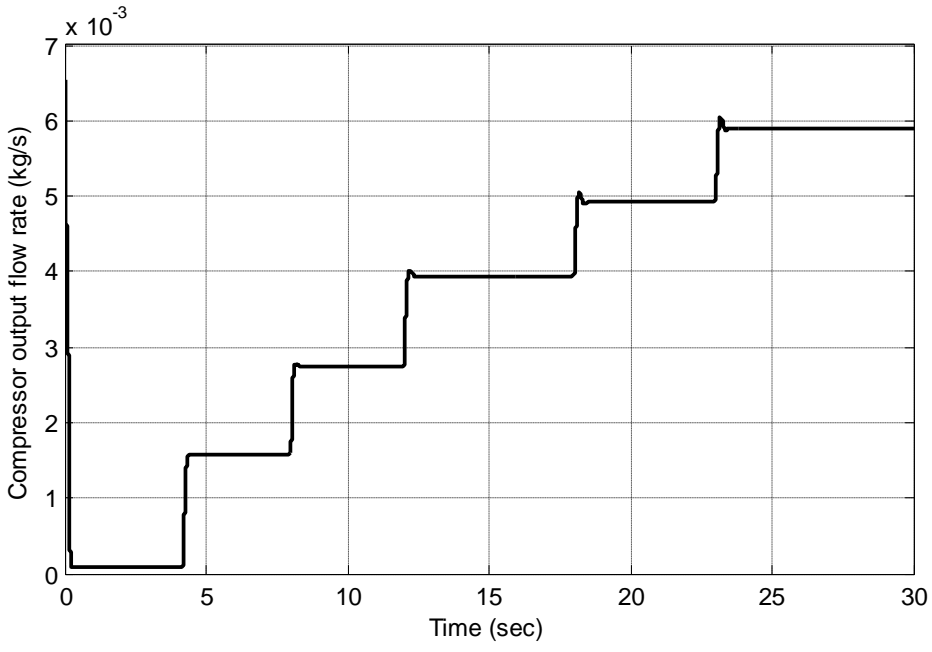


Figure 6.3 Response of compressor output flow to current changes

It is observed that the compressor responds to the current changes rapidly. Within the simulations of Figure 6.3-6.5, although some overshoots are observed the system can recover in small durations and reject oxygen starvation.

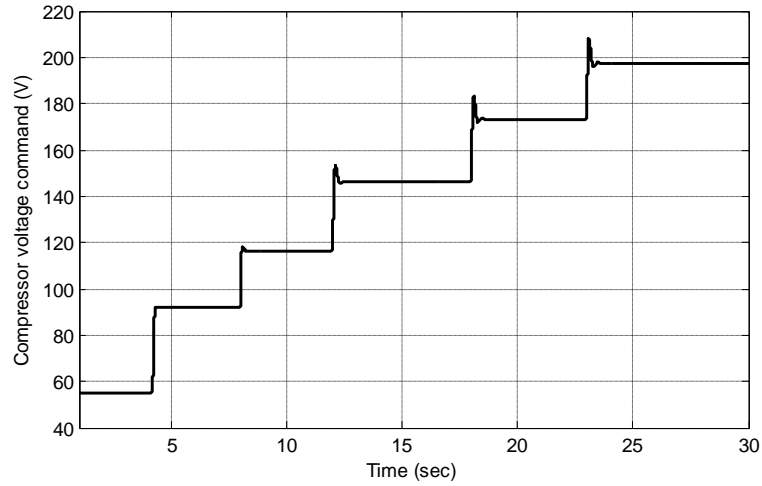


Figure 6.4 Response of compressor voltage command to current changes.

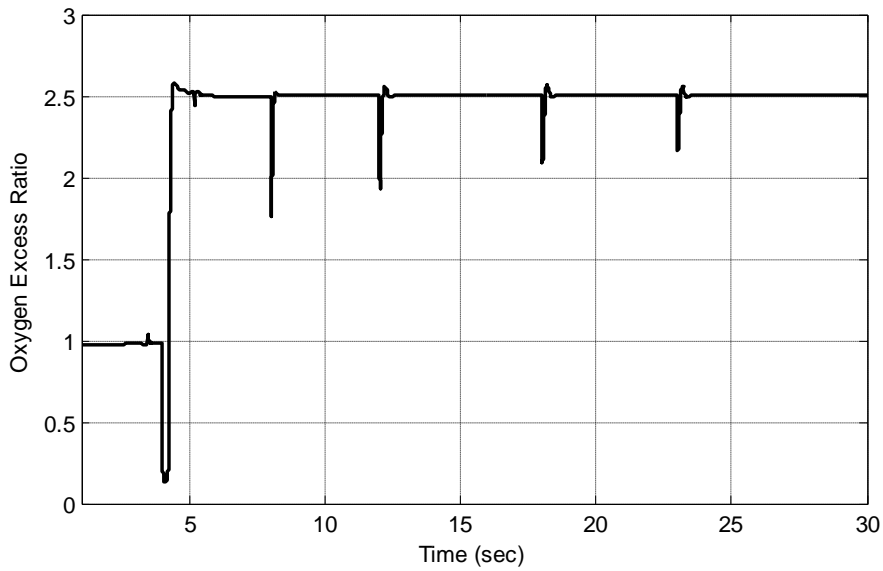


Figure 6.5 Response of oxygen excess ratio with current changes.

## 6.2. Cooling System

The cooling system is aimed to keep the stack at 338 K while operating at any stack current. In order to achieve proper cooling in the system three strategies are developed. These strategies are then compared in terms of stack temperature, ITAE (Integral of time weighted absolute error given in Equation (6.2)) and parasitic energy losses.

$$ITAE = \int_0^{\infty} t|e(t)|dt \quad (6.2)$$

In control strategy-1, pump voltage is set to a constant value at 6.8 V while fan voltage is adjusted according to the feedback of stack temperature with a PI controller. For second control strategy pump, voltage is determined according to the voltage command to the compressor, while fan is operated with an on/off controller. Fan is operated when the difference between the stack temperature and desired temperature exceeds 2 K until this difference becomes -2 K. Third control strategy is implemented by setting the pump voltage by a PI controller while voltage is operated by an on/off controller as stated above. The corresponding block diagrams for the controller strategies are shown at Figure 6.6-6.8. The on/off controller involved for fan operation is given in Figure 6.9.

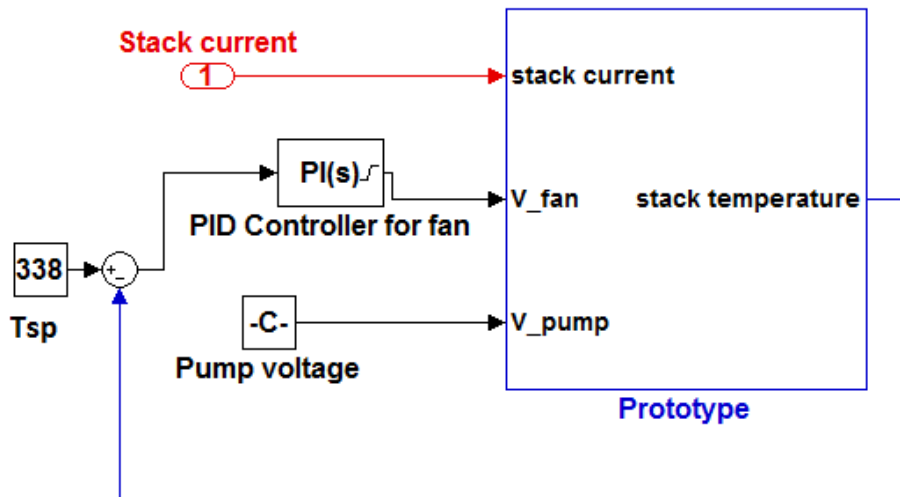


Figure 6.6 Control strategy-1 (Fan voltage:PI, Pump voltage:constant)

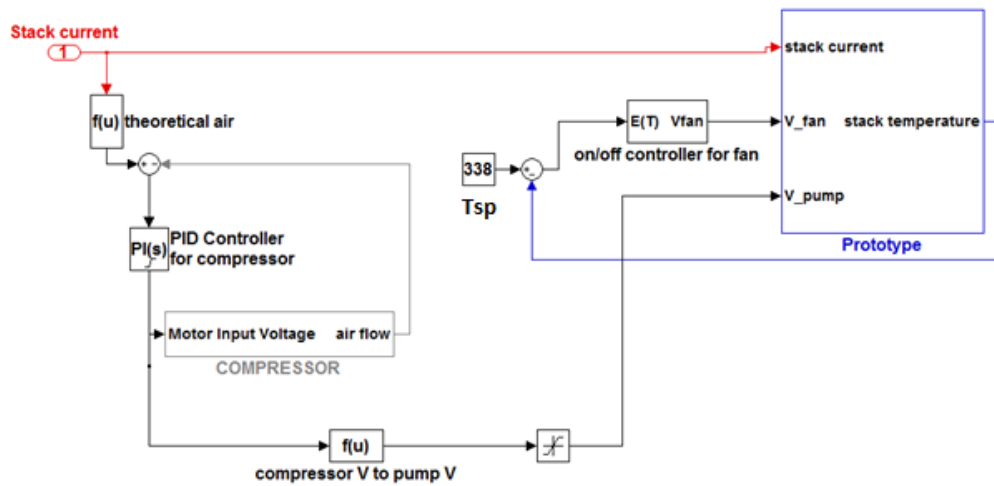


Figure 6.7 Control strategy-2 (Fan voltage:on/off, Pump voltage:follows compressor voltage)

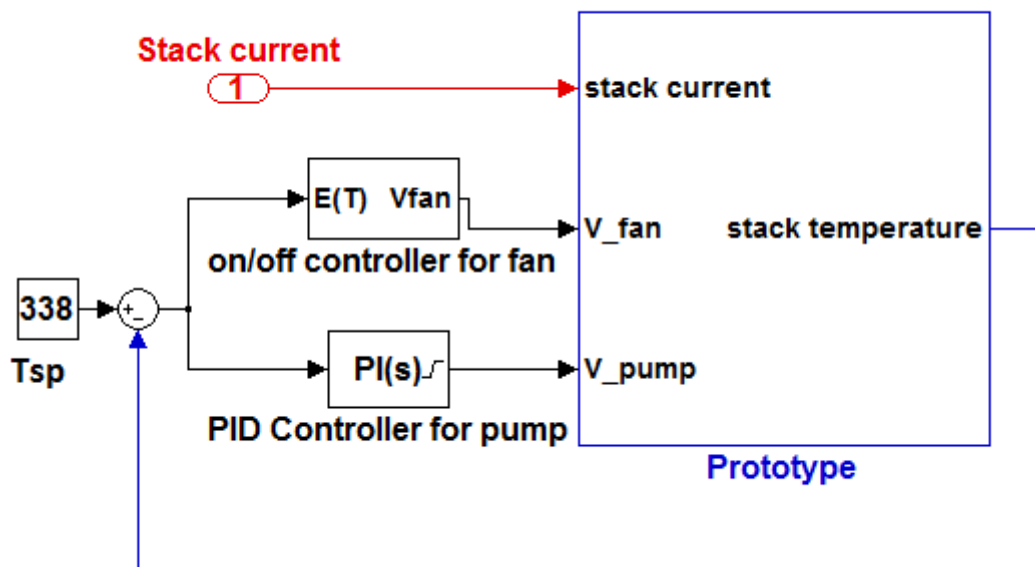


Figure 6.8 Control strategy-3 (Fan voltage:on/off, Pump voltage:PI)

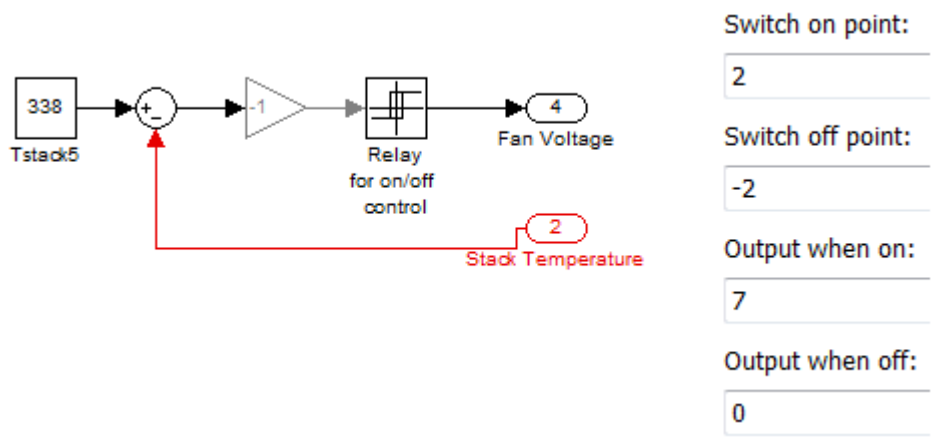


Figure 6.9 On/off controller in Simulink

Stack current step change are applied to the system as given in Figure 6.10 as the disturbance. By assuming full humidification, voltages of pump and fan, ITAE and parasitic losses are compared.

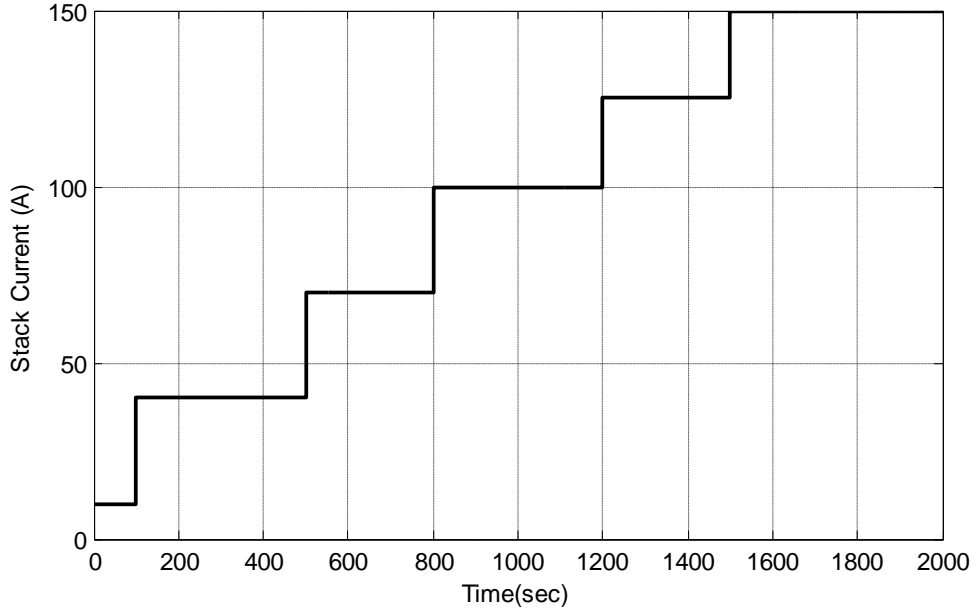


Figure 6.10 Stack current step change as disturbance

At Figure 6.11 the temperature profiles for three cooling system strategies are given. While the fan is operating in on/off mode, the stack temperature is kept  $\pm 2$  K close to the set point. On/off control strategy for the fan may be considered as proper for cooling system in terms of stack temperature analysis. By setting pump voltage a constant value and adding a PI controller for the fan, higher deviations from the set point are observed during the

simulation. Setting a constant value for the pump is not a good approach for the systems that subjected to dynamic changes that affect the heat generation thus the stack temperature sharply. For a 3kW system the heat generation will be smaller at low stack currents, but when the loads are increased the heat generation can be higher than 3 kW according to the stack efficiency. Operating at low pump voltages cannot achieve a sufficient heat removal at high loads as observed after the 500<sup>th</sup> second of Figure 6.11. On the other hand higher pump voltages will remove more heat than the required amount, so the temperature will be lower than the set point.

In Figure 6.12 the behavior of the fan voltages are represented by the stack current changes. While operating the fan with a PI controller with constant pump voltage, at high loads the fan operates continuously. To apply such a method, the fans should be tested in terms of the continuous working ability. While fan is operated at on/off mode, it just operates when the pump is insufficient to remove heat and the stack temperature increase 2 K above the set point of temperature. Pump and fan both operates until the stack temperature is reduced to 2 K below the set point. Therefore the pump voltage defines the start point and duration of the fan operation. While pump follows the compressor voltage command, the fan step in operation earlier, and fan working durations are higher. For the third controller where pump operation is supplied by a PI controller, it is observed that fan engages in the operation lately with small durations. As given in Figure 6.13, the pump voltage is slower for second controller strategy in which fan is operated more than the third controller.

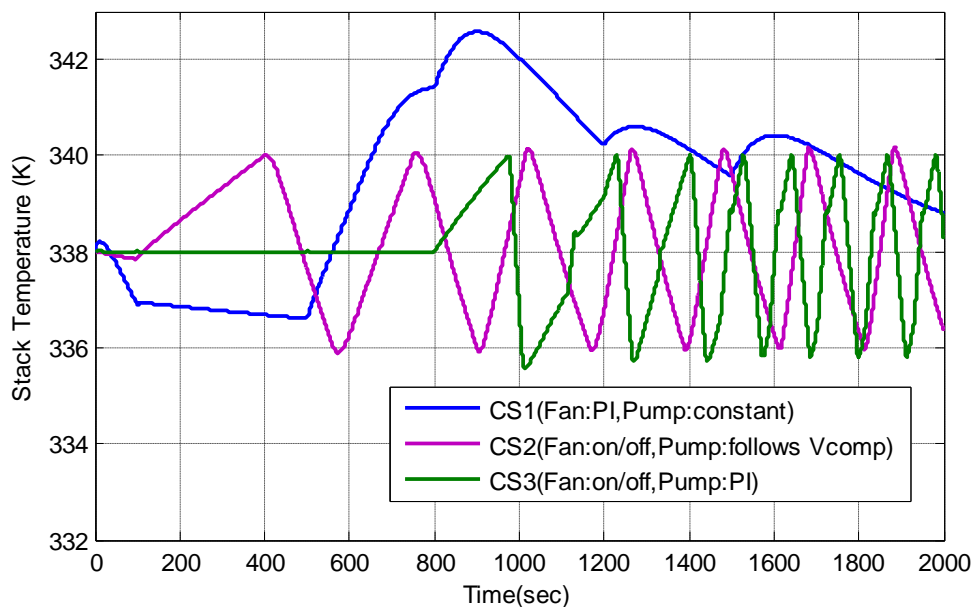


Figure 6.11 Stack temperature change by a stack current changes

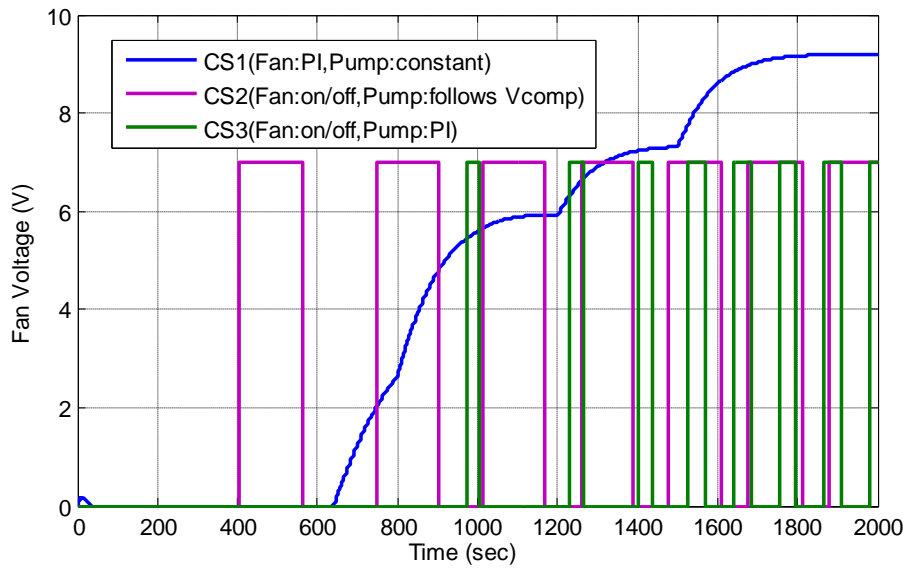


Figure 6.12 Response of fan voltage

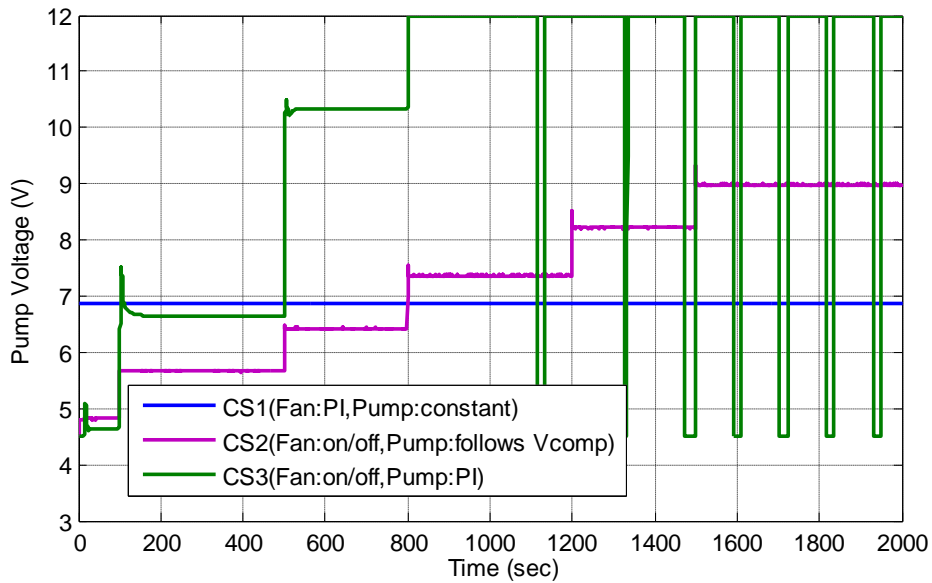


Figure 6.13 Response of pump voltage

The performance of the controller strategies can be compared in terms of ITAE and the parasitic losses which are shown by Figures 6.14-6.16. As expected the ITAE of the CS1, is higher since the method is not capable of achieving a proper heat removal due to constant pump voltage. CS2 and CS1 shows similar ITAE values in which fans are operated both in on/off mode.

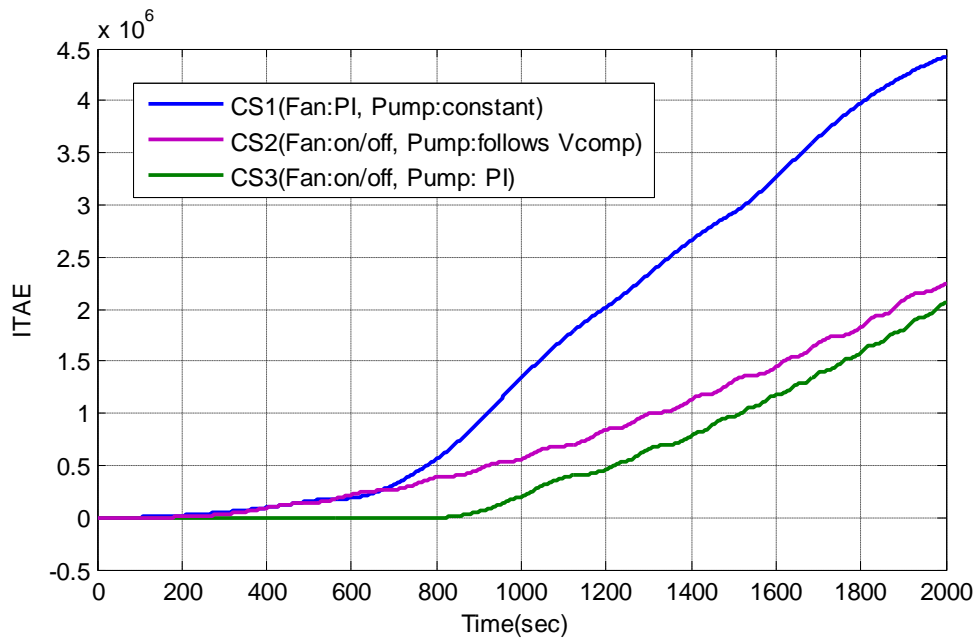


Figure 6.14 ITAE values for the three control strategies.

Figure 6.15 and 6.16 represents the parasitic power and energy requirements for the three control strategies. From Figure 6.15 it can be stated that fan constitutes the parasitic power more than the pump. Also Figure 6.16 shows that fan usage with longer durations results in high parasitic energy. So fan usage should be kept in minimum to avoid high power consumption. Analyzing both ITAE and parasitic power, CS3 can be considered as the best cooling strategy among the ones described in this work.

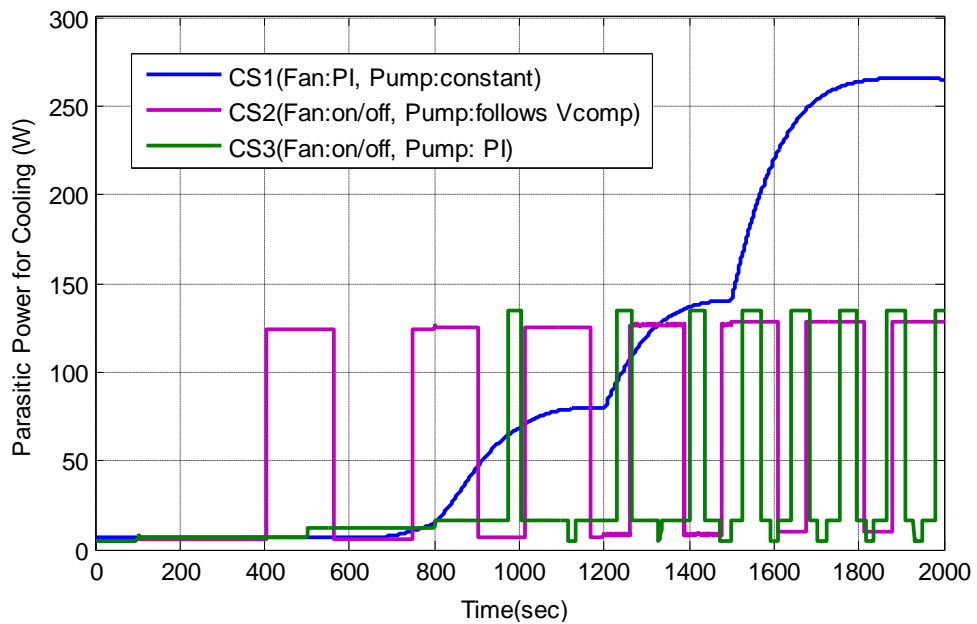


Figure 6.15 Parasitic power required for three control strategies

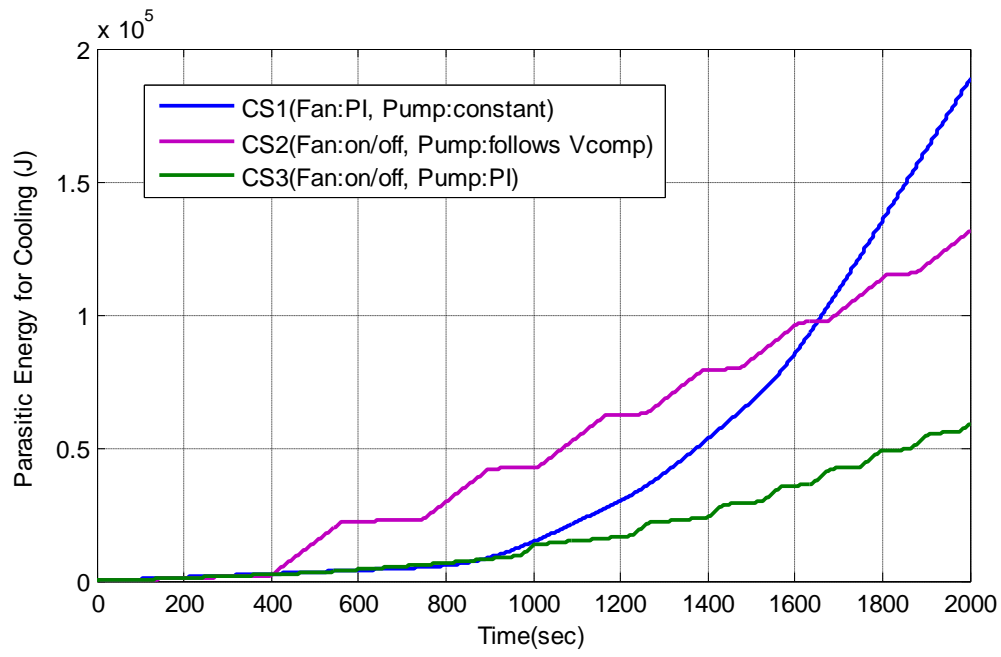


Figure 6.16 Total parasitic energy requirements during the simulation.

## CHAPTER 7

### CONCLUSION AND RECOMMENDATIONS

In this thesis PEM fuel cell modeling and control studies are conducted. Model development is completed by the stack and cooling system tests. Humidifier model is compared by the models available in literature and a reasonable agreement is observed. Compressor model is directly adapted from the literature and a feedback coupled static controller is applied for the control of air flow. For thermal management subsystem, different controller algorithms are developed and analyzed on the Simulink model.

Models are the necessary tools for understanding the system behavior within different conditions. For process control the model should be optimized in terms of the simplifications and covered details. For cooling system a simplified semi-empirical model is derived which allows simulations with small durations. Instead of creating equipment based model by modeling pump and fan, just the effect of voltages of these components on cooling system is analyzed with the experimental data. This method resulted in a simple and system specific model which makes it proper for temperature control.

To keep the stack at a desired temperature different operating conditions are determined for fan and pump. Step changes in stack current are applied as a disturbance and the responses are observed on Simulink. The performances for different controller implementations are compared in terms of stack temperature, ITAE and the parasitic energy losses. It is observed that minimizing fan voltage by setting higher pump voltages gives better results with smaller parasitic loss and ITAE value. Therefore a PI controller for the pump and an on/off controller for the fan are suggested for this system.

The compressor model adapted from the literature having a higher capacity is assumed to have the same dynamics with a small compressor suitable for 3kW fuel cell and the outlet air flow rate is multiplied by a factor to obtain suitable flow rates. This approach is used as a temporary solution to the lack of experimental data of a proper compressor. Performing compressor tests and derivation of a simpler model is recommended for the future study. Since electrochemical reactions have very small time constants, the reactant supply system should have small response times to any kind of disturbance. Therefore the compressor control should be studied in detail with the sophisticated process control techniques.

Although a detailed modeling is available in literature, experimental analysis of humidifier is not satisfactory. The humidifier model requires initial guesses for simulation which is related with lack of experimental evaluations. Humidifier tests are recommended both for simplifying the model for smaller simulation durations, and requirement for the initial guesses.



## REFERENCES

- [1] Miah M.S., Ahmed N.U., Ghowdhury M., Optimum policy for integration of renewable energy sources into the power generation system. *Energy Economics* 2012, 34, 558–567.
- [2] Oh S., Kim K., Oh S., Kwok H., Optimal operation of a 1-kW PEMFC-based CHP system for residential applications. *Applied Energy* 2012, 95, 93-101.
- [3] Barbir F., *PEM Fuel Cells: Theory and Practice*. Elsevier Inc., 2005.
- [4] Djilali N., Computational modeling of polymer electrolyte membrane (PEM) fuel cells: Challenges and Opportunities., *Energy* 2007, 32, 269-280.
- [5] Editorial Polymer electrolytes for a hydrogen economy., *Internal Journal of Hydrogen Energy* 2012, 37, 6120-6131.
- [6] Smitha B., Sridhar A., Khan A.A., Solid polymer electrolyte membranes for fuel cell applications-a review., *Journal of Membrane Science* 2005, 259, 10-26.
- [7] Kreuer K., Paddison S.J., Spohr E., Schuster M., Transport in Proton Conductors for Fuel-Cell Applications: Simulations, Elementary Reactions, and Phenomenology., *Chem. Rev.* 2004, 104,4637-4678.
- [8] Fernandes A.C., Ticianelli E.A., A performance and degradation study of Nafion 212 membrane for proton exchange membrane fuel cells., *Journal of Power Sciences* 2009,193, 547-554.
- [9] Othman R., Dicks A.L., Zhu Z., Non precious metal catalysts for the PEM fuel cell cathode., *International Journal of Hydrogen Energy* 2012,37, 357-372.
- [10] Litster S., McLean G., PEM fuel cell electrodes., *Journal of Power Sources* 2004, 130, 61–76.
- [11] Bayrakçeken A., Erkan S., Türker L., Eroğlu İ., Effects of membrane electrode assembly components on proton exchange membrane fuel cell performance, *International Journal of Hydrogen Energy* 2008,33, 165 – 170.
- [12] Park S., Lee J., Popov B.N., A review of gas diffusion layer in PEM fuel cells: Materials and designs., *International Journal of Hydrogen Energy* 2012,37,5850-5865.
- [13] Antunes R.A., Oliveira M.C.L., Ett G., Ett V., Corrosion of metal bipolar plates for PEM fuel cells: A review., *International Journal of Hydrogen Energy* 2010,35, 3632-3647.

- [14] Yang X., Ye Q., Cheng P., Hydrogen pumping effect induced by fuel starvation in a single cell of a PEM fuel cell stack at galvanostatic operation., *International Journal of Hydrogen Energy* 2012,37, 14430-14453.
- [15] Yousfi-Steiner N., Moçotéguy P., Candusso D., Hissel D., A review on polymer electrolyte membrane fuel cell catalyst degradation and starvation issues: Causes, consequences and diagnostic for mitigation., *Journal of Power Sources* 2009, 194, 130–145.
- [16] Matraji I., Laghrouche S., Jemei S., Wack M., Robust control of the PEM fuel cell air-feed system via sub-optimal second order sliding mode., *Applied Energy* 2013,104, 945-957.
- [17] Vega-Leal A.P., Palomo F.R., Barragán F., García C., Brey J.J., Design of control systems for portable PEM fuel cells., *Journal of Power Sources* 2007,169, 194-197.
- [18] Pukrushpan J.T., Stefanopoulou A.G., Peng H., *Control of Fuel Cell Power Systems. Principles, Modeling, Analysis and Feedback Design*, Springer, 2004.
- [19] He J., Ahn J., Choe S., Analysis and control of a fuel delivery system considering a two-phase anode model of the polymer electrolyte membrane fuel cell stack., *Journal of Power Sources* 2011, 196, Issue 10, 4655-4670.
- [20] Panos C., Kouramas K.I., Georgiadis M.C., Pistikopoulos E.N., Modeling and explicit model predictive control for PEM fuel cell systems., *Chemical Engineering Science* 2012,67,15-25.
- [21] Park S., Choe S., Choi S., Dynamic modeling and analysis of a shell-and-tube type gas to gas membrane humidifier for a PEM fuel cell applications., *International Journal of Hydrogen Energy* 2008, 33,2273-2282.
- [22] Chen D., Li W., Peng H., An experimental study and model validation of a membrane humidifier for PEM fuel cell humidification control., *Journal of Power Sciences* 2008,180,461-467.
- [23] Kang S., Min K., Yu S., Two dimensional dynamic modeling of a shell-and-tube water-to-gas membrane humidifier for proton exchange membrane fuel cell., *International Journal of Hydrogen Energy* 2010, 35,1727-1741.
- [24] Chen D., Peng H., A Thermodynamic Model of Membrane Humidifiers for PEM Fuel Cell Humidification Control., *Transactions of the ASME* 2005,127, 424-432.
- [25] Woo-Ann J., *Control and Analysis of Air, Water and Thermal Systems for a Polymer Electrolyte Membrane Fuel Cell*. In Phd Thesis in Mechanical Engineering. Alabama, Auburn University, 2011.

- [26] Park Y. H., Caton J. A., Development of a PEM stack and performance analysis including the effects of water content in the membrane and cooling method., *Journal of Power Sources* 2008, 179, 584-591.
- [27] Hu P., Cao G., Zhu X., Hu M., Coolant circuit modeling and temperature fuzzy control of proton exchange membrane fuel cells., *International Journal of Hydrogen Energy* 2010, 35, 9110-9123.
- [28] Rabbani A., Rokni M., Dynamic characteristics of an automotive fuel cell system for transitory load changes., *Sustainable Energy Technologies and Assessments* 2013, 1, 34-43.
- [29] Cho K. T., Mench M.M., Coupled effects of flow field geometry and diffusion media material structure on evaporative water removal from polymer electrolyte fuel cells., *International Journal of Hydrogen Energy* 2010, 35, 12329-12340.
- [30] Belvedere B., Bianchi M., Borghetti A., Pascale A.D., Paolone M., Vecci R., Experimental Analysis of a PEM fuel cell performance at variable load with anodic exhaust management optimization., *International Journal of Hydrogen Energy* 2013, 38, 385-393.
- [31] Chen J., Siegel J.B., Stefanopoulou A.G., Waldecke J.R., Optimization of purge cycle for dead-ended anode fuel cell operation., *International Journal of Hydrogen Energy* 2013, 38, 5092-5105.
- [32] Zhang Y., Zhou B., Modeling and Control of a Portable proton exchange membrane fuel cell-battery power system., *Journal of Power Sciences* 2011, 196, 8413-8423.
- [33] Kim Y.B., Kang S.J., Time delay control for fuel cells with bidirectional DC/DC converter and battery., *International Journal of Hydrogen Energy* 2010, 35, 8792-8803.
- [34] Mulder G., Ridder F.J., Coenen P., Weyen D., Martens A., Evaluation of an on-site cell voltage monitor for fuel cell systems., *International Journal of Hydrogen Energy* 2008, 33, 5728-5737.
- [35] Mulder G., Coenen P., Ridder F.J., Martens A., An advanced cell voltage monitoring device for fuel cell control ., *Vlaamse Instelling voor Technologisch Onderzoek, Boeretang 200, B-2400 Mol, Belgium*
- [36] Ous T., Arcoumanis C., Degradation aspects of water formation and transport in Proton Exchange Membrane Fuel Cell: A review., *Journal of Power Sciences* 2013, 240, 558-582.
- [37] Collier A., Wang H., Yuan X.Z., Zhang J., Wilkinson D.P., Degradation of polymer electrolyte membranes., *International Journal of Hydrogen Energy* 2006, 35, 1838-1854.

- [38]Bequette B.W.,Process Dynamics Modeling, Analysis and Simulation., Prentice Hall.,1998.
- [39]Seidenberger K., Wilhelm F., Schmitt T., Lehnert W., Scholta J., Estimation of water distribution and degradation mechanisms in polymer electrolyte membrane fuel cell gas diffusion layers using a 3D Monte Carlo model.,Journal of Power Sources 2011,196, 5317–5324.
- [40]Fiçıcılar B.,Electrocatalyst Development and Modeling of Nonisothermal two-phase flow for pem fuel cells.,. In Phd Thesis in Chemical Engineering, Ankara, Middle East Technical University,2011.
- [41]Khandelwal M., Lee S., Mench M.M., Model to predict temperature and capillary pressure driven water transport in PEFCs after shutdown.,Journal of Electrochemical Society2009, 156(6),B703-B715.
- [42]Khandelwal M.,Lee S.,Mench M.M., One-dimensional thermal model of cold-start in a polymer electrolyte fuel cell stack., Journal of Power Sciences 2007,172,816-830.
- [43]Grötsch M., Mangold M., A two-phase PEMFC model for process control purposes., Chemical Engineering Science 2008, 63,434-447.
- [44]Mann R.F., Amphlett J.C., Peppley B.A., Thurgood C.P., Application of Butler-Volmer equations in the modeling of activation polarization for PEM fuel cells. Journal of Power Sources 2006, 161( 2), 775-781.
- [45] Nguyen T.V., White R.E., A water and heat management model for proton exchange membrane fuel cells. Journal of Electrochemical Society 1993, 140(8), 2178-2186 .
- [46] Springer T.E., Zawodzinski T.A., Gottesfeld S.,Polymer electrolyte fuel cell model. Journal of Electrochemical Society 1991,138(8),2334-2342.
- [47] Dutta S., Shimpalee S., Van Zee J.W., Numerical prediction of mass-exchange between cathode and anode channels in a PEM fuel cell., International Journal of Heat and Mass Transfer 2001,44,2029-2042.
- [48] Incropera, DeWitt.,Bergman.,Lavine.,Fundamentals of Heat and Mass Transfer..6<sup>th</sup> edition.Wiley 2007.
- [49] McCabe, Smith, Harriott. Unit Operations of Chemical Engineering, Sixth Edition, McGraw-Hill.

## APPENDIX A

### EQUIPMENT SPECIFICATIONS

#### A.1. Water Circulation Pump

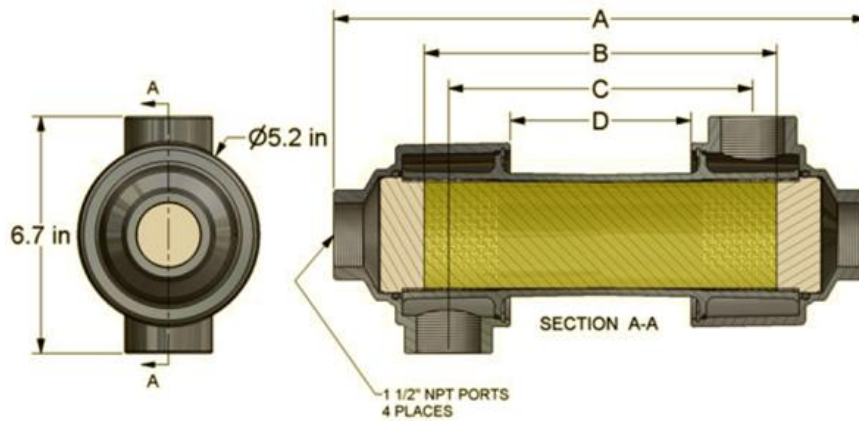
A water circulating pump (Kormas centrifugal Pump-671 143 35) will be used in order to operate the 3kW PEMFC stack at the desired temperature as given in Figure A.1. Pump operates with 24VDC, with maximum flow rate of 4500 l/h and 0.2 bar pressure [51].



Figure A.1 Water circulating pump (<http://www.kormas.com/urunler.asp?id=311> accessed at 20.06.2013.)

## A.2. Humidifier

A shell-and-tube structured membrane humidifier is selected to be used in the system which is shown in Figure A-2. Specifications for the humidifier are given in Table A.1.



Model	A		B (Nom.)		C		D	
	inch	mm.	inch	mm.	inch	mm.	inch	mm.
FC300-1660-7LP	12.1	307.3	7	177.8	5.6	142.2	2.1	53.3
FC300-1660-10LP/HP	15.1	383.5	10	254	8.6	218.4	5.1	129.5
FC300-1660-15LP	20.1	510.5	15	381	13.6	345.4	10.1	256.5

Shell diameter 3.4 inches (86.4mm)

Figure A.2 Structure of the membrane humidifier (<http://www.permapure.com/prod-sub-pages/fc300/?ind=Product%20Support%20Pages&prod> = accessed at 20.06.2013.)

Table A.1 Humidifier Specifications

Construction materials	Housing-GE Norly or ABS Seals-EPDM (peroxide cured) Tube bundle headers-polyurethane Membrane tubing-Nafion ®
Maximum operating pressure	Low pressure model-10 psig High pressure model-45 psig
Operating fluid temperature	1-90°C
Pressure differential on tubing	35kPa
Storage temperature	-30 to 60°C
Fittings	ABS or Nylon fittings are recommended

## APPENDIX B

### PROGRAM CODES FOR DATA ANALYSIS

#### B.1. Cooling system regression code

Cooling system regression function is coded as below:

```
function uA=lsq_uA(x,xdata)

    uA=x(1).*((x(2).*xdata(:,1)+x(3)).^x(6)).*((x(4).*xdata(:,2)+x(5)).^x(7));

end
```

Data is imported and the initial conditions are described with a Matlab script as below:

```
xdata(:,1)=data(:,1);
xdata(:,2)=data(:,2);
ydata=data(:,3);

x = lsqcurvefit(@lsq_uA, [0.78, 0.551,3.639,0.913,-3.97,2.08,0.815],
xdata, ydata)
```

#### B.2. Polarization curve regression code

The function for polarization curve is coded as below:

```
function L=lsq_polarization(x,xdata)

    L=44*((1.191-(0.235+0.2642.*(1-exp(-x(1).*xdata)))-(xdata.*0.1706))-
(xdata.*((x(2).*xdata)./x(3)).^x(4))));

end
```

The data loading and initial condition determination for the nonlinear regression is achieved by the code given as below:

```
clear all
A=importdata('polarizationdata.xlsx');
xdata=A.Sayfal(:,1);
ydata=A.Sayfal(:,2);
x = lsqcurvefit(@lsq_polarization, [10,0.1086,2.2,2], xdata, ydata)
```

### B.3. JMP Script for reducing test data

JMP.8 is used for data reduction.

```
dt=current data table();
for(i=0, i<3624,i++;
x=i;
y=i+998;
mylist=Index(x,y);
dt<<Delete rows(mylist),
if(i<3624,continue()));
```

### B.4. Humidifier Model Subsystems

Humidifier Model consists of the subsystems of heat transfer, inlet gas properties, mass balances and energy balances. In Simulink each of these subsystems are developed by using the equations given in Section 3.2.3.

- **Heat Transfer Subsystem**

In heat transfer subsystem overall heat transfer coefficient is calculated with a script given as below, by knowing the tube side and shell side air flow rates and temperatures.

```
function y = fcn(m1,m4,T1,T4)
%#codegen

Da=0.00097;
Db=0.00107;
Db_re=0.254;
mua=184.6*10^(-7);
mub=208.2*10^(-7);
Pra=0.707;
Prb=0.70;
Ain=0.000774;
Dout=0.00102;
```

```

Din=0.00097;
pi=3.14;
L=0.254;
kmemb=0.21;
km=0.02642;
Aout=0.000997;
Aino=0.0264;
Aouto=0.000814;
Axf=0.0047;

Rea= 4*m4/(pi*Da*mua)/780;
Reb=4*m1/(pi*Db*mub)/780;

if Reb<=4;
m=0.989;
n=0.330;

elseif 4<Reb<=40;
m=0.911;
n=0.385;

elseif 40<Reb<=4000;
m=0.683;
n=0.466;

elseif 4000<Reb<=40000;
m=0.193;
n=0.618 ;

else 40000<Reb;
m=0.027;
n=0.805 ;
end

Nua=0.023*(Rea^0.8)*(Prb^0.4);
Nub=m*(Reb^n)*(Prb^0.33);
ha=Nua*km/Da;
hb=Nub*km/Db;

y=((1/(ha*Ain*780))+((log(Dout/Din))/(2*pi*L*780*kmemb)))+(1/(hb*Aout*780))
)^(-1); %OVERALL HEAT TRANSFER COEFFICIENT

```

- **Subsystem of Inlet Gas Properties**

In the subsystem of inlet gas properties, the tube side and shell side dry air and vapor flow rates, vapor mass fractions and vapor pressures are calculated by knowing temperature, relative humidity, mass flow rate and pressure as given in Figure B.1. In Simulink program by clicking on the blocks involved in the model we can see the related equations, which are the ideal gas law, saturation pressure and some algebraic equations in this subsystem.

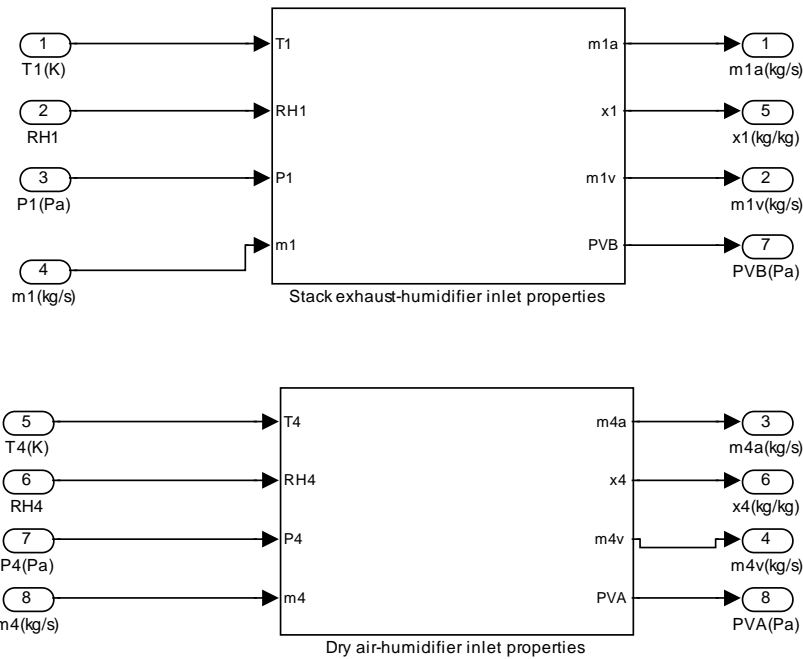


Figure B.1 Inlet gas properties subsystem involved in humidifier model

- **Mass Balance Subsystem involved in humidifier**

Mass balance subsystem involved in humidifier model calculates the mass involved in tube side and shell side, output vapor and air mass flow rates, and the vapor transfer from shell side to the tube side. Figure B.2 shows the Simulink model which includes the humidifier mass balance equations (3.70)-(3.74) and vapor transfer equations (3.89)-(3.94).

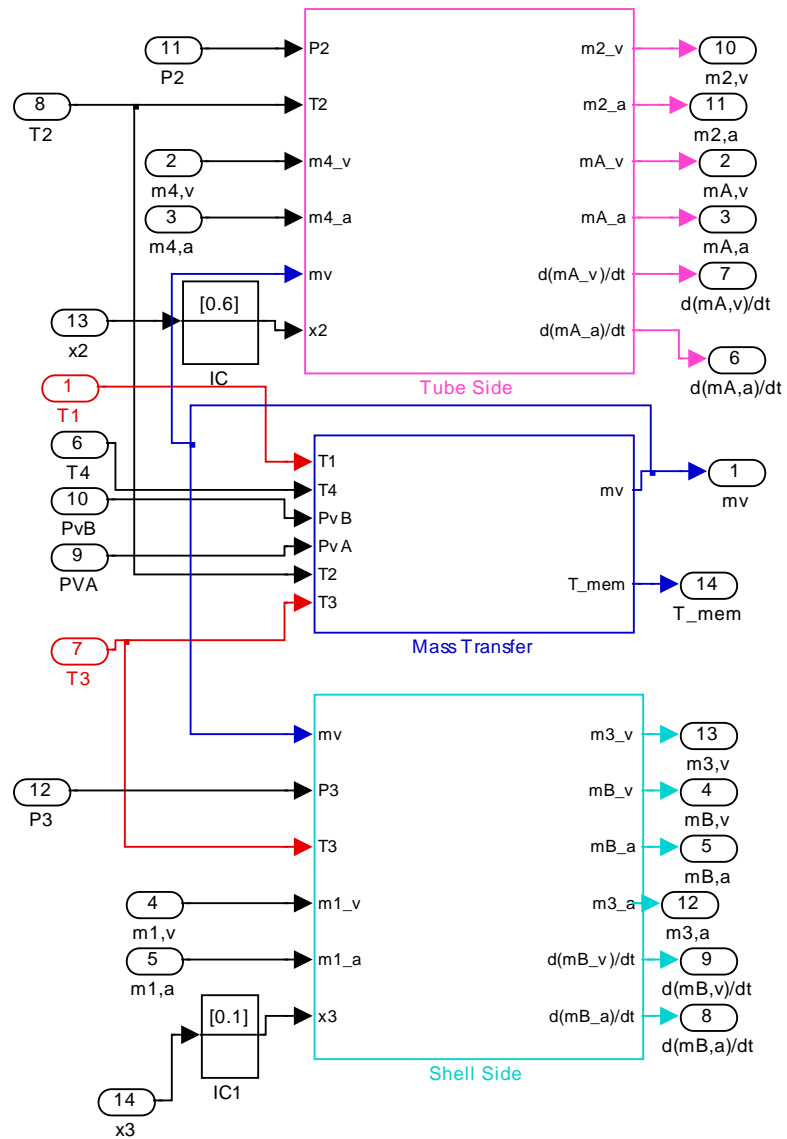


Figure B.2 Mass balance subsystem involved in humidifier model

- **Energy Balance Subsystem involved in humidifier**

Energy balance subsystem involved in the humidifier includes the energy balance equations developed for the tube and shell sides, equations (3.75)-(3.80).

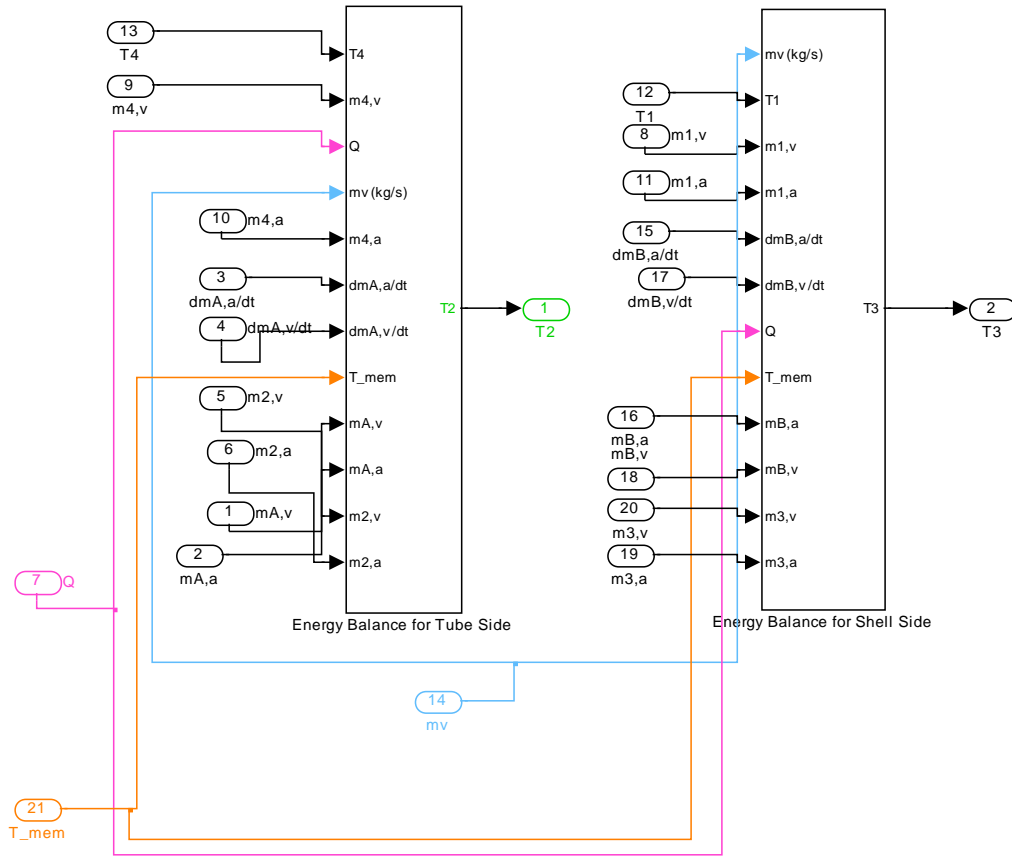


Figure B.3 Energy balance subsystem involved in humidifier model

### B.5. Model Parameters

```

%% Data for stack model
nanode=2;
ncathode=4;
Faradaysconstant=96485;
Hydrogenmolarmass=2*(10^(-3));
Watermolarmass=18*(10^(-3));
Nitrogenmolarmass=28*(10^(-3));
Oxygenmolarmass=32*(10^(-3));
R=8.314;
Anodevolume=0.000384*2;
Cathodevolume=0.000384*2;
Membranedrydensity=0.002;
Membraneequivalentweight=1.1;

```

```

Cellarea=400 ;
%%cell area (cm^2)

fc_outlet_flow_constant=2.1776*10^(-6);

ncell=44;

tm=0.0128;
% PARAMETERS FOR HUMIDIFIER MODEL

pi=3.14;

R=8.314; %J/(mol.K)
L=0.254; %m _tube length
A=0.666*2.12; %m2 _total heat and mass transfer area

Vb=0.000588*2.12;

Va=0.0001464*2.12;

ro=0.001;

Meq=1;
tm_h=0.00005; %m
Mw=18/1000;

cpa=1005;
cva=717;
cvv=1463;
cpv=1952;

Da=0.00097;
Db=0.00102;
Db_re=0.254;
mua=184.6*10^(-7);
mub=208.2*10^(-7);
Pra=0.707;
Prb=0.70;
Ain=0.000774;
Dout=0.00102;
Din=0.00097;

kmemb=0.21;
km=0.02642;
Aout=0.000997;
Aino=0.0264;
Aouto=0.000814;
Axf=0.0047;

```

- **Stack Model involved in fuel cell system**

Stack model includes the anode flow model (equations (3.1)-(3.18)), cathode flow model (equations (3.19)-(3.26)), membrane vapor transport model (equations (3.40)-(3.45)) and stack voltage model (equations (3.27)-(3.39)).

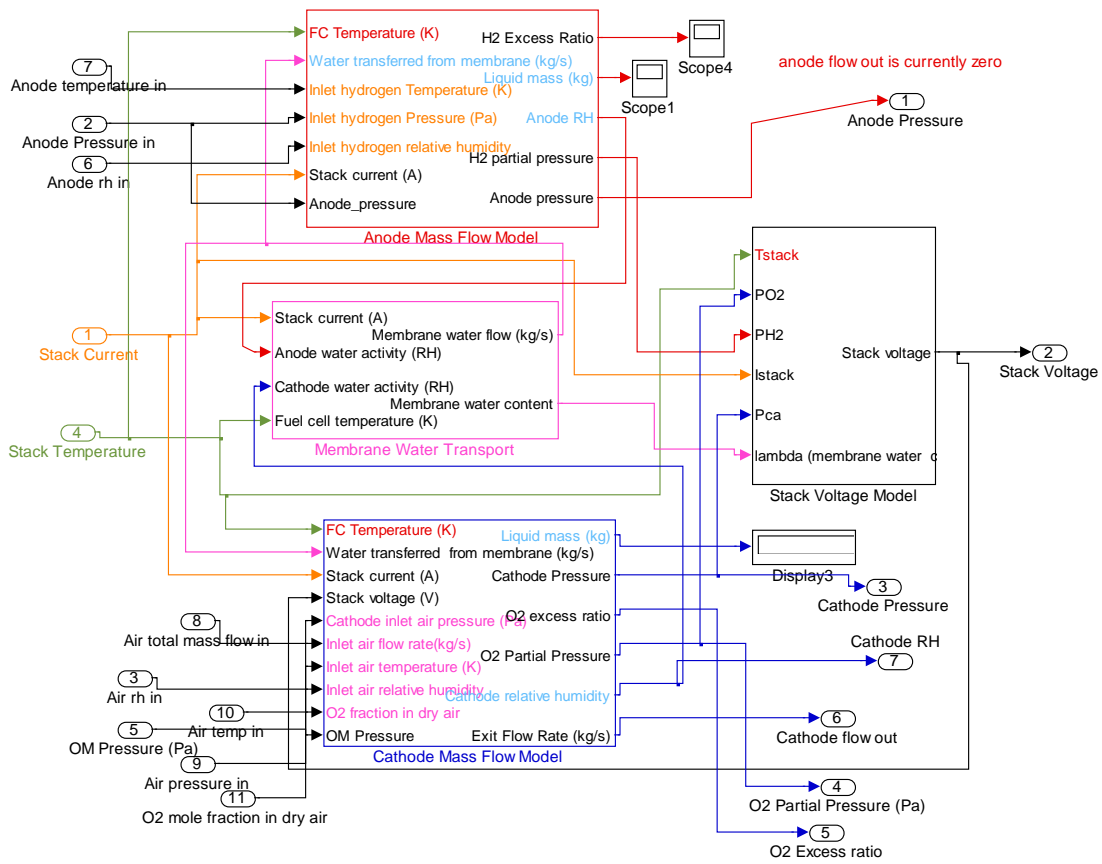


Figure B.4 Stack model involved in fuel cell system